Comparison of Ellipsoidal and Spherical Harmonics for Gravitational Field Modeling of Non-spherical Bodies

Thesis

Presented in Partial Fulfillment of the Requirements for the Degree
Master of Science in the Graduate School of The Ohio State University

By

Xuanyu Hu, M.S.
Graduate Program in Geodetic Science

The Ohio State University
2012

Thesis Committee
Dr. Christopher Jekeli, Advisor
Dr. C.K. Shum
Dr. Ralph von Frese

Abstract

Two harmonic expansions are compared on modeling the gravitational field of non-spherical attracting bodies. As a solution to the Laplace's equation based on spherical coordinates, the spherical harmonic series (SHS) is uniformly convergent outside a certain reference sphere that encloses the entire body mass. The convergence can be doubtful in close proximity to the body. On the other hand, a tri-axial ellipsoid, being more arbitrary-shaped than a sphere, is more apt to be closely fitting to the attracting body. It would be desirable to apply the ellipsoidal harmonic series (EHS) for field modeling if the body is distinctly non-spherical. To obtain the EHS one solves the Laplace's equation in ellipsoidal coordinates. In theory, the EHS is akin to the SHS in terms of representation, properties and relation to the field potential problem. It can be shown that EHS is convergent outside a certain reference ellipsoid, thus could have more convergence region than the SHS. However, the application of the EHS for field modeling is obscured by many numerical difficulties. The theoretical formulation is far from practical and needs to be modified at the cost of computational complexity. The numerical scheme of applying the EHS for field modeling presented by Garmier and Barriot has been reviewed and adopted for application in this work. The numerical accuracy of the EHS may deteriorate from a certain degree, e.g., around 15, which limits the use of higher-degree expansions.

In simulation we choose to compare the performance of EHS and SHS in modeling the gravitational field of the Martian moon Phobos and asteroid 433 Eros, both assumed to be homogeneous. Of the two bodies, Phobos has moderate shape non-sphericity, while Eros is highly irregular-shaped. Results suggest that the EHS and SHS models are comparable in performance in their respective convergence regions. Outside the convergence region, both models are subject to divergence, i.e., incurring substantial modeling errors. And the further outside the convergence region, the greater the errors. The divergence will be aggravated by increasing the degree of

expansions rather than be abated. With smaller convergence region than the EHS, the SHS becomes more vulnerable to divergence in close range of the body, e.g., on the reference ellipsoid. On the other hand, even if the EHS is applied outside its convergence region, e.g., on the surface of the body, it is less error-prone than the SHS, as the surface points usually reside at more shallow depth below the reference ellipsoid than below the reference sphere. The comparison of simulation results on Phobos and Eros suggest that the EHS is a more consistent model than the SHS for the non-spherical bodies, at the expense of increased computational effort. And the more non-spherical the body is, the more advantageous it is to apply the EHS.

Vita

July, 2006…….…….. B.E., Northwestern Polytechnical University, China

July, 2009……..... M.S., Shanghai Observatory, Chinese Academy of Sciences, China

September, 2009 to present…..... Graduate student, Geodetic Science Division, School of Earth Sciences, The Ohio State University

September, 2010 to present…… Graduate Teaching Associate, School of Earth Sciences, The Ohio State University

Fields of Study

Major Field: Geodetic Science

Acknowledgements

I would like to express my utmost gratitude to my advisor Dr. Christopher Jekeli for his supervision for this thesis. It has been a true privilege to learn from him and have his guidance throughout this work which helped me not only comprehend the technical details but also have them fit in the big picture of physical geodesy. I also greatly appreciate his instructions in a series of core courses in geodesy that inspired my interest in this field. I want to express my thanks to Dr. C.K. Shum for reviewing my thesis with constructive criticism, and for the unreserved help I received from him in research all along. Not least of all, I am thankful for his earlier effort in recruiting me into this prestigious program. I wish to thank Dr. Ralph von Frese for serving on the thesis committee and providing insightful comments that help me better understand the role of this work in the geophysical context. My sincere gratitude also goes to Dr. Alan Saalfeld for his instructions on various interesting courses as well as his kind encouragement. Thanks to Dr. Yuchan Yi, Mr. Peter Luk for their support during my studies. Last but not least, to my dearest friends the Sellerses, thank you so much for all your help and care ever since I arrived and making me feel at home in the US.

Table of Contents

List of Tables

List of Figures

Chapter 1: Introduction

In the last half a century or so there has been immense interest in exploring extraterrestrial objects, most notably the Moon[1] and other major planets such as Mars[2], Jupiter[3] etc. Space missions that involved sending spacecrafts with scientific instruments to approach or even land on the mission target[4] have greatly improved our understanding of formation, condition and possible inhabitability of these planets[5,6]. Meanwhile, smaller objects in the solar system such as comets, asteroids have also been subject of scrutiny; more are being marked as future targets of exploration[7]. To name but a few reasons for this, these small bodies denote a significant departure from major planets, dwarf planets and some planetary satellites such as the Moon in size, shape, mass and interior structure etc.[8] Knowledge of these small bodies may well complement our knowledge of the solar system[9]. Furthermore, some planets, e.g. Mars, Saturn have planetary moons of which some are small ones, exploring them may facilitate the understanding of the origin and evolution of the respective planetary system. Last but not least, there are numerous asteroids in the solar system, many whose trajectories come close to the Earth may pose risks of future crashing with potential damage, even devastation[10].

As a spacecraft approaches a celestial body, it is subject to the body's gravitation. Modeling the gravitational field is therefore an indispensable task for accurately tracking and controlling the spacecraft, which is a requisite condition for the functionality of onboard research instruments, e.g., satellite altimetry relies heavily on orbital accuracy especially the radial component[11,12]. Another major motivation is that, since gravitation is essentially determined by the mass distribution of the attracting body, knowledge of the field may shed light on the interior condition such as composition and structure of the body. In general, to represent the gravitational field one can use either forward or backward modeling methods. The former is an intuitive yet not always realistic method based on the fact that the mass distribution

of the attracting body, if known, uniquely determines the gravitational field [13,14,15], while the reverse, unfortunately, is usually not true. The dilemma, however, is that not only is the mass distribution not easily known, but also it is likely the riddle itself we try to solve (e.g., in geophysics). On the other hand, backward-modeling may be of more practical significance. In this case, rather than pursuing the mass distribution, one uses measurements on or outside the attracting body to comprehensively characterize the exterior gravitational field. For example, a common practice in geodesy is to use ground-based and airborne gravimetric measurements of local accelerations for studying the Earth gravity* field[16,17]. With the advent and later pervasiveness of space technology, satellite laser ranging[18,19], satellite-to-satellite tracking[20,21], GPS[22] etc. were also found to be highly serviceable and complementary for field modeling. Although the actual specifics vary, the above geodetic principle can be readily (have been) extended to extraterrestrial bodies, e.g., making use of Doppler, VLBI tracking data of the nearing spacecraft to derive the gravitational field of the attracting object[23,24,25].

Appropriate mathematical methods are also crucial for field modeling. The basis of representing the gravitational field in free space is expressed by the Laplace's equation, a solution to which would form a field model. These solutions are known as harmonic functions whose forms vary according to the coordinate system used. For the Earth and other bodies whose shape is nearly spherical, a natural choice is the set of spherical coordinates. Accordingly the gravitational model is expressed by the series expansion of spherical harmonics. Specifically, the backward modeling is to determine a set of coefficients for the spherical harmonics that conform to the true field. Spherical harmonic series is prevalently used for gravitational field modeling due to its elegant form, straightforward formulation, and being probably the easiest solution to find. As a series solution the use of spherical harmonics is not unconditional. To model the exterior field, for instance, the series is uniformly convergent outside a certain reference sphere enclosing the entire attracting body. Inside the sphere the convergence can be doubtful. The implication is that, spherical harmonics are better suited for spherical bodies as their shape is more likely to fill up

* Gravity is related to but differs from gravitation which we neglect for the moment.

the reference sphere. The unoccupied area inside the sphere known as divergence region is where spherical harmonics would be subject to errors in practice. For planets such as Earth and Mars, the figure oblateness is typically on the order of 0.001 or less, which suggests slight deviations of their shape from a sphere. We need not worry about related errors except for exacting applications. In case the errors are not tolerable, one remedy is to resort to the spheroidal harmonics[26] for which the reference surface is an ellipsoid of revolution to reduce the divergence region.

Problems arise when the attracting object assumes a more arbitrary or irregular shape. In this case since the body does not fit snugly into the (any) reference sphere (or spheroid) there is a considerable region of divergence inside the reference surface where the spherical (or spheroidal) harmonic model might incur errors. This could become a significant issue, e.g., when we evaluate the landing trajectory of the spacecraft close to the arbitrary-shaped body. Intuitively, the body is more likely to be fitted by an arbitrary or tri-axial ellipsoid, for which sphere and spheroid are but special cases. The divergence region is expected to be well restricted in the ellipsoid of proper choice. Therefore we are curious about the possible solution to the Laplace's equation based on ellipsoidal coordinates: the ellipsoidal harmonics. In particular, a fundamental issue we wish to explore is the convergence behavior of the ellipsoidal harmonics. Furthermore, we are interested in how ellipsoidal harmonics perform compared to their counterpart spherical harmonics in terms of complexity, effectiveness as well as necessity of application.

The theoretical aspects of ellipsoidal harmonics were well addressed as early as the 1800's. Comprehensive discussions on this topic can be found in Hobson[27], Byerly[28]. The ellipsoidal harmonics are based on Lamé's functions. With a tri-axial ellipsoid as the reference surface, ellipsoidal harmonics are analogous to spherical harmonics in formulation, and come with similar properties. Most desirably, it will be shown that the ellipsoidal harmonics are convergent outside the reference ellipsoid, therefore expected to have greater convergence region than spherical harmonics near the attracting body. On the other hand, the computational complexity of ellipsoidal harmonics far exceeds that of spherical harmonics, largely due to the

lack of recurrence relation for the Lamé's functions, and the fact that the theoretical form of the ellipsoidal harmonics can be numerically unstable. We will review and apply a numerical scheme presented by Garmier and Barriot[29] for gravitational field modeling via the ellipsoidal harmonics. Certain frequently encountered numerical issues such as singularities, loss of significant digits, and etc., will be investigated. Some complementary notes and formulae will be provided for handling the singularities, especially for computing the higher-order derivatives of the ellipsoidal harmonics.

The application is to model the gravitational field of the Martian moon Phobos and the asteroid 433 Eros. The performance of the spherical and ellipsoidal harmonic models will be compared. Eros is an archetype of the non-spherical, irregularly shaped bodies, and the motivation to exploit the ellipsoidal harmonics in prior works[30,31]. The limitation of spherical harmonic model can be fully revealed for these bodies. On the other hand, Phobos is less remarkable as an irregular-shaped body. We recall several gravitational field models developed so far for Phobos[13,15,32,33], and note that an ellipsoidal harmonic model has yet to be presented. A goal of this work is then to apply ellipsoidal harmonics to model the field of Phobos. Moreover, with its distinct but still moderate non-sphericity among the irregular bodies, We deem Phobos to be a supplementary case for model comparison. For example, whether the ellipsoidal and spherical harmonics tend to concur for less non-spherical bodies, and how their performance varies for different shapes of the body, and etc.

The contents of this thesis are organized as follows: in chapter 2, we shall only briefly introduce the background of gravitational field modeling based on spherical harmonics, as the subject can be easily found in a great many reference. In chapter 3, we will revisit the theory of ellipsoidal harmonics based on Hobson's discussions with some explanatory notes. The computation of the ellipsoidal harmonics will be discussed in chapter 4, based on the numerical method by Garmier. In chapter 5, we will provide simulation results of comparing the performance of the ellipsoidal and spherical harmonics for modeling the gravitational field of Phobos and 433 Eros,

both assumed to have constant density. Finally, concluding discussions will be presented in chapter 6.

Chapter 2: Background of Gravitational Field Modeling

2.1 Gravitational potential, acceleration and gradient

The gravitational potential V of a point mass M at a certain exterior point in space can be expressed as[34]

$$V = \frac{GM}{r} \tag{2.1}$$

where G is the Newton's gravitational constant, r the distance from M to the given point. If we adopt a rectangular coordinate system of x,y,z, r can be expressed as

$$r = \left((x-x_0)^2 + (y-y_0)^2 + (z-z_0)^2\right)^{\frac{1}{2}}$$

Here $(x\ y\ z)^T$ is the vectorized position of the given point, and $(x_0\ y_0\ z_0)^T$ that of the point mass. The gravitational acceleration at x,y,z is obtained by taking the gradient of (2.1) such as

$$\begin{aligned} \mathbf{a} = \nabla V &= \begin{pmatrix} \frac{\partial V}{\partial x} & \frac{\partial V}{\partial y} & \frac{\partial V}{\partial z} \end{pmatrix}^T \\ &= \begin{pmatrix} -\frac{GM}{r^3}(x-x_0) & -\frac{GM}{r^3}(y-y_0) & -\frac{GM}{r^3}(z-z_0) \end{pmatrix}^T \end{aligned} \tag{2.2}$$

Taking the second order derivative of the three components of **a** with respect to x,y,z yields

$$\begin{aligned} \mathbf{\Gamma} = \nabla \mathbf{a} &= \begin{pmatrix} \frac{\partial^2 V}{\partial x^2} & \frac{\partial^2 V}{\partial x \partial y} & \frac{\partial^2 V}{\partial x \partial z} \\ \frac{\partial^2 V}{\partial y \partial x} & \frac{\partial^2 V}{\partial y^2} & \frac{\partial^2 V}{\partial y \partial z} \\ \frac{\partial^2 V}{\partial z \partial x} & \frac{\partial^2 V}{\partial z \partial y} & \frac{\partial^2 V}{\partial z^2} \end{pmatrix} = \begin{pmatrix} \Gamma_{xx} & \Gamma_{xy} & \Gamma_{xz} \\ \Gamma_{yx} & \Gamma_{yy} & \Gamma_{yz} \\ \Gamma_{zx} & \Gamma_{zy} & \Gamma_{zz} \end{pmatrix} \\ &= \frac{GM}{r^5} \begin{pmatrix} 3(x-x_0)^2 - r^2 & 3(x-x_0)(y-y_0) & 3(x-x_0)(z-z_0) \\ 3(y-y_0)(x-x_0) & 3(y-y_0)^2 - r^2 & 3(y-y_0)(z-z_0) \\ 3(z-z_0)(x-x_0) & 3(z-z_0)(y-y_0) & 3(z-z_0)^2 - r^2 \end{pmatrix} \end{aligned} \tag{2.3}$$

$\mathbf{\Gamma}$ is known as the gravitational gradient matrix. Here we define explicitly that for

∇ acting on column vector such as **a**, the result is a matrix such as

$$\nabla \mathbf{a} = \begin{pmatrix} \nabla a_x & \nabla a_y & \nabla a_z \end{pmatrix}^T = \begin{pmatrix} \frac{\partial a_x}{\partial x} & \frac{\partial a_x}{\partial y} & \frac{\partial a_x}{\partial z} \\ \frac{\partial a_y}{\partial x} & \frac{\partial a_y}{\partial y} & \frac{\partial a_y}{\partial z} \\ \frac{\partial a_z}{\partial x} & \frac{\partial a_z}{\partial y} & \frac{\partial a_z}{\partial z} \end{pmatrix} \tag{2.4}$$

We note that[35]

$$\begin{aligned} &\Gamma_{xx} + \Gamma_{yy} + \Gamma_{zz} = 0, \\ &\Gamma_{xy} = \Gamma_{yx}, \Gamma_{yz} = \Gamma_{zy,} \Gamma_{zx} = \Gamma_{xz} \end{aligned} \tag{2.5}$$

If mass *M* is not a point but an attracting body that occupies a certain volume, (2.1) needs to be modified as follows,

$$V = \int_M \frac{G}{r} dM = \iiint_v \frac{G\rho}{r} dv \tag{2.6}$$

in which case *M* is decomposed into various point mass *dM* occupying infinitesimal volume *dv* with density ρ, the potential at the given point is then integrated over the entire body (Figure 2.1). Likewise, the expressions for **a** and $\mathbf{\Gamma}$ based on (2.2) and (2.3) would both involve volume integrals. However, though we obtained (2.5) assuming that *M* is a point mass, this relation also holds for *M* that occupies a certain volume[35]. We note that, to be able to apply (2.6), we must know the mass or density distribution of the attracting body.

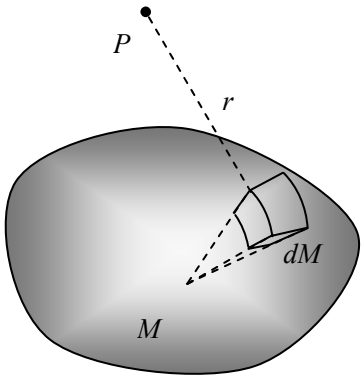

Figure 2.1 Decomposition of *M* into infinitesimal mass elements

2.2 Laplace's equation in relation to gravitational potential

The gravitational potential in the free space must satisfy the Laplace's equation[34],

$$\Delta V = 0 \tag{2.7}$$

The Laplacian operator Δ, in some orthogonal coordinate system of ξ_1, ξ_2, ξ_3 can be expressed as

$$\Delta = \frac{1}{h_1 h_2 h_3}\left[\frac{\partial}{\partial \xi_1}\left(\frac{h_2 h_3}{h_1}\frac{\partial}{\partial \xi_1}\right)+\frac{\partial}{\partial \xi_2}\left(\frac{h_3 h_1}{h_2}\frac{\partial}{\partial \xi_2}\right)+\frac{\partial}{\partial \xi_3}\left(\frac{h_1 h_2}{h_3}\frac{\partial}{\partial \xi_3}\right)\right] \tag{2.8}$$

where h_i is the distance scale along ξ_i, with i = 1,2,3. In the rectangular coordinates (2.8) simply becomes

$$\Delta = \frac{\partial^2}{\partial x^2}+\frac{\partial^2}{\partial y^2}+\frac{\partial^2}{\partial z^2} \tag{2.9}$$

Of particular interest is expressing (2.8) in the spherical coordinates of radius r, latitude φ and longitude λ (Figure 2.2), for which the distance scales are

$$h_r = 1,\ h_\varphi = r,\ h_\lambda = r\cos\varphi \tag{2.10}$$

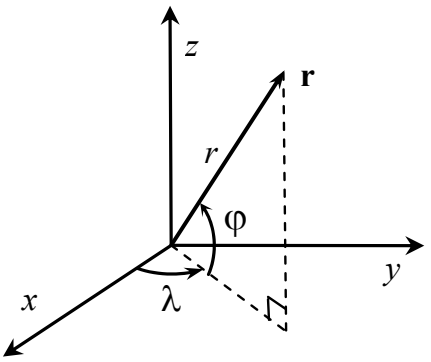

Figure 2.2 Spherical coordinates in relation to rectangular coordinates

Eq. (2.8) then becomes

$$\Delta = \frac{\partial^2 V}{\partial r^2}+\frac{2}{r}\frac{\partial V}{\partial r}+\frac{1}{r^2}\frac{\partial^2 V}{\partial \varphi^2}-\frac{\tan\varphi}{r^2}\frac{\partial V}{\partial \varphi}+\frac{1}{r^2\cos^2\varphi}\frac{\partial^2 V}{\partial \lambda^2} \tag{2.11}$$

(2.11) can be solved via separation of variables to seek such a V that has the form

$$V = f(r)g(\varphi)h(\lambda) \tag{2.12}$$

The solution to be found is given by the spherical harmonic expansion series whose form is either

$$V = \sum_{n=0}^{\infty} r^n \sum_{m=0}^{n} P_n^m(\sin\varphi)\left(A_{nm}\cos m\lambda + B_{nm}\sin m\lambda\right) \tag{2.13-1}$$

or

$$V = \sum_{n=0}^{\infty} \frac{1}{r^{n+1}} \sum_{m=0}^{n} P_n^m(\sin\varphi)\left(A_{nm}\cos m\lambda + B_{nm}\sin m\lambda\right) \tag{2.13-2}$$

The integers n, m denote the degree and order of the series, respectively. P_n^m are the Legendre's functions if m=0, or associated Legendre's functions for $m\neq 0$, defined as

$$\begin{aligned} P_n^0(x) &= P_n(x) = \frac{1}{2^n n!}\frac{d^n}{dx^n}(x^2-1)^n, \\ P_n^m(x) &= (1-x^2)^{\frac{m}{2}}\frac{d^m P_n(x)}{dx^m} \end{aligned} \tag{2.14}$$

A_{nm}, B_{nm} are the coefficients to be determined.

The exterior gravitational potential should vanish at infinity, i.e.,

$$\lim_{r\to\infty} V = 0 \tag{2.15}$$

Therefore (2.13-2) is a viable solution while (2.13-1) is not, since $V\to\infty$ as $r\to\infty$.

2.3 Spherical harmonic expansions

As was mentioned in the previous part, the spherical harmonic series (SHS) provide a form of solution to the Laplace's equation in spherical coordinates. There are several interesting properties associated with the SHS. Among them orthogonality is of great importance to us, and shall be briefly discussed in this part. First let us contract the notations of harmonic functions in (2.13-2) as

$$\begin{aligned} R_n^m(\varphi,\lambda) &= P_n^m(\sin\varphi)\cos m\lambda, \\ S_n^m(\varphi,\lambda) &= P_n^m(\sin\varphi)\sin m\lambda \end{aligned} \tag{2.16}$$

also known as the spherical surface harmonics. Then we have

$$\iint_{\sigma} R_n^m R_p^q d\sigma = 0,\ \iint_{\sigma} S_n^m S_p^q d\sigma = 0 \text{ , if } \ m \neq q \ \text{ or } \ n \neq p \tag{2.17}$$

Here the integration is over a unit sphere with surface area $\sigma = 4\pi$, centered at the origin of the coordinate system. And $d\sigma = h_\varphi h_\lambda d\varphi d\lambda = \cos\varphi d\varphi d\lambda$ for r=1. On the other hand, we have

$$\iint_{\sigma}\left(R_n^0\right)^2 d\sigma=\frac{4\pi}{2n+1},$$
$$\iint_{\sigma}\left(R_n^m\right)^2 d\sigma=\iint_{\sigma}\left(S_n^m\right)^2 d\sigma=\frac{2\pi}{2n+1}\frac{(n+m)!}{(n-m)!},\ \text{for } m\neq 0 \tag{2.18}$$

If we multiply V by R_n^m or S_n^m, and integrate the resulting product over a certain sphere of radius $r=r_0$ with $d\sigma=r_0^2\cos\varphi d\varphi d\lambda$, since r_0^2 being a constant can be dropped out we get

$$\iint_{\sigma}V(r_0,\varphi,\lambda)R_n^m d\sigma=\frac{A_{nm}}{r_0^{n+1}}\iint_{\sigma}\left(R_n^m\right)^2 d\sigma$$
$$\iint_{\sigma}V(r_0,\varphi,\lambda)S_n^m d\sigma=\frac{B_{nm}}{r_0^{n+1}}\iint_{\sigma}\left(S_n^m\right)^2 d\sigma \tag{2.19}$$

Hence (2.19) suggests a way of determining the coefficients A_{nm}, B_{nm}, given that V on such a sphere of r_0 is known. This leads to one kind of the boundary value problem known as Dirichlet's problem. We shall hereafter discuss a slight variant of the SHS and accordingly a different form of (2.19) for evaluating coefficients.

For the purpose of modeling the gravitational potential at an exterior point, it is often insightful to rewrite (2.13-2) as

$$V=\frac{GM}{r}\sum_{n=0}^{\infty}\left(\frac{R}{r}\right)^n\sum_{m=0}^{n}\left(C_{nm}R_n^m(\varphi,\lambda)+S_{nm}S_n^m(\varphi,\lambda)\right) \tag{2.20}$$

where R is the radius of some reference sphere and C_{nm}, S_{nm} are the new coefficients. C_{nm}, S_{nm} characterize the gravitational field, and they may be determined in the same manner as determining A_{nm}, B_{nm} via solving the Dirichlet's problem given that V on the reference sphere is known. Please note that $C_{0,0}=1, S_{n0}=0$.

The advantage of (2.20) is that now C_{nm}, S_{nm} are all (for different n and m) dimensionless quantities[36]. Furthermore, to prevent the values of C_{nm}, S_{nm} to vary too much for different n or m, the normalized spherical harmonics $\bar{R}_n^m, \bar{S}_n^m$ are favored for computations, in which case the integrals in (2.18) all become unity

$$\iint_{\sigma}\left(\bar{R}_n\right)^2 d\sigma=1,$$
$$\iint_{\sigma}\left(\bar{R}_n^m\right)^2 d\sigma=\iint_{\sigma}\left(\bar{S}_n^m\right)^2 d\sigma=1,\ \text{for } m\neq 0 \tag{2.21}$$

(2.20) can be expressed as

$$V = \frac{GM}{r}\sum_{n=0}^{\infty}\left(\frac{R}{r}\right)^n \sum_{m=0}^{n}\left(\bar{C}_{nm}\bar{R}_n^m(\varphi,\lambda) + \bar{S}_{nm}\bar{S}_n^m(\varphi,\lambda)\right) \tag{2.22}$$

with

$$\begin{aligned}
&\bar{R}_n^m = \bar{P}_n^m(\sin\varphi)\cos m\lambda,\ \ \bar{S}_n^m = \bar{P}_n^m(\sin\varphi)\sin m\lambda \\
&\bar{P}_n = N_n P_n,\ \ \bar{C}_{n0} = C_{n0}/N_n,\ \ N_n = (2n+1)^{1/2} \\
&\bar{P}_n^m = N_{nm}P_n^m,\ \left\langle \begin{matrix} \bar{C}_{nm} = C_{nm}/N_{nm} \\ \bar{S}_{nm} = S_{nm}/N_{nm} \end{matrix} \right\rangle,\ \ N_{nm} = \left(2(2n+1)\frac{(n+m)!}{(n-m)!}\right)^{1/2}
\end{aligned} \tag{2.23}$$

And $\bar{P}_n^m$ are the associated Legendre's functions normalized by the normalization constants N_{nm}.

So a practical form of (2.19) for us is as follows, applied on the sphere of radius R,

$$\begin{aligned}
\iint_{\sigma} V(R,\varphi,\lambda)\bar{R}_n^m(\varphi,\lambda)d\sigma &= \frac{GM}{R}\bar{C}_{nm} = \hat{C}_{nm} \\
\iint_{\sigma} V(R,\varphi,\lambda)\bar{S}_n^m(\varphi,\lambda)d\sigma &= \frac{GM}{R}\bar{S}_{nm} = \hat{S}_{nm}
\end{aligned} \tag{2.24}$$

In simulations GM may be assumed a known quantity, therefore we can obtain $\bar{C}_{nm}, \bar{S}_{nm}$ directly. However, in reality GM is usually not known beforehand, in this case we could always determine $\hat{C}_{0,0}$ first and then use

$$GM = \frac{\hat{C}_{0,0}R}{\bar{C}_{0,0}} = \hat{C}_{0,0}R \tag{2.25}$$

And other $\bar{C}_{nm}, \bar{S}_{nm}$ can be subsequently obtained based on (2.24).

Eq. (2.20) expresses the gravitational potential. The gravitational acceleration is the gradient of the potential. Using the SHS, the acceleration in the rectangular coordinates can be computed by

$$\mathbf{a}=\begin{pmatrix}a_x\\a_y\\a_z\end{pmatrix}=\nabla V=\begin{pmatrix}\frac{\partial r}{\partial x}&\frac{\partial \varphi}{\partial x}&\frac{\partial \lambda}{\partial x}\\\frac{\partial r}{\partial y}&\frac{\partial \varphi}{\partial y}&\frac{\partial \lambda}{\partial y}\\\frac{\partial r}{\partial z}&\frac{\partial \varphi}{\partial z}&\frac{\partial \lambda}{\partial z}\end{pmatrix}\begin{pmatrix}\frac{\partial V}{\partial r}\\\frac{\partial V}{\partial \varphi}\\\frac{\partial V}{\partial \lambda}\end{pmatrix}$$
$$=\begin{pmatrix}\cos\varphi\cos\lambda&-\sin\varphi\cos\lambda&-\sin\lambda\\\cos\varphi\sin\lambda&-\sin\varphi\sin\lambda&\cos\lambda\\\sin\varphi&\cos\varphi&0\end{pmatrix}\begin{pmatrix}\frac{\partial V}{\partial r}\\\frac{1}{h_\varphi}\frac{\partial V}{\partial \varphi}\\\frac{1}{h_\lambda}\frac{\partial V}{\partial \lambda}\end{pmatrix} \tag{2.26}$$

The gravitational gradient can be found in a similar fashion, and is of the form

$$\mathbf{\Gamma}=\nabla(\mathbf{a}^T)=\begin{pmatrix}\frac{\partial r}{\partial x}&\frac{\partial \varphi}{\partial x}&\frac{\partial \lambda}{\partial x}\\\frac{\partial r}{\partial y}&\frac{\partial \varphi}{\partial y}&\frac{\partial \lambda}{\partial y}\\\frac{\partial r}{\partial z}&\frac{\partial \varphi}{\partial z}&\frac{\partial \lambda}{\partial z}\end{pmatrix}\begin{pmatrix}\frac{\partial a_x}{\partial r}&\frac{\partial a_y}{\partial r}&\frac{\partial a_z}{\partial r}\\\frac{\partial a_x}{\partial \varphi}&\frac{\partial a_y}{\partial \varphi}&\frac{\partial a_z}{\partial \varphi}\\\frac{\partial a_x}{\partial \lambda}&\frac{\partial a_y}{\partial \lambda}&\frac{\partial a_z}{\partial \lambda}\end{pmatrix} \tag{2.27}$$

The expressions for elements in $\mathbf{\Gamma}$ are nevertheless complicated. Being of no further interest to us in the ensuing text, they are omitted here for the sake of brevity.

2.3.1 A condition of using spherical harmonics

It is important to note that (2.13-2) and (2.20) are both infinite series. It is easily understood that (2.20) is uniformly convergent outside reference sphere of radius *R*, i.e.,

$$\frac{R}{r}<1 \tag{2.28}$$

As $r\to R$ they will converge to the prescribed values of V on the reference sphere[27]. Inside the reference sphere the convergence is not unconditional[1]. In practice, we always truncate (2.20) at a certain degree. Using (2.20), we are not concerned with the divergence of the series (in the mathematical sense) so much as

[1] It can be shown that (2.13-2) and (2.20) are uniformly convergent outside the smallest bounding sphere of the body, known as the Brillouin sphere, which is not necessarily the reference sphere. However, we do not distinguish such difference as we will later investigate the convergence of the series numerically.

the errors that will be introduced due to the violation of (2.28). Quite obviously, the further inside the reference sphere, the larger R/r is, the larger errors are likely to be introduced. However, in order to distinguish such error as is caused by the divergence of the series from others, we will sometimes refer to it as divergence errors or simply divergence.

In principle, in order for (2.20) to accurately describe the gravitational potential outside the reference sphere, the entire attracting body should be inside the reference sphere, i.e., no mass is left outside.

2.4 Centrifugal effect

When it comes to describing the dynamics of particles in a rotating coordinate system, e.g., at the surface of the Earth, it is often more straightforward to introduce the gravity potential W, defined as

$$W = V + \Phi \tag{2.29}$$

V is the aforementioned gravitational potential and Φ the centrifugal potential. In the rectangular coordinate system fixed to the rotating body with the z-axis coincident with the axis of rotation, Φ can be expressed as

$$\Phi = \frac{1}{2}\omega^2 (x^2 + y^2) \tag{2.30}$$

where ω is the rotation rate. Taking the gradient of Φ yields the centrifugal acceleration such as

$$\mathbf{a}_\Phi = \nabla\Phi = \begin{pmatrix} \omega^2 x \\ \omega^2 y \\ 0 \end{pmatrix} \tag{2.31}$$

Then the gravity acceleration can be expressed by

$$\mathbf{g} = \nabla W = \mathbf{a} + \mathbf{a}_\Phi \tag{2.32}$$

The second order derivatives of centrifugal potential can be easily calculated as

$$\mathbf{G} = \begin{pmatrix} G_{xx} & G_{xy} & G_{xz} \\ G_{yx} & G_{yy} & G_{yz} \\ G_{zx} & G_{zy} & G_{zz} \end{pmatrix} = \mathbf{\Gamma} + \mathbf{\Gamma}_\Phi, \ \mathbf{\Gamma}_\Phi = \nabla\mathbf{a} = \begin{pmatrix} \omega^2 & 0 & 0 \\ 0 & \omega^2 & 0 \\ 0 & 0 & 0 \end{pmatrix} \tag{2.33}$$

Similar to (2.5), if we consider the centrifugal effects we have

$$G_{xx} + G_{yy} + G_{zz} = 2\omega^2,$$
$$G_{xy} = G_{yx}, G_{yz} = G_{zy,} G_{zx} = G_{xz} \tag{2.34}$$

Chapter 3: Ellipsoidal Harmonic Expansions

The spherical harmonics are solution to the Laplace's equation in the spherical coordinates. In this chapter, we will discuss another solution to the Laplace's equation, based on the ellipsoidal coordinates.

3.1 Ellipsoidal coordinates

The ellipsoidal coordinates can be found by solving the roots of the equation of λ^2

$$\frac{x^2}{\lambda^2}+\frac{y^2}{\lambda^2-h^2}+\frac{z^2}{\lambda^2-k^2}=1 \tag{3.1}$$

where x,y,z are the rectangular coordinates, and $h<k$ are two positive real constants. Rearranging (3.1), we have

$$\begin{aligned}&\left(\lambda^2\right)^3+a_2\left(\lambda^2\right)^2+a_1\lambda^2+a_0=0,\\&a_0=-x^2h^2k^2,\ a_1=x^2(h^2+k^2)+y^2k^2+z^2h^2+h^2k^2,\\&a_2=-(x^2+y^2+z^2+h^2+k^2),\end{aligned} \tag{3.2}$$

Therefore (3.1) is a cubic equation of λ^2. It can be shown that there are three distinct real roots for (3.2)[37], denote these roots as $\lambda_1^2,\ \lambda_2^2,\ \lambda_3^2$ that satisfy

$$\lambda_1^2\ge k^2,\quad k^2\ge\lambda_2^2\ge h^2,\quad h^2\ge\lambda_3^2\ge 0 \tag{3.3}$$

Then (3.1) can be expressed as

$$\frac{x^2}{\lambda_1^2}+\frac{y^2}{\lambda_1^2-h^2}+\frac{z^2}{\lambda_1^2-k^2}=1, \tag{3.4-1}$$

$$\frac{x^2}{\lambda_2^2}+\frac{y^2}{\lambda_2^2-h^2}-\frac{z^2}{k^2-\lambda_2^2}=1, \tag{3.4-2}$$

$$\frac{x^2}{\lambda_3^2}-\frac{y^2}{h^2-\lambda_3^2}-\frac{z^2}{k^2-\lambda_3^2}=1. \tag{3.4-3}$$

which represent an ellipsoid, a one-sheet hyperboloid and a two-sheet hyperboloid, respectively (Figure 3.1). Particularly, for the ellipsoid with three semi-axes, $a > b >$

c, we have

$$k = \sqrt{a^2 - c^2}, \quad h = \sqrt{a^2 - b^2} \tag{3.5}$$

thus k and h are the focal lengths.

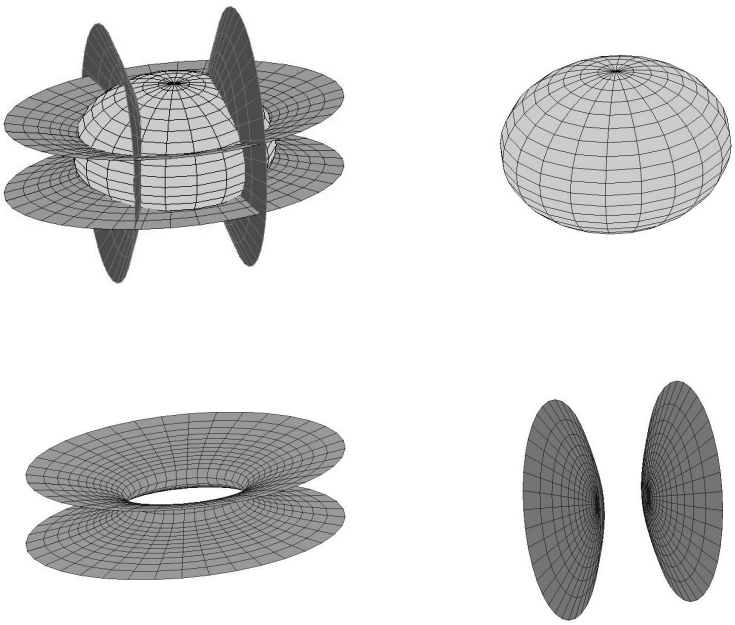

Figure 3.1 The three orthogonal surfaces that correspond to the fixed ellipsoidal coordinates. Upper-right: ellipsoid; lower-left: one-sheet hyperboloid; lower-right: two-sheet hyperboloid.

The solution of (3.4) can be found by the following expressions,

$$\begin{aligned} \lambda_1^2 &= 2Q\cos\frac{\theta}{3} - \frac{a_2}{3}, \\ \lambda_2^2 &= 2Q\cos\frac{\theta + 4\pi}{3} - \frac{a_2}{3}, \\ \lambda_3^2 &= 2Q\cos\frac{\theta + 2\pi}{3} - \frac{a_2}{3} \end{aligned} \tag{3.6}$$

where

$$\cos\theta = \frac{R}{Q^3},\ Q = \sqrt{\frac{-p}{3}},\ R = -\frac{q}{2},$$
$$p = \frac{3a_1 - a_2^2}{3},\ q = \frac{2a_2^3 - 9a_2a_1 + 27a_0}{27} \tag{3.7}$$

Note that the coefficients a_0,a_1,a_2 come from (3.2). So that (3.6), (3.7) in conjunction with (3.2) give the expressions of transformation from the rectangular to ellipsoidal coordinates.

The numerical results by (3.6) and (3.7) via trigonometric expressions may not be accurate enough and need to be refined. We could always take such results as initial values and use numerical schemes such as the Newton-Raphson method to obtain more accurate results.

To prevent subscripts cluttering the notations, we shall also denote the three ellipsoidal coordinates as follows

$$\rho = \lambda_1,\ \mu = \lambda_2,\ \upsilon = \lambda_3 \tag{3.8}$$

And throughout this text we shall use both notations interchangeably unless stated otherwise. Moreover, hereafter we shall reserve $\lambda_j,\ j = 1,2,3$ with or without the subscript j for the ellipsoidal coordinates, rather than for the longitude of spherical coordinates.

On the other hand, the transformation from the ellipsoidal to rectangular coordinates can be expressed by

$$x^2 = \frac{\rho^2\mu^2\upsilon^2}{h^2k^2} \tag{3.9-1}$$

$$y^2 = \frac{\left(\rho^2 - h^2\right)\left(\mu^2 - h^2\right)\left(h^2 - \upsilon^2\right)}{h^2\left(k^2 - h^2\right)} \tag{3.9-2}$$

$$z^2 = \frac{\left(\rho^2 - k^2\right)\left(k^2 - \mu^2\right)\left(k^2 - \upsilon^2\right)}{k^2\left(k^2 - h^2\right)} \tag{3.9-3}$$

We can easily verify that the three surfaces of (3.4) are orthogonal to one another. For example, consider the normal vectors to surfaces expressed by (3.4-1) and (3.4-2)

$$\mathbf{n}_1 = \left(\frac{x}{\rho^2} \quad \frac{y}{\rho^2 - h^2} \quad \frac{z}{\rho^2 - k^2}\right)^T \tag{3.10-1}$$

$$\mathbf{n}_2 = \begin{pmatrix} \dfrac{x}{\mu^2} & \dfrac{y}{\mu^2 - h^2} & -\dfrac{z}{k^2 - \mu^2} \end{pmatrix}^T \tag{3.10-2}$$

Taking the product of $\mathbf{n}_1$ and $\mathbf{n}_2$ yields

$$\mathbf{n}_1 \cdot \mathbf{n}_2 = \frac{x^2}{\rho^2 \mu^2} + \frac{y^2}{\left(\rho^2 - h^2\right)\left(\mu^2 - h^2\right)} - \frac{z^2}{\left(\rho^2 - k^2\right)\left(k^2 - \mu^2\right)} \tag{3.11}$$

Substituting equations (3.9) into the above expression,

$$\begin{aligned} \mathbf{n}_1 \cdot \mathbf{n}_2 &= \frac{\upsilon^2}{h^2 k^2} + \frac{\left(h^2 - \upsilon^2\right)}{h^2\left(k^2 - h^2\right)} - \frac{\left(k^2 - \upsilon^2\right)}{k^2\left(k^2 - h^2\right)} \\ &= \frac{\upsilon^2\left(k^2 - h^2\right) + k^2\left(h^2 - \upsilon^2\right) - h^2\left(k^2 - \upsilon^2\right)}{h^2 k^2\left(k^2 - h^2\right)} = 0 \end{aligned} \tag{3.12}$$

Other two orthogonal relations can be shown in a similar manner.

It is noted that in (3.9) the correspondence between the ellipsoidal and rectangular coordinates are not one-to-one because of the squares. For the time being we ignore the sign ambiguity and consider,

$$\begin{aligned} &x = \frac{\rho\mu\upsilon}{hk}, \quad y = \frac{\sqrt{\rho^2 - h^2}\sqrt{\mu^2 - h^2}\sqrt{h^2 - \upsilon^2}}{h\sqrt{k^2 - h^2}}, \\ &z = \frac{\sqrt{\rho^2 - k^2}\sqrt{k^2 - \mu^2}\sqrt{k^2 - \upsilon^2}}{k\sqrt{k^2 - h^2}} \end{aligned} \tag{3.13}$$

and introduce the following entities

$$\begin{aligned} &\frac{\mu\upsilon}{hk} = \sin\phi, \quad \frac{\sqrt{\mu^2 - h^2}\sqrt{h^2 - \upsilon^2}}{h\sqrt{k^2 - h^2}} = \cos\phi\cos\gamma, \\ &\frac{\sqrt{k^2 - \mu^2}\sqrt{k^2 - \upsilon^2}}{k\sqrt{k^2 - h^2}} = \cos\phi\sin\gamma \end{aligned} \tag{3.14}$$

ϕ, γ are as illustrated in Figure 3.2. We noted that

$$\begin{aligned} &x = \rho\sin\phi, \quad y = \sqrt{\rho^2 - h^2}\cos\phi\cos\gamma, \\ &z = \sqrt{\rho^2 - k^2}\cos\phi\sin\gamma \end{aligned} \tag{3.15}$$

Therefore (3.15) further illustrates the meaning of h and k as two focal lengths for the ellipsoid with semi-major axis ρ.

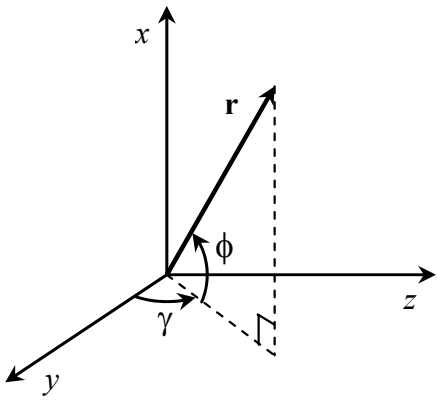

Figure 3.2 Spherical coordinates based on ϕ, γ

Taking the total derivatives of (3.9) with respect to the ellipsoidal coordinates we have

$$
\begin{aligned}
dx &= \frac{\mu\upsilon}{hk}d\rho + \frac{\rho\upsilon}{hk}d\mu + \frac{\rho\mu}{hk}d\upsilon \\
dy &= \frac{\rho\sqrt{\mu^2-h^2}\sqrt{h^2-\upsilon^2}}{h\sqrt{k^2-h^2}\sqrt{\rho^2-h^2}}d\rho + \frac{\mu\sqrt{\rho^2-h^2}\sqrt{h^2-\upsilon^2}}{h\sqrt{k^2-h^2}\sqrt{\mu^2-h^2}}d\mu \\
&\quad - \frac{\upsilon\sqrt{\rho^2-h^2}\sqrt{\mu^2-h^2}}{h\sqrt{k^2-h^2}\sqrt{h^2-\upsilon^2}}d\upsilon \\
dz &= \frac{\rho\sqrt{k^2-\mu^2}\sqrt{k^2-\upsilon^2}}{k\sqrt{k^2-h^2}\sqrt{\rho^2-k^2}}d\rho - \frac{\mu\sqrt{\rho^2-k^2}\sqrt{k^2-\upsilon^2}}{k\sqrt{k^2-h^2}\sqrt{k^2-\mu^2}}d\mu \\
&\quad - \frac{\upsilon\sqrt{\rho^2-k^2}\sqrt{k^2-\mu^2}}{k\sqrt{k^2-h^2}\sqrt{k^2-\upsilon^2}}d\upsilon
\end{aligned}
\tag{3.16}
$$

Thus the infinitesimal distance is related to the differential increments in ellipsoidal coordinates via

$$
\begin{aligned}
dl^2 &= dx^2 + dy^2 + dz^2 \\
&= \left[\frac{\mu^2\upsilon^2}{h^2k^2} + \frac{\rho^2\left(\mu^2-h^2\right)\left(h^2-\upsilon^2\right)}{h^2\left(k^2-h^2\right)\left(\rho^2-h^2\right)} + \frac{\rho^2\left(k^2-\mu^2\right)\left(k^2-\upsilon^2\right)}{k^2\left(k^2-h^2\right)\left(\rho^2-k^2\right)}\right]d\rho^2 + \\
&\left[\frac{\rho^2\upsilon^2}{h^2k^2} + \frac{\mu^2\left(\rho^2-h^2\right)\left(h^2-\upsilon^2\right)}{h^2\left(k^2-h^2\right)\left(\mu^2-h^2\right)} + \frac{\mu^2\left(\rho^2-k^2\right)\left(k^2-\upsilon^2\right)}{k^2\left(k^2-h^2\right)\left(k^2-\mu^2\right)}\right]d\mu^2 + \\
&\left[\frac{\rho^2\mu^2}{h^2k^2} + \frac{\upsilon^2\left(\rho^2-h^2\right)\left(\mu^2-h^2\right)}{h^2\left(k^2-h^2\right)\left(h^2-\upsilon^2\right)} + \frac{\upsilon^2\left(\rho^2-k^2\right)\left(k^2-\mu^2\right)}{k^2\left(k^2-h^2\right)\left(k^2-\upsilon^2\right)}\right]d\upsilon^2 \qquad (3.17) \\
&= \frac{\left(\rho^2-\mu^2\right)\left(\rho^2-\upsilon^2\right)}{\left(\rho^2-k^2\right)\left(\rho^2-h^2\right)}d\rho^2 + \frac{\left(\rho^2-\mu^2\right)\left(\mu^2-\upsilon^2\right)}{\left(k^2-\mu^2\right)\left(\mu^2-h^2\right)}d\mu^2 + \\
&\frac{\left(\rho^2-v^2\right)\left(\mu^2-\upsilon^2\right)}{\left(h^2-\upsilon^2\right)\left(k^2-\upsilon^2\right)}d\upsilon^2
\end{aligned}
$$

It follows that the distance scales for ρ, μ and υ are

$$
h_\rho = \frac{\sqrt{\rho^2-\mu^2}\sqrt{\rho^2-\upsilon^2}}{\sqrt{\rho^2-k^2}\sqrt{\rho^2-h^2}},\quad h_\mu = \frac{\sqrt{\rho^2-\mu^2}\sqrt{\mu^2-\upsilon^2}}{\sqrt{k^2-\mu^2}\sqrt{\mu^2-h^2}},
$$

$$
h_\upsilon = \frac{\sqrt{\rho^2-\upsilon^2}\sqrt{\mu^2-\upsilon^2}}{\sqrt{h^2-\upsilon^2}\sqrt{k^2-\upsilon^2}} \qquad (3.18)
$$

3.2 Ellipsoidal harmonics

To introduce the ellipsoidal harmonics, it is helpful to first look at the Laplace's equation in the sphero-conal coordinates r,μ,υ which are related to the rectangular coordinates via[27]

$$
\begin{aligned}
x^2 &= \frac{r^2\mu^2\upsilon^2}{h^2k^2},\quad y^2 = \frac{r^2(\mu^2-h^2)(h^2-\upsilon^2)}{h^2(k^2-h^2)}, \\
z^2 &= \frac{r^2(k^2-\mu^2)(k^2-\upsilon^2)}{k^2(k^2-h^2)}
\end{aligned} \qquad (3.19)
$$

It can be verified that the sphero-conal coordinates are also orthogonal, and the distance scales are given by

$$
h_r = 1,\quad h_\mu = \frac{r\sqrt{\mu^2-\upsilon^2}}{\sqrt{k^2-\mu^2}\sqrt{\mu^2-h^2}},\quad h_\upsilon = \frac{r\sqrt{\mu^2-\upsilon^2}}{\sqrt{h^2-\upsilon^2}\sqrt{k^2-\upsilon^2}} \qquad (3.20)
$$

The Laplace's equation is, substituting the above expressions into (2.8),

$$\begin{aligned}&\left(\mu^2-\upsilon^2\right)\frac{\partial}{\partial r}\left(r^2\frac{\partial V}{\partial r}\right)+\\&\sqrt{\mu^2-h^2}\sqrt{k^2-\mu^2}\,\frac{\partial}{\partial\mu}\left(\sqrt{\mu^2-h^2}\sqrt{k^2-\mu^2}\,\frac{\partial V}{\partial\mu}\right)+\\&\sqrt{h^2-\upsilon^2}\sqrt{k^2-\upsilon^2}\,\frac{\partial}{\partial\upsilon}\left(\sqrt{h^2-\upsilon^2}\sqrt{k^2-\upsilon^2}\,\frac{\partial V}{\partial\upsilon}\right)=0\end{aligned}\tag{3.21}$$

If we introduce the following two intermediate variables

$$\eta=\int_h^{\mu}\frac{dt}{\sqrt{t^2-h^2}\sqrt{k^2-t^2}},\tag{3.22-1}$$

$$\zeta=\int_0^{\upsilon}\frac{dt}{\sqrt{h^2-t^2}\sqrt{k^2-t^2}}\tag{3.22-2}$$

Then (3.21) can be written as

$$\left(\mu^2-\upsilon^2\right)\frac{\partial}{\partial r}\left(r^2\frac{\partial V}{\partial r}\right)+\frac{\partial^2 V}{\partial\eta^2}+\frac{\partial^2 V}{\partial\zeta^2}=0\tag{3.23}$$

Assume that $V=r^n u(\eta,\zeta)$, then (3.23) becomes

$$\left(\mu^2-\upsilon^2\right)n(n+1)u+\frac{\partial^2 V}{\partial\eta^2}+\frac{\partial^2 V}{\partial\zeta^2}=0\tag{3.24}$$

Further assume that *u* has the form of $E(\mu)E(\upsilon)$, and substitute this expression into (3.24), we get

$$\left(\mu^2-\upsilon^2\right)n(n+1)E(\mu)E(\upsilon)+\frac{d^2E(\mu)}{d\eta^2}E(\upsilon)+\frac{d^2E(\upsilon)}{d\zeta^2}E(\mu)=0\tag{3.25}$$

And we must have

$$\begin{aligned}&\left[\frac{d^2E(\mu)}{d\eta^2}+\mu^2n(n+1)E(\mu)\right]E(\upsilon)\\&+\left[\frac{d^2E(\upsilon)}{d\zeta^2}-\upsilon^2n(n+1)E(\upsilon)\right]E(\mu)=0\end{aligned}\tag{3.26}$$

Particularly, for some constant *p*, the above equation can be manipulated as follows,

$$\begin{aligned}&\left[\frac{d^2E(\mu)}{d\eta^2}+\mu^2n(n+1)E(\mu)-pE(\mu)\right]E(\upsilon)+\\&\left[\frac{d^2E(\upsilon)}{d\zeta^2}-\upsilon^2n(n+1)E(\upsilon)+pE(\upsilon)\right]E(\mu)=0\end{aligned}\tag{3.27}$$

Therefore, the expressions in the two brackets satisfy

$$\frac{d^2E(\mu)}{d\eta^2} + \mu^2 n(n+1)E(\mu) - pE(\mu) = 0 \tag{3.28-1}$$

$$\frac{d^2E(\upsilon)}{d\zeta^2} - \upsilon^2 n(n+1)E(\upsilon) + pE(\upsilon) = 0 \tag{3.28-2}$$

Upon substituting (3.22-1) into (3.28-1), we get

$$\begin{aligned}&\left(\mu^2 - k^2\right)\left(\mu^2 - h^2\right)\frac{d^2E(\mu)}{d\mu^2} + \mu(2\mu^2 - h^2 - k^2)\frac{dE(\mu)}{d\mu} + \\ &\left[p(h^2 + k^2) - n(n+1)\mu^2\right]E(\mu) = 0\end{aligned} \tag{3.29}$$

And for υ we would get an expression of the exact same form as (3.29).

Now we consider the Laplace's equation for the ellipsoidal coordinates. Substituting (3.18) into (2.8) yields

$$\begin{aligned}&\left(\mu^2 - \upsilon^2\right)\sqrt{\rho^2 - k^2}\sqrt{\rho^2 - h^2}\,\frac{\partial}{\partial\rho}\left(\sqrt{\rho^2 - k^2}\sqrt{\rho^2 - h^2}\,\frac{\partial V}{\partial\rho}\right) + \\ &\left(\rho^2 - \upsilon^2\right)\sqrt{k^2 - \mu^2}\sqrt{\mu^2 - h^2}\,\frac{\partial}{\partial\mu}\left(\sqrt{k^2 - \mu^2}\sqrt{\mu^2 - h^2}\,\frac{\partial V}{\partial\mu}\right) + \\ &\left(\rho^2 - \mu^2\right)\sqrt{k^2 - \upsilon^2}\sqrt{h^2 - \upsilon^2}\,\frac{\partial}{\partial v}\left(\sqrt{k^2 - \upsilon^2}\sqrt{h^2 - \upsilon^2}\,\frac{\partial V}{\partial\upsilon}\right) = 0\end{aligned} \tag{3.30}$$

Again refer to (3.22) but introduce another intermediate variable

$$\xi = \int_k^\rho \frac{dt}{\sqrt{t^2 - h^2}\sqrt{t^2 - k^2}} \tag{3.31}$$

The Laplace's equation then becomes

$$\left(\mu^2 - \upsilon^2\right)\frac{\partial^2 V}{\partial\xi^2} + \left(\rho^2 - \upsilon^2\right)\frac{\partial^2 V}{\partial\eta^2} + \left(\rho^2 - \mu^2\right)\frac{\partial^2 V}{\partial\zeta^2} = 0 \tag{3.32}$$

This time we assume

$$V = \sum cE(\rho)E(\mu)E(\upsilon) \tag{3.33}$$

where c is some constant. Substitute (3.28) in (3.32) for $E(\mu)$ and $E(\upsilon)$, we find that

$$\frac{d^2E(\rho)}{d\xi^2} - \rho^2 n(n+1)E(\rho) + pE(\rho) = 0 \tag{3.34}$$

And furthermore, we see that

$$\left(\rho^2-k^2\right)\left(\rho^2-h^2\right)\frac{d^2E(\rho)}{d\rho^2}+\rho(2\rho^2-h^2-k^2)\frac{dE(\rho)}{d\rho}+$$
$$\left[p(h^2+k^2)-n(n+1)\rho^2\right]E(\rho)=0 \tag{3.35}$$

Therefore $E(\rho), E(\mu), E(\upsilon)$ satisfy the differential equation of the same form. However, ρ,μ,υ each has different ranges of values as given by (3.3).

3.2.1 Lamé's functions

We see that the solution to the Laplace's equation in the ellipsoidal coordinates is of the form $E(\rho)E(\mu)E(\upsilon)$. Moreover, $E(\lambda_j)$, $j=1,2,3$ satisfies the second order differential equation of (3.29) for all three ellipsoidal coordinates. In this part we discuss the form of $E(\lambda_j)$.

Referring back to the SHS, (2.13-1) suggests spherical harmonics are of the form $r^n P_n^m(\sin\phi)\cos m\gamma$ or $r^n P_n^m(\sin\phi)\sin m\gamma$. Note that we have substituted ϕ,γ for the original spherical coordinates φ,λ in (2.13-1). The associated Legendre's functions can be expressed as[36]

$$P_n^m(\sin\phi)=\cos^m\phi\sum_{j=0}^{s}\alpha_{n,m,j}\sin^{n-m-2j}\phi,\quad s=\left\lfloor\frac{n-m}{2}\right\rfloor \tag{3.36}$$

where $\alpha_{n,m,j}$ is constant, and '$\lfloor\bullet\rfloor$' means that the result is rounded down to the nearest integer. On the other hand,

$$\cos m\gamma=\mathrm{Re}(e^{\mathrm{i}m\gamma})=\mathrm{Re}\left((\cos\gamma+\mathrm{i}\sin\gamma)^m\right) \tag{3.37}$$

and

$$(\cos\gamma+\mathrm{i}\sin\gamma)^m=\sum_{l=0}^{m}\mathrm{i}^{m-l}\binom{m}{l}\cos^l\gamma\sin^{m-l}\gamma \tag{3.38}$$

where the binomial coefficient is given by

$$\binom{m}{l}=\frac{m!}{l!(m-l)!} \tag{3.39}$$

Taking the real part of the $(\cos\gamma+\mathrm{i}\sin\gamma)^m$ forces terms associated with i^{m-l} when m-l is odd number to vanish. Therefore we need to distinguish between the even and odd values of m for $\sin m\gamma$ and $\cos m\gamma$.

If m is even, i.e., $m = 2l, l = 0,1,\cdots,\left\lfloor \frac{n}{2} \right\rfloor$

$$\cos m\gamma = \sum_{i=0}^{l} (-1)^{l-i} \binom{m}{2i} \cos^{2i}\gamma \sin^{m-2i}\gamma \tag{3.40}$$

Therefore

$$\begin{aligned} & P_n^m(\sin\phi)\cos m\gamma \\ &= \left(\cos^m\phi \sum_{j=0}^{s} \alpha_{n,m,j} \sin^{n-m-2j}\phi \right) \cdot \sum_{i=0}^{l} (-1)^{l-i} \binom{m}{2i} \cos^{2i}\gamma \sin^{m-2i}\gamma \\ &= \left(\sum_{j=0}^{s} \alpha_{n,m,j} \sin^{n-m-2j}\phi \right) \cdot \sum_{i=0}^{l} (-1)^{l-i} \binom{m}{2i} \left(\cos^{2i}\phi\cos^{2i}\gamma\right)\left(\cos^{m-2i}\phi\sin^{m-2i}\gamma\right) \end{aligned} \tag{3.41}$$

Referring to (3.14), we see that

$$\begin{aligned} & P_n^m(\sin\phi)\cos m\gamma \\ &= \left(\sum_{j=0}^{s} \alpha_{n,m,j} \left(\frac{\mu\upsilon}{hk} \right)^{n-m-2j} \right) \cdot \\ & \sum_{i=0}^{l} (-1)^{l-i} \binom{m}{2i} \left(\frac{\sqrt{\mu^2-h^2}\sqrt{h^2-\upsilon^2}}{h\sqrt{k^2-h^2}} \right)^{2i} \left(\frac{\sqrt{k^2-\mu^2}\sqrt{k^2-\upsilon^2}}{k\sqrt{k^2-h^2}} \right)^{m-2i} \end{aligned} \tag{3.42}$$

Remembering that m is even, the above expression will be of the following form

$$\begin{aligned} & P_n^m(\sin\phi)\cos m\gamma = \\ & \left(a_0\mu^n + a_1\mu^{n-2} + \cdots a_r\mu^{n-2r}\right)\left(a_0\upsilon^n + a_1\upsilon^{n-2} + \cdots a_r\upsilon^{n-2r}\right),\ r = \left\lfloor \frac{n}{2} \right\rfloor \end{aligned} \tag{3.43}$$

where a_i, i=1,2,…,r are constants. The scale of the expression is arbitrary.

On the other hand, if m is odd, i.e., $m = 2l+1, l = 0,1,\cdots,\left\lfloor \frac{n-1}{2} \right\rfloor$

$$\cos m\gamma = \sum_{i=0}^{l} (-1)^{l-i} \binom{m}{2i+1} \cos^{2i+1}\gamma \sin^{m-2i-1}\gamma \tag{3.44}$$

Then

$$
\begin{aligned}
&P_n^m(\sin\phi)\cos m\gamma \\
&=\left(\sum_{j=0}^{s}\alpha_{n,m,j}\sin^{n-m-2j}\phi\right)\cdot\sum_{i=0}^{l}(-1)^{l-i}\binom{m}{2i+1}\left(\cos\phi\cos\gamma\right)^{2i+1}\left(\cos\phi\sin\gamma\right)^{m-2i-1} \\
&=\left(\sum_{j=0}^{s}\alpha_{n,m,j}\left(\frac{\mu\upsilon}{hk}\right)^{n-m-2j}\right)\cdot \\
&\sum_{i=0}^{l}(-1)^{l-i}\binom{m}{2i+1}\left(\frac{\sqrt{\mu^2-h^2}\sqrt{h^2-\upsilon^2}}{h\sqrt{k^2-h^2}}\right)^{2i+1}\left(\frac{\sqrt{k^2-\mu^2}\sqrt{k^2-\upsilon^2}}{k\sqrt{k^2-h^2}}\right)^{m-2i-1}
\end{aligned}
\tag{3.45}
$$

For odd m, m-2i-1 is even but 2i+1 is odd in the above expression, it follows that $P_n^m(\sin\phi)\cos m\gamma$ for odd m is of the following form

$$
\begin{aligned}
P_n^m(\sin\phi)\cos m\gamma=\sqrt{\mu^2-h^2}\left(a_0\mu^{n-1}+a_1\mu^{n-3}+\cdots a_r\mu^{n-2r-1}\right)\cdot \\
\sqrt{h^2-\upsilon^2}\left(a_0\upsilon^{n-1}+a_1\upsilon^{n-3}+\cdots a_r\upsilon^{n-2r-1}\right),
\end{aligned}
\tag{3.46}
$$

with $r=\left\lfloor\frac{n-1}{2}\right\rfloor$. In the similar fashion, one can show that for even m

$$
\begin{aligned}
P_n^m(\sin\phi)\sin m\gamma=\sqrt{k^2-\mu^2}\left(a_0\mu^{n-1}+a_1\mu^{n-3}+\cdots a_r\mu^{n-2r-1}\right)\cdot \\
\sqrt{k^2-\upsilon^2}\left(a_0\upsilon^{n-1}+a_1\upsilon^{n-3}+\cdots a_r\upsilon^{n-2r-1}\right)
\end{aligned}
\tag{3.47}
$$

And for odd m, we have

$$
\begin{aligned}
P_n^m(\sin\phi)\sin m\gamma=\sqrt{\mu^2-h^2}\sqrt{k^2-\mu^2}\left(a_0\mu^{n-2}+a_1\mu^{n-4}+\cdots a_r\mu^{n-2r-2}\right)\cdot \\
\sqrt{h^2-\upsilon^2}\sqrt{k^2-\upsilon^2}\left(a_0\upsilon^{n-2}+a_1\upsilon^{n-4}+\cdots a_r\upsilon^{n-2r-2}\right)
\end{aligned}
\tag{3.48}
$$

with $r=\left\lfloor\frac{n}{2}\right\rfloor-1$.

So we know that the spherical surface harmonics correspond to four distinct classes of functions, which we define as follows

$$
\begin{aligned}
&K(\lambda)=u_K(\lambda),\quad L(\lambda)=\sqrt{\left|\lambda^2-h^2\right|}u_L(\lambda) \\
&M(\lambda)=\sqrt{\left|k^2-\lambda^2\right|}u_M(\lambda),\quad N(\lambda)=\sqrt{\left|\lambda^2-h^2\right|}\sqrt{\left|k^2-\lambda^2\right|}u_N(\lambda)
\end{aligned}
\tag{3.49-1}
$$

with

$$
\begin{aligned}
&u_K(\lambda)=a_0^{(K)}\lambda^n+a_1^{(K)}\lambda^{n-2}+\cdots a_r^{(K)}\lambda^{n-2r},\ r=\left\lfloor\frac{n}{2}\right\rfloor \\
&u_L(\lambda)=a_0^{(L)}\lambda^{n-1}+a_1^{(L)}\lambda^{n-3}+\cdots a_r^{(L)}\lambda^{n-2r-1},\ r=\left\lfloor\frac{n-1}{2}\right\rfloor
\end{aligned}
\tag{3.49-2}
$$

$$u_M(\lambda) = a_0^{(M)}\lambda^{n-1} + a_1^{(M)}\lambda^{n-3} + \cdots a_r^{(M)}\lambda^{n-2r-1},\ r = \left\lfloor \frac{n-1}{2} \right\rfloor$$

$$u_N(\lambda) = a_0^{(N)}\lambda^{n-2} + a_1^{(N)}\lambda^{n-4} + \cdots a_r^{(N)}\lambda^{n-2r-2},\ r = \left\lfloor \frac{n}{2} \right\rfloor - 1$$

$a_i^{(\bullet)}, i = 1, 2, \cdots, r$ are constants for any of the four classes of functions[1]. Next we seek to determine these constants so that *K*,*L*,*M*,*N* will satisfy (3.28), which is rewritten as follows

$$\begin{aligned} &\left(\lambda^4 - \alpha\lambda^2 + \beta\right)\frac{d^2E(\lambda)}{d\lambda^2} + \lambda(2\lambda^2 - \alpha)\frac{dE(\lambda)}{d\lambda} + \\ &\left[p\alpha - n(n+1)\lambda^2\right]E(\lambda) = 0,\ \ \alpha = h^2 + k^2, \beta = h^2k^2 \end{aligned} \tag{3.50}$$

And please note that we dropped the subscript *j* for λ_j and are reminded again that it should not be confused with longitude of the spherical harmonics. The *K*-, *L*-, *M*- and *N*-functions that satisfy (3.50) are defined as the four classes of Lamé's functions. Eq. (3.50) is known as the Lamé's equation.

Determination of coefficients of the Lamé's functions

Let us first look at the class-*K* function. Dropping the superscript '(*K*)' of $a_i^{(K)}$ in (3.49-2) and differentiating *K* gives

$$\frac{dK}{d\lambda} = na_0\lambda^{n-1} + \cdots + (n-2i)a_i\lambda^{n-2i-1} + \cdots \tag{3.51-1}$$

$$\frac{d^2K}{d\lambda^2} = n(n-1)a_0\lambda^{n-2} + \cdots + (n-2i)(n-2i-1)a_i\lambda^{n-2i-2} + \cdots \tag{3.51-2}$$

Note that the negative powers of λ vanish in (3.51). Substituting (3.51) into (3.50), evidently, the coefficients for various powers of λ must all equal zero. For instance, the coefficient for λ^n is $\alpha(p - n^2)a_0 - 2(2n-1)a_1 = 0$.

More generally for $\lambda^{n-2i}, 0 \le i \le r = \left\lfloor \frac{n}{2} \right\rfloor$ the coefficient is

$$f_i a_{i-1} + (g_i - \alpha p)a_i + h_i a_{i+1} = 0 \tag{3.52}$$

with

[1] Please note that in our text the integer *r* takes different values according to the degree *n* and class, whereas in Hobson[27] $r = \lfloor n/2 \rfloor$.

$$
\begin{aligned}
f_i &= -\beta(n-2i+2)(n-2i+1),\\
g_i &= \alpha(n-2i)^2,\\
h_i &= 2(i+1)(2n-2i-1)
\end{aligned}
\tag{3.53}
$$

And, please distinguish the difference between focal length h and coefficient h_i. It is worth pointing out that there is no $a_{(-1)}$, so f_0 is unimportant. On the other hand, we assumed $a_{r+1} = 0$ when $i = r$, in which case h_r becomes trivial. And the same is true with $a_{r+2}, a_{r+3}, \cdots$. Therefore we end up with a tri-diagonal r+1 by r+1 matrix

$$
\mathbf{T}_K = \begin{pmatrix}
g_0 & h_0 & & & & \\
f_1 & g_1 & h_1 & & & \\
 & \ddots & \ddots & \ddots & & \\
 & & f_i & g_i & h_i & \\
 & & & \ddots & \ddots & \ddots \\
 & & & & f_r & g_r
\end{pmatrix}
\tag{3.54}
$$

that satisfies

$$
\mathbf{T}_K \mathbf{x} - \alpha p \mathbf{x} = \mathbf{0},\ \mathbf{x} = \begin{pmatrix} a_0 & a_1 \cdots a_r \end{pmatrix}^T
$$

Since p is a constant that needs to be determined, we drop the preceding coefficient of α, so the above expression becomes

$$
\mathbf{T}_K \mathbf{x} - p\mathbf{x} = \mathbf{0} \tag{3.55}
$$

It becomes clear that determining $a_0, a_1, \ldots a_r$ is basically to solve (3.55) for the r+1 eigenvectors of $\mathbf{T}_K$ that correspond to different eigenvalues of p.

The above discussion applies to the Lamé's functions of class K. And the coefficients for classes L, M, N can be determined in the same fashion. For the sake of brevity, we omit the derivations and only include results below.

For class L, the elements in the tri-diagonal matrix $\mathbf{T}_L$ are as follows

$$
\begin{aligned}
f_i &= -\beta(n-2i+1)(n-2i),\\
g_i &= \alpha(n-2i-1)^2 + k^2(2n-4i-1),\\
h_i &= 2(i+1)(2n-2i-1)
\end{aligned}
\tag{3.56}
$$

where $0 \le i \le r,\ r = \left\lfloor \dfrac{n-1}{2} \right\rfloor$.

For class M, the elements in $\mathbf{T}_M$ are

$$
\begin{aligned}
f_i &= -\beta(n-2i+1)(n-2i),\\
g_i &= \alpha(n-2i-1)^2 + h^2(2n-4i-1),\\
h_i &= 2(i+1)(2n-2i-1)
\end{aligned}
\tag{3.57}
$$

And r is the same as for class L.

For class N, the elements in $\mathbf{T}_N$ are

$$
\begin{aligned}
f_i &= -\beta(n-2i)(n-2i-1),\\
g_i &= \alpha(n-2i-1)^2,\\
h_i &= 2(i+1)(2n-2i-1)
\end{aligned}
\tag{3.58}
$$

with $r = \left\lfloor \frac{n}{2} \right\rfloor - 1$.

For a given degree n, we have $\lfloor n/2 \rfloor + 1$ K-functions, $\lfloor (n-1)/2 \rfloor + 1$ L- or M-functions, $\lfloor n/2 \rfloor$ N-functions. Therefore the number of Lamé's functions for a given degree is $2n+1$, the same as for the spherical harmonics.

As a brief summary for this section, we have found that, in relation to the spherical harmonics, $E(\lambda)$ is of four forms given by K,L,M,N, satisfying (3.50). For a given degree n there should be $2n+1$ such $E(\lambda)$. And we shall seek $2n+1$ distinct values of p so as to determine the same number of Lamé's functions. The correspondence between the Lamé's functions and the surface spherical harmonics can be expressed by

$$
P_n^m(\sin\phi)\begin{Bmatrix}\cos m\gamma\\ \sin m\gamma\end{Bmatrix} = \begin{Bmatrix}R_n^m(\phi,\gamma)\\ S_n^m(\phi,\gamma)\end{Bmatrix} = \sum_i c_i E_n^i(\mu)E_n^i(\upsilon)
\tag{3.59}
$$

with

$E(\lambda) \in K(\lambda)$, if m as in $\cos m\gamma$ is even.

$E(\lambda) \in L(\lambda)$, if m as in $\cos m\gamma$ is odd.

$E(\lambda) \in M(\lambda)$, if m as in $\sin m\gamma$ is even.

$E(\lambda) \in N(\lambda)$, if m as in $\sin m\gamma$ is odd.

And c_i are some constants. We also use subscript 'n' to indicate the degree of $E(\lambda)$.

3.2.2 Properties of Lamé's functions

There are several properties associated with Lamé's functions that serve as the basis of application of ellipsoidal harmonics, which are comprehensively discussed

by Hobson[27]. Of those, three properties will be reviewed in brief in this section. Firstly, we shall see that Lamé's functions are linearly independent, that is, one cannot be expressed as a linear combination of others. Secondly, the orthogonality[1] is an essential condition for the expressibility of a function by ellipsoidal harmonics. Thirdly, we will also show that the zeros of Lamé's functions, i.e., the roots of the Lamé's equation, are all located in the range [-*k*,*k*] and they are all distinct.

Linear independence

Suppose $E_n^1(\mu)$ and $E_n^2(\mu)$ of degree *n* and of the same class satisfy

$$\frac{d^2E_n}{d\eta^2} + \mu^2 n(n+1)E_n - pE_n = 0 \tag{3.60}$$

where μ has been suppressed for E_n in this part. We have

$$\frac{d^2E_n^1}{d\eta^2} + \mu^2 n(n+1)E_n^1 - p_1E_n^1 = \frac{d^2E_n^2}{d\eta^2} + \mu^2 n(n+1)E_n^2 - p_2E_n^2 \tag{3.61}$$

Then

$$E_n^2\frac{d^2E_n^1}{d\eta^2} - E_n^1\frac{d^2E_n^2}{d\eta^2} = (p_1 - p_2)E_n^1E_n^2 \tag{3.62}$$

Rearrange (3.62) as follows,

$$E_n^2\frac{d^2E_n^1}{d\eta^2} + \frac{dE_n^2}{d\eta}\frac{dE_n^1}{d\eta} - \frac{dE_n^2}{d\eta}\frac{dE_n^1}{d\eta} - E_n^1\frac{d^2E_n^2}{d\eta^2} = (p_1 - p_2)E_n^1E_n^2 \tag{3.63}$$

and integrate the (3.63) on both sides from 0 to ω where

$$\omega = \int_h^k \frac{d\mu}{\sqrt{\mu^2 - h^2}\sqrt{k^2 - \mu^2}} \tag{3.64}$$

We get

$$\left[E_n^2\frac{dE_n^1}{d\eta} - E_n^1\frac{dE_n^2}{d\eta}\right]_0^{\omega} = \int_0^{\omega}(p_1 - p_2)E_n^1E_n^2 d\eta \tag{3.65}$$

Alternatively, the left-hand side (LHS) is

$$\left[\sqrt{k^2 - \mu^2}\sqrt{\mu^2 - h^2}\left(E_n^2\frac{dE_n^1}{d\mu} - E_n^1\frac{dE_n^2}{d\mu}\right)\right]_h^k \tag{3.66}$$

[1] This relation was referred to as 'The evaluation of a certain double integral' by Hobson in [27]. Somehow it plays an analogous role to the orthogonality relation of the spherical harmonics, and is therefore simply called the orthogonality for the ellipsoidal harmonics in this text.

It can be shown that this expression will vanish for all four classes of Lamé's functions. Therefore the right-hand side (RHS) of (3.65) is

$$\int_0^{\omega} (p_1 - p_2) E_n^1 E_n^2 d\eta = 0 \tag{3.67}$$

Subsequently we have

$$\int_0^{\omega} E_n^1 E_n^2 d\eta = 0 \tag{3.68}$$

unless $p_1 = p_2$, in which case the integral in (3.67) becomes $\int_0^{\omega} (E_n)^2 d\eta$ which certainly cannot vanish.

It follows that $E_n(\mu)$ of the same class are linearly independent. For instance, let us assume

$$\sum_{i=1}^{r} c_i E_n^i = 0 \tag{3.69}$$

and multiply the LHS of (3.69) by E_n^i, and then integrate it from 0 to ω. We note that $\int_0^{\omega} (E_n^i)^2 d\eta$ does not vanish, thus (3.69) cannot hold. Therefore all $E(\mu)$ of the same degree and of the same class must be linearly independent. Of course this result holds for Lamé's functions based on other ellipsoidal coordinates.

Orthogonality

Denote $E(\mu)$ for degree *n* associated with a certain eigenvalue *p* by $E_n^p(\mu)$, and that for degree *m* and eigenvalue *q* by $E_m^q(\mu)$. Consider

$$\frac{d^2 E_n^p(\mu)}{d\eta^2} + \mu^2 n(n+1) E_n^p(\mu) - p E_n^p(\mu) = 0 \tag{3.70-1}$$

$$\frac{d^2 E_m^q(\mu)}{d\eta^2} + \mu^2 m(m+1) E_m^q(\mu) - q E_m^q(\mu) = 0 \tag{3.70-2}$$

Multiplying the LHS of (3.70-1) by $E_m^q(\mu)$ and subtracting from it the LHS of (3.70-2) multiplied by $E_n^p(\mu)$, we get

$$\begin{aligned} &E_m^q(\mu)\frac{d^2 E_n^p(\mu)}{d\eta^2} - E_n^p(\mu)\frac{d^2 E_m^q(\mu)}{d\eta^2} = \\ &\left\{\mu^2\left[n(n+1) - m(m+1)\right] - (p-q)\right\} E_m^q(\mu) E_n^p(\mu) \end{aligned} \tag{3.71}$$

Integrate both sides of the equation from 0 to ω, the LHS of (3.71) vanishes, therefore

$$\int_0^{\omega}\left\{\mu^2\left[n(n+1)-m(m+1)\right]-(p-q)\right\}E_m^q(\mu)E_n^p(\mu)d\eta=0$$

or

$$\begin{aligned}&\left[n(n+1)-m(m+1)\right]\int_0^{\omega}\mu^2E_m^q(\mu)E_n^p(\mu)d\eta\\&=(p-q)\int_0^{\omega}E_m^q(\mu)E_n^p(\mu)d\eta\end{aligned}\qquad(3.72\text{-}1)$$

In the same way for $E_n^p(\upsilon)$ we can get

$$\begin{aligned}&\left[n(n+1)-m(m+1)\right]\int_0^{\sigma}\upsilon^2E_m^q(\upsilon)E_n^p(\upsilon)d\zeta\\&=(p-q)\int_0^{\sigma}E_m^q(\upsilon)E_n^p(\upsilon)d\zeta\end{aligned}\qquad(3.72\text{-}2)$$

Here σ refers to ζ such as

$$\sigma=\int_0^h\frac{d\upsilon}{\sqrt{h^2-\upsilon^2}\sqrt{k^2-\upsilon^2}}\qquad(3.73)$$

We get, by multiplying the RHS of (3.72-1) with LHS of (3.72-2), and the LHS of (3.72-1) with RHS of (3.72-2), and then subtracting the results, that

$$\begin{aligned}&\left[n(n+1)-m(m+1)\right](p-q)\\&\int_0^{\omega}\int_0^{\sigma}(\mu^2-\upsilon^2)E_n^p(\mu)E_m^q(\mu)E_n^p(\upsilon)E_m^q(\upsilon)d\eta d\zeta=0\end{aligned}\qquad(3.74)$$

Therefore the integral $\int_0^{\omega}\int_0^{\sigma}(\mu^2-\upsilon^2)E_m^q(\mu)E_n^p(\mu)E_m^q(\upsilon)E_n^p(\upsilon)d\eta d\zeta$ vanishes, unless

$$n=m \quad\text{and}\quad p=q$$

If n≠*m* and *p*≠*q*, we know from (3.74) that the integral vanishes.

If *n*=*m* and *p*≠*q*, $\int_0^{\omega}E_n^q(\mu)E_n^p(\mu)d\eta=0$ as we know from (3.68). The same is true with $\int_0^{\sigma}E_n^q(\upsilon)E_n^p(\upsilon)d\zeta=0$, therefore the integral in (3.74) must vanish.

If *n*≠*m* and *p*=*q*, we know from (3.72) that $\int_0^{\omega}\mu^2E_m^q(\mu)E_n^p(\mu)d\eta=0$ and $\int_0^{\sigma}\upsilon^2E_m^q(\upsilon)E_n^p(\upsilon)d\zeta=0$. Therefore the integral in (3.74) vanishes.

When *n*=*m* and *p*=*q*,

$$\int_0^{\omega}\int_0^{\sigma}(\mu^2-\upsilon^2)E_m^q(\mu)E_n^p(\mu)E_m^q(\upsilon)E_n^p(\upsilon)d\eta d\zeta$$
$$=\int_0^{\omega}\int_0^{\sigma}(\mu^2-\upsilon^2)\left[E_n^p(\mu)E_n^p(\upsilon)\right]^2 d\eta d\zeta \tag{3.75}$$

It will be shown later (in section 3.2.3) that

$$\int_0^{\omega}\int_0^{\sigma}(\mu^2-\upsilon^2)\left[E_n^p(\mu)E_n^p(\upsilon)\right]^2 d\eta d\zeta=\gamma_n^p \tag{3.76}$$

γ_n^p is some constant which can be used to normalize E_n^p so that

$$\int_0^{\omega}\int_0^{\sigma}(\mu^2-\upsilon^2)\left[\bar{E}_n^p(\mu)\bar{E}_n^p(\upsilon)\right]^2 d\eta d\zeta=1 \tag{3.77}$$

$\bar{E}_n^p$ is the normalized Lamé's function. We will discuss the normalization in the next section.

Assume that a certain function $f(\mu,\upsilon)$ can be expressed by

$$f(\mu,\upsilon)=\sum_i\sum_p c_i^p E_i^p(\mu)E_i^p(\upsilon)$$

where c_i^p is some constant. If we multiply both sides by $(\mu^2-\upsilon^2)E_n^p(\mu)E_n^p(\upsilon)$ and integrate from 0 to ω for η and from 0 to σ for ζ, we get

$$c_n^p\int_0^{\omega}\int_0^{\sigma}(\mu^2-\upsilon^2)\left[E_n^p(\mu)E_n^p(\upsilon)\right]^2 d\eta d\zeta=\int_0^{\omega}\int_0^{\sigma}(\mu^2-\upsilon^2)f(\mu,\upsilon)E_n^p(\mu)E_n^p(\upsilon)d\eta d\zeta$$

From (3.76), we get

$$c_n^p=\frac{\int_0^{\omega}\int_0^{\sigma}(\mu^2-\upsilon^2)f(\mu,\upsilon)E_n^p(\mu)E_n^p(\upsilon)d\eta d\zeta}{\gamma_n^p} \tag{3.78}$$

This is how the coefficients c_i^p in $f(\mu,\upsilon)$ can be obtained.

Zeros for the Lamé's functions

The real roots of the Lamé's equation $E(\lambda)=0$ all fall in the range of [-*k*,*k*]. First of all, it can be shown that $u(\lambda)$ as in (3.49-2) must satisfy the following equation

$$(\lambda^2-h^2)(\lambda^2-k^2)\frac{d^2u}{d\lambda^2}+P(\lambda)\frac{du}{d\lambda}+Q(\lambda)u=0 \tag{3.79}$$

In this case neither *P* nor *Q* contains factors of λ^2-h^2 or λ^2-k^2. If we assume that $u(\lambda)=0$ has roots at $\lambda=\pm h$ or $\pm k$, according to (3.79) $\frac{du}{d\lambda}$ must also vanish at $\lambda=\pm h,\pm k$. Differentiating (3.79) again gives

$$(\lambda^2 - h^2)(\lambda^2 - k^2)\frac{d^3u}{d\lambda^3} + \left(2\lambda(2\lambda^2 - h^2 - k^2) + P\right)\frac{d^2u}{d\lambda^2} + \\ + \left(\frac{dP}{d\lambda} + Q\right)\frac{du}{d\lambda} + \frac{dQ}{d\lambda}u = 0 \tag{3.80}$$

Hence $\left.\frac{d^2u}{d\lambda^2}\right|_{\pm k,\pm h} = 0$ since its coefficient is non-zero. One can go on differentiating (3.80) to show that higher derivatives of *u* all vanish if *u* vanishes at $\lambda = \pm h$ or ±*k*. Therefore we know that $u(\lambda) = 0$ must not have roots at $\lambda = \pm h$ or ±*k*. Similarly, the above reasoning can be applied to show that $u(\lambda) = 0$ can not have equal roots and neither can $E(\lambda) = 0$.

On the other hand, based on (3.74) we see that

$$\int_0^{\omega}\int_0^{\sigma}(\mu^2 - \upsilon^2)E(\mu)E(\upsilon)d\eta d\zeta = 0 \tag{3.81}$$

Because $(\mu^2 - \upsilon^2)$ is always non-negative, so either $E(\mu)$ or $E(\upsilon)$ must have a zero between the respective integration limits. Let

$$f(r) = (\mu^2 - r^2)(\upsilon^2 - r^2) \tag{3.82}$$

where $0 < r^2 < k^2$ that satisfies $E(r) = 0$. Applying the condition of orthogonality, we see that, assuming the polynomial $f(r)$ to be of a different degree than that of $E(\mu)E(\upsilon)$,

$$\int_0^{\omega}\int_0^{\sigma}(\mu^2 - \upsilon^2)f(r)E(\mu)E(\upsilon)d\eta d\zeta = 0 \tag{3.83}$$

This suggests that either $E(\mu)$ or $E(\upsilon)$ must have zeros between $(0, r)$ or (r, k). In this manner one can go on to show that all roots are between 0 and *k* and unequal. Note that $E(\lambda) = 0$ may have a root at $\lambda = 0$.

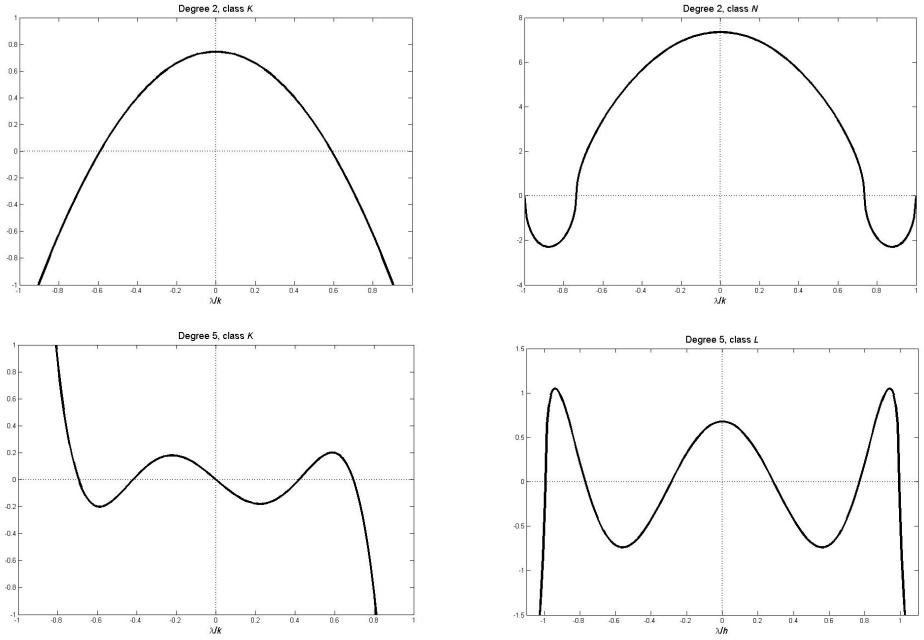

Figure 3.3 Behavior of Lamé's functions. Top: degree 2 class *K* (left) and *N* (right). Bottom: degree 5, class *K* (left) and *L* (right)

Figure 3.3 shows the behavior of Lamé's functions for different classes and different degrees. The change in λ is expressed as the ratio of either λ/h or λ/k. The scale of the Lamé's functions can be arbitrarily set. Additionally, the sign of the preceding factor $\sqrt{|\lambda^2-k^2|}, \sqrt{|\lambda^2-h^2|}$ as in (3.49-1) is chosen such that whenever λ passes $\pm h$ or $\pm k$ the sign changes.

3.2.3 Normalization factor of Lamé's functions

It is often desirable to use the normalized Lamé's functions that satisfy (3.77). For example, one of the advantages is the ease to apply (3.78). The expression on the LHS of (3.76) can be rearranged as

$$\begin{aligned}&\int_0^{\omega}\int_0^{\sigma}(\mu^2-\upsilon^2)\left[E_n^p(\mu)E_n^p(\upsilon)\right]^2 d\eta d\zeta = \\ &\int_0^{\sigma}\left[E_n^p(\upsilon)\right]^2 d\zeta\int_0^{\omega}\mu^2\left[E_n^p(\mu)\right]^2 d\eta - \int_0^{\omega}\left[E_n^p(\mu)\right]^2 d\eta\int_0^{\sigma}\upsilon^2\left[E_n^p(\upsilon)\right]^2 d\zeta\end{aligned} \tag{3.84}$$

Specifically,

$$\int_0^{\omega}\left[E_n^p(\mu)\right]^2 d\eta = \int_h^k \frac{\left[E_n^p(\mu)\right]^2 d\mu}{\sqrt{\mu^2-h^2}\sqrt{k^2-\mu^2}} \tag{3.85-1}$$

$$\int_0^{\sigma}\left[E_n^p(\upsilon)\right]^2 d\zeta = \int_0^{h} \frac{\left[E_n^p(\upsilon)\right]^2 d\upsilon}{\sqrt{h^2-\upsilon^2}\sqrt{k^2-\upsilon^2}} \tag{3.85-2}$$

Now without loss of generality, we assume E_n^p is of class *K*, so that

$$E_n^p(\mu) = a_0\mu^n + a_1\mu^{n-2} + \cdots = \sum_{i=0}^{r} a_i\mu^{n-2i}$$

$r = \left\lfloor \frac{n}{2} \right\rfloor$ being an integer. Therefore $\left[E_n^p(\mu)\right]^2$ is essentially a polynomial of the form

$$\left[E_n^p(\mu)\right]^2 = \sum_{i=0}^{n} a_i'\mu^{2i} \tag{3.86}$$

where a_i' are some constants to be determined from the coefficients of the Lamé's functions as $a_i^{(K)}$ in (3.49). Eq. (3.85-1) becomes

$$\int_0^{\omega}\left[E_n^p(\mu)\right]^2 d\eta = \int_h^{k} \frac{\sum_{i=0}^{n} a_i'\mu^{2i}}{\sqrt{-\mu^4+\alpha\mu^2-\beta}} d\mu \tag{3.87}$$

And α, β are the same as in (3.50). It is realized that

$$\begin{aligned} &\frac{d}{d\mu}\left(\mu^m\sqrt{-\mu^4+\alpha\mu^2-\beta}\right) \\ &= \frac{-(m+2)\mu^{m+3}+(m+1)\alpha\mu^{m+1}-m\beta\mu^{m-1}}{\sqrt{-\mu^4+\alpha\mu^2-\beta}} \end{aligned} \tag{3.88}$$

And obviously we have

$$\left[\mu^m\sqrt{-\mu^4+\alpha\mu^2-\beta}\right]_h^k = 0 \tag{3.89}$$

If we integrate the RHS of (3.88) with respect to μ from *h* to *k*, we have

$$\int_h^{k} \frac{-(m+2)\mu^{m+3}+(m+1)\alpha\mu^{m+1}-m\beta\mu^{m-1}}{\sqrt{-\mu^4+\alpha\mu^2-\beta}} d\mu = 0 \tag{3.90}$$

Therefore, (3.90) can be used as a recurrence algorithm, e.g., to express $\int_0^{\omega}\mu^{m+3}d\eta$ by $\int_0^{\omega}\mu^{m+1}d\eta$ and $\int_0^{\omega}\mu^{m-1}d\eta$. Note that for (3.90) the recurrence holds if *m* descends as odd numbers through *m*=1, when $\int_0^{\omega}\mu^4 d\eta$ shall be expressed by

$\int_0^{\omega} \mu^2 d\eta, \int_0^{\omega} d\eta$. Eventually, we will have

$$\int_0^{\omega} \left[E_n^p(\mu) \right]^2 d\eta = A \int_0^{\omega} \mu^2 d\eta + B \int_0^{\omega} d\eta, \tag{3.91}$$

where *A* and *B* are certain constants. It can be easily shown that

$$\int_0^{\sigma} \left[E_n^p(\upsilon) \right]^2 d\zeta = A \int_0^{\sigma} \upsilon^2 d\zeta + B \int_0^{\sigma} d\zeta \tag{3.92}$$

Using the same reasoning, we have

$$\begin{aligned} \int_0^{\omega} \mu^2 \left[E_n^p(\mu) \right]^2 d\eta &= A' \int_0^{\omega} \mu^2 d\eta + B' \int_0^{\omega} d\eta, \\ \int_0^{\sigma} \upsilon^2 \left[E_n^p(\upsilon) \right]^2 d\zeta &= A' \int_0^{\sigma} \upsilon^2 d\zeta + B' \int_0^{\sigma} d\zeta \end{aligned} \tag{3.93}$$

A', B' are likewise constants. Finally, based on (3.91) through (3.93), eq. (3.84) can be effectively reduced to

$$\begin{aligned} &\int_0^{\omega} \int_0^{\sigma} (\mu^2 - \upsilon^2) \left[E_n^p(\mu) E_n^p(\upsilon) \right]^2 d\eta d\zeta = \\ &(A'B - AB') \int_0^{\omega} \int_0^{\sigma} (\mu^2 - \upsilon^2) d\eta d\zeta \end{aligned} \tag{3.94}$$

It can be shown that

$$\int_0^{\omega} \int_0^{\sigma} (\mu^2 - \upsilon^2) d\eta d\zeta = \frac{\pi}{2} \tag{3.95}$$

Therefore, to normalize the Lamé's functions, we need to compute *A*, *B*, *A'* and *B'* and use

$$\bar{E}_n^p(\mu) = E_n^p(\mu) \Big/ \left(\gamma_n^p \right)^{1/4} \tag{3.96}$$

with

$$\gamma_n^p = (A'B - AB') \frac{\pi}{2} \tag{3.97}$$

as the normalization factor. This will ensure that (3.77) holds, and $\bar{E}_n^p(\mu)$ is now the normalized Lamé's function. To simplify notations, we drop the bar in $\bar{E}_n^p(\mu)$ in (3.77), considering that the scale of Lamé's functions as determined by (3.55) is arbitrary. Therefore we will hereafter assume the following relation to hold in this text, unless stated otherwise,

$$\int_0^{\omega} \int_0^{\sigma} (\mu^2 - \upsilon^2) \left[E_n^p(\mu) E_n^p(\upsilon) \right]^2 d\eta d\zeta = 1 \tag{3.98}$$

3.2.4 Lamé's functions of the second kind

The ellipsoidal harmonics discussed so far are applicable to representing the interior potential. For example, eq. (3.33) suggests that

$$V = \sum cE(\rho)E(\mu)E(\upsilon)$$

for a certain set of constants *c*. Suppose $E(\rho)$ belongs to class *K*, $E(\rho)$ is to be the following form

$$E(\rho) = a_0\rho^n + a_1\rho^{n-2} + \cdots$$

$E(\rho)$ becomes infinity as ρ reaches infinity. Therefore (3.33) cannot be used to model the exterior gravitational potential. The same is true for other classes of *L*,*M*,*N*. A different expression is needed such that when ρ approaches infinity, the potential vanishes. It has been found that $E(\rho)$ is the solution to

$$\frac{d^2E(\rho)}{d\xi^2} - \rho^2 n(n+1)E(\rho) + pE(\rho) = 0 \tag{3.99}$$

Another solution to this equation, namely, the Lamé's function of the second kind $F(\rho)$, can be found as follows. First, it also satisfies

$$\frac{d^2F(\rho)}{d\xi^2} - \rho^2 n(n+1)F(\rho) + pE(\rho) = 0 \tag{3.100}$$

Multiplying the LHS of (3.99) with $F(\rho)$ and subtracting it from LHS of (3.100) multiplied with $E(\rho)$ yields

$$F(\rho)\frac{d^2E(\rho)}{d\xi^2} - E(\rho)\frac{d^2F(\rho)}{d\xi^2} = 0 \tag{3.101}$$

then

$$\begin{aligned} &F(\rho)\frac{d^2E(\rho)}{d\xi^2} + \frac{dE(\rho)}{d\xi}\frac{dF(\rho)}{d\xi} - \frac{dE(\rho)}{d\xi}\frac{dF(\rho)}{d\xi} - E(\rho)\frac{d^2F(\rho)}{d\xi^2} = 0 \\ &\Rightarrow \frac{d}{d\xi}\left[F(\rho)\frac{dE(\rho)}{d\xi} - E(\rho)\frac{dF(\rho)}{d\xi}\right] = 0 \end{aligned} \tag{3.102}$$

Therefore,

$$F(\rho)\frac{dE(\rho)}{d\xi} - E(\rho)\frac{dF(\rho)}{d\xi} = C \tag{3.103}$$

where *C* is some constant. The above equation can be written as

$$\left[E(\rho)\right]^2 \frac{d}{d\xi}\left[\frac{F(\rho)}{E(\rho)}\right] = C \tag{3.104}$$

Then

$$\frac{F(\rho)}{E(\rho)} = \int_a^b \frac{C}{\left[E(\rho)\right]^2} d\xi \tag{3.105}$$

The limits of integration *a*,*b* are chosen in such a way that when ρ reaches infinity, $F(\rho)/E(\rho)$ becomes zero. Upon substituting $dt = \sqrt{t^2-k^2}\sqrt{t^2-h^2}\,d\xi$ in (3.105), we get

$$\frac{F(\rho)}{E(\rho)} = \int_\rho^{+\infty} \frac{C}{\left[E(t)\right]^2 \sqrt{t^2-h^2}\sqrt{t^2-k^2}} dt \tag{3.106}$$

Furthermore, the constant *C* is to be determined such that when ρ becomes a very large quantity,

$$F(\rho) = \frac{1}{\rho^{n+1}} \quad \text{or} \quad \frac{F(\rho)}{E(\rho)} = \frac{1}{\rho^{2n+1}} \tag{3.107}$$

Of course $F(\rho)$ in this case would be analogous to the attenuation factor of $1/r^{n+1}$ for the spherical harmonics. Eq. (3.107) suggests that, for very large ρ

$$\frac{F(\rho)}{E(\rho)} = \frac{1}{\rho^{2n+1}} = C\int_\rho^{\infty} \frac{dt}{t^{2n+2}} \tag{3.108}$$

Hence

$$C = 2n+1 \tag{3.109}$$

In this case a_0, which is the coefficient for ρ^n in (3.49-2), is taken to be one. Finally, we have

$$F(\rho) = (2n+1)E(\rho)\int_\rho^{+\infty} \frac{dt}{\left[E(t)\right]^2 \sqrt{t^2-h^2}\sqrt{t^2-k^2}} \tag{3.110}$$

And the exterior potential can be represented by

$$V = \sum cF(\rho)E(\mu)E(\upsilon) \tag{3.111}$$

where *c* is some constant.

3.3 Gravitational field modeling via ellipsoidal harmonics

Our interest is to apply the ellipsoidal harmonic series (EHS) to model the gravitational potential of the attracting body at the exterior point. We found that

(3.111) is a promising form of EHS for such a purpose. In analogy with the SHS of the following form

$$V = \sum_{n=0}^{\infty} \frac{1}{r^{n+1}} \sum_{m=0}^{n} P_n^m(\sin\varphi)\left(A_{nm}\cos m\lambda + B_{nm}\sin m\lambda\right)$$

we shall look for the EHS of the form

$$V = \sum_{n=0}^{\infty} \sum_{m=1}^{2n+1} c_{nm} F_n^m(\rho) E_n^m(\mu) E_n^m(\upsilon) \tag{3.112}$$

In (3.112), n as always is the degree number. c_{nm}, analogous to A_{nm} and B_{nm}, are the coefficients that characterize the gravitational field of the attracting body. For a given n there are $2n+1$ E_n^m and F_n^m that are associated with different eigenvalues of p_m. These functions are numbered as $m = 1, 2, \cdots, 2n+1$. The correspondence between different m and four classes of E_n^m we define as follows:

$$E_n^m \in K, \quad \text{if } 1 \le m \le n_K \tag{3.113-1}$$

$$E_n^m \in L, \quad \text{if } n_K < m \le n_K + n_L \tag{3.113-2}$$

$$E_n^m \in M, \quad \text{if } n_K + n_L < m \le n_K + 2n_L \tag{3.113-3}$$

$$E_n^m \in N, \quad \text{if } n_K + 2n_L < m \le 2n+1 \tag{3.113-4}$$

with n_K and n_L denoting the number of K- and L-functions, respectively, such as

$$n_K = 1 + \left\lfloor \frac{n}{2} \right\rfloor, \quad n_L = \left\lfloor \frac{n+1}{2} \right\rfloor \tag{3.114-1}$$

For the sake of clarity, we also re-write explicitly the number of M- and N-functions,

$$n_M = n_L, \quad n_N = \left\lfloor \frac{n}{2} \right\rfloor \tag{3.114-2}$$

And of course we must have $n_K + n_M + n_L + n_N = 2n+1$. Note that if any inequality in (3.113) does not hold then that particular class simply does not exist. For example, there are no functions of class L, M for degree zero, whereas there is no N for either degree zero or one.

3.3.1 Field coefficients of ellipsoidal harmonics

Eq. (3.112) can be used to model the exterior gravitational field of the attracting body. The coefficients c_{nm} should be chosen in such a way that as the degree n

approaches infinity, the EHS modeled V shall converge to the true potential. One possible way in which c_{nm} can be determined is to apply the orthogonality of the EHS. We first re-express equation (3.78) as follows, with slight changes in notation in conformity with (3.112)

$$c_{nm} = \int_0^{\omega}\int_0^{\sigma}(\mu^2-\upsilon^2)f(\mu,\upsilon)E_n^m(\mu)E_n^m(\upsilon)d\eta d\zeta \tag{3.115}$$

Note that we dropped the normalization factor γ_n^m assuming that E_n^m has already been normalized. Substituting V for $f(\mu,\upsilon)$, where V is the potential given on a certain ellipsoid with semi-major axis of ρ_0 (Figure 3.4)

$$V = V(\rho=\rho_0,\mu,\upsilon) = \sum_{n=0}^{\infty}\sum_{m=1}^{2n+1} c_{nm}F_n^m(\rho_0)E_n^m(\mu)E_n^m(\upsilon)$$

would result in

$$\begin{aligned}&\int_0^{\omega}\int_0^{\sigma}(\mu^2-\upsilon^2)V(\mu,\upsilon)E_n^m(\mu)E_n^m(\upsilon)d\eta d\zeta\\ &= c_{nm}F_n^m(\rho_0)\int_0^{\omega}\int_0^{\sigma}(\mu^2-\upsilon^2)\left[E_n^m(\mu)E_n^m(\upsilon)\right]^2 d\eta d\zeta = c_{nm}F_n^m(\rho_0)\end{aligned} \tag{3.116}$$

The integration is over the entire ellipsoidal surface. Therefore we have

$$c_{nm} = \frac{\int_0^{\omega}\int_0^{\sigma}(\mu^2-\upsilon^2)V(\mu,\upsilon)E_n^m(\mu)E_n^m(\upsilon)d\eta d\zeta}{F_n^m(\rho_0)} \tag{3.117}$$

By deriving c_{nm} this way we ensure that the EHS-modeled potential V_{EHS} will conform to the prescribed values of V on the ellipsoid. It is found that it is more convenient to express (3.112) as follows

$$V_{\mathrm{EHS}} = \sum_{n=0}^{\infty}\sum_{m=1}^{2n+1} c_{nm}\frac{F_n^m(\rho)}{F_n^m(\rho_0)}E_n^m(\mu)E_n^m(\upsilon) \tag{3.118}$$

Please note the difference of c_{nm} in (3.112) and (3.118). We see that now $\dfrac{F_n^m(\rho)}{F_n^m(\rho_0)}$ plays the same role as $\left(\dfrac{R}{r}\right)^{n+1}$ for the SHS. We shall hereafter refer to c_{nm} as the gravitational field coefficients or simply field coefficients for ellipsoidal harmonics.

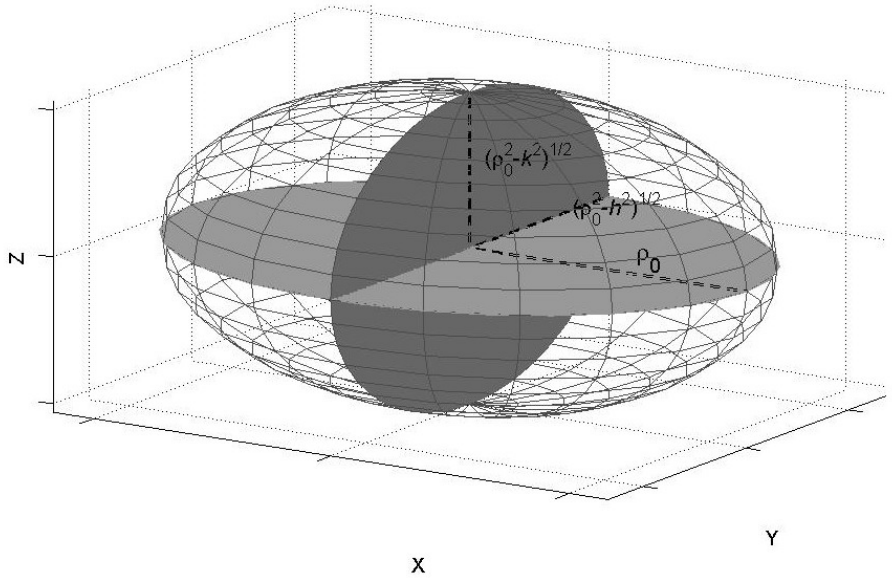

Figure 3.4 The ellipsoid on which V is proscribed, with semimajor axis ρ_0 and focal lengths h,k

3.3.2 Brief notes on the convergence of ellipsoidal harmonics

So far we have not attended to the convergence of the EHS. For the SHS of (2.20), we know that it is uniformly convergent outside the reference sphere of radius R. Because the attenuation factor $\left(\frac{R}{r}\right)^{n+1}$ is smaller than unity hence the convergence is guaranteed (provided that the field coefficients are bounded). In this section we shall show (but not with indisputable rigor) that (3.118) is uniformly convergent outside the ellipsoid given by $\rho = \rho_0$, by discussing the role of $\frac{F_n^m(\rho)}{F_n^m(\rho_0)}$.

First of all, we remind ourselves that $F(\rho)$ is given by

$$F(\rho) = (2n+1)E(\rho)\int_{\rho}^{+\infty} \frac{dt}{\left[E(t)\right]^2 \sqrt{t^2-h^2}\sqrt{t^2-k^2}} \tag{3.119}$$

Without loss of generality, let us assume that $E(\rho)$ is of class K. In this case

$$\frac{E(\rho)}{E(\rho_0)} = \frac{\rho^{n-2r}(\rho^2-q_1)(\rho^2-q_2)\cdots(\rho^2-q_r)}{\rho_0^{n-2r}(\rho_0^2-q_1)(\rho_0^2-q_2)\cdots(\rho_0^2-q_r)} \le \left(\frac{\rho}{\rho_0}\right)^n \tag{3.120}$$

where $r = n_K = \left\lfloor \frac{n}{2} \right\rfloor$, and $q_1, q_2, \ldots$ are the zeros of Lamé's functions. Hence $F(\rho)$ shall satisfy

$$\frac{F(\rho)}{F(\rho_0)} \le \left(\frac{\rho}{\rho_0} \right)^n \frac{I(\rho)}{I(\rho_0)} \tag{3.121}$$

where

$$I(\rho) = \int_\rho^{+\infty} \frac{dt}{\left[E(t)\right]^2 \sqrt{t^2 - k^2}\sqrt{t^2 - h^2}} \tag{3.122}$$

Because the zeros of Lamé's functions are all in range [-k,k] and let us assume $\rho > k$, we have

$$\left[E(\rho)\right]^2 \le \left[E(t)\right]^2, \rho \le t$$

Moreover, for $t \ge \rho$ we could find such constants C_0, C_0' that satisfy

$$E(t) = t^n (1 - \frac{q_1}{t^2})(1 - \frac{q_2}{t^2}) \cdots (1 - \frac{q_r}{t^2}) \ge \frac{t^n}{C_0} \tag{3.123}$$

and

$$\sqrt{t^2 - h^2}\sqrt{t^2 - k^2} = t^2 \sqrt{1 - \frac{h^2}{t^2}}\sqrt{1 - \frac{k^2}{t^2}} \ge \frac{t^2}{C_0'} \tag{3.124}$$

Combining (3.123) and (3.124), we have

$$I(\rho) \le \left(C_0\right)^2 \int_\rho^{+\infty} \frac{dt}{t^{2n}\sqrt{t^2 - k^2}\sqrt{t^2 - h^2}} \le C_1 \int_\rho^{+\infty} \frac{dt}{t^{2n+2}} \tag{3.125}$$

And $C_1 = (C_0)^2 C_0'$ is some constant. Changing the integration variable via

$$t = \frac{1}{s}, \ dt = -\frac{1}{s^2} ds \tag{3.126}$$

in the integral of (3.125) results in

$$I(\rho) \le C_1 \int_0^{1/\rho} s^{2n} dt = \frac{C_1}{(2n+1)} \frac{1}{\rho^{2n+1}} \tag{3.127}$$

On the other hand, again referring to (3.123) and (3.124), we could find such a constant C_2 that satisfies

$$I(\rho_0) \ge C_2 \int_\rho^{+\infty} \frac{dt}{t^{2n+2}} \tag{3.128}$$

Therefore

$$I(\rho_0) \geq C_2 \int_0^{1/\rho} s^{2n} dt = \frac{C_2}{(2n+1)} \frac{1}{\rho_0^{2n+1}} \tag{3.129}$$

By substituting the inequalities (3.127) and (3.129) into (3.121), we obtain

$$\frac{F(\rho)}{F(\rho_0)} \leq C \left(\frac{\rho_0}{\rho} \right)^{n+1}, C = \frac{C_1}{C_2} \tag{3.130}$$

The fact that the attenuation factor $\frac{F(\rho)}{F(\rho_0)}$ for the EHS is equivalent to the form of $\left(\frac{\rho_0}{\rho} \right)^{n+1}$ suggests that (3.118) will be convergent outside the ellipsoid of ρ_0. For other classes of Lamé's functions, (3.130) can be derived in a similar way, and is not discussed here.

It can also be shown that (3.118) will indeed converge to the prescribed values of V on the ellipsoid as $\rho \to \rho_0$. Furthermore, we understand that, to apply (3.118), the mass of the attracting body must be all inside the ellipsoid of ρ_0, just as the entire mass must be inside the reference sphere for the SHS. Now (3.118) is ever more promising to be applied to model the gravitational field of the attracting body. In the following chapter, we shall discuss the numerical computations of the EHS.

Chapter 4: Numerical Considerations for Computing Ellipsoidal Harmonics

The theory of ellipsoidal harmonic expansions was reviewed in chapter 3 based on Hobson's discussions of the subject. Unfortunately, when it comes to numerical computations of Lamé's functions and the application of (3.118) etc., the afore-adopted formulation of the EHS is far from applicable. A more practical numerical scheme of applying the EHS for gravitational field modeling was elaborated by Garmier[29] that could accommodate the numerical difficulties, which is the focus of this chapter.

4.1 Computation of Lamé's functions

The first and foremost task of using the EHS is to generate Lamé's functions. All these functions satisfy (3.50). We are seeking the solution as a power series as given by (3.49), and solve for the eigenvalues and eigenvectors of the following tri-diagonal real matrix **T** as in (3.54).

$$\mathbf{T} = \begin{pmatrix} g_0 & h_0 & & & \\ f_1 & g_1 & h_1 & & \\ & \ddots & \ddots & \ddots & \\ & & f_{r-1} & g_{r-1} & h_{r-1} \\ & & & f_r & g_r \end{pmatrix}$$

Depending on the class of Lamé's functions, coefficients f_i,g_i,h_i will take on different values, as are given by (3.53) and (3.56) through (3.58). We note that f_i are all multiples of $\beta = h^2k^2$, while g_i are the multiples of $\alpha = h^2 + k^2$. Since h and k both have the dimension of distance, elements on different diagonals of **T** can be sometimes severely 'out of balance', i.e., the magnitude of f_i is likely greater than h_i. Another distinct issue is with the dimension of coefficients for the Lamé's functions. Namely, since λ_j has the dimension of distance as h and k, the coefficients of a_i as in (3.49) will each be of different dimensions. This is certainly not desirable (e.g.,

compared to C_{nm}, S_{nm} for the SHS). To address the above issues, we could introduce another set of variables[38]

$$\Lambda_j = 1 - t_j^2,\ t_j = \frac{\lambda_j}{h},\ j = 1,2,3 \tag{4.1}$$

Again λ_j is the ellipsoidal coordinate. Subsequently, corresponding to (3.49) the Lamé's functions of four classes are as follows

$$K(\lambda_j) = t_j^{n-2r} u_n^m(\Lambda_j) \tag{4.2-1}$$

$$L(\lambda_j) = t_j^{n-2r-1} \sqrt{\left|t_j^2 - 1\right|} u_n^m(\Lambda_j) \tag{4.2-2}$$

$$M(\lambda_j) = t_j^{n-2r-1} \sqrt{\left|t_j^2 - \kappa^2\right|} u_n^m(\Lambda_j) \tag{4.2-3}$$

$$N(\lambda_j) = t_j^{n-2r-2} \sqrt{\left|t_j^2 - 1\right|} \sqrt{\left|t_j^2 - \kappa^2\right|} u_n^m(\Lambda_j) \tag{4.2-4}$$

with

$$\kappa = \frac{k}{h} \tag{4.3}$$

Here we assume

$$u_n^m(\Lambda_j) = b_0 + b_1 \Lambda_j + \cdots b_r \Lambda_j^r \tag{4.4}$$

with $r = \left\lfloor \frac{n}{2} \right\rfloor$ for class K, $r = \left\lfloor \frac{n-1}{2} \right\rfloor$ for class L or M. $r = \left\lfloor \frac{n}{2} \right\rfloor - 1$ for class N.

Since t_j as well as Λ_j are dimensionless, b_i are all (for different i) of the same dimension.

The coefficients b_i can be determined in the exact same way as determining a_i in (3.49). Suppose we want to find b_i for class K. First, we have

$$\frac{du_K}{dt} = -2t\left(b_1 + 2b_2\Lambda + \cdots + rb_r\Lambda^{r-1}\right) = \cdots + (-2ib_i t\Lambda^{i-1}) + \cdots \tag{4.5-1}$$

It follows that

$$\frac{d^2u_K}{dt^2} = \ldots + -2ib_i\Lambda^{i-2}[(2i-1)\Lambda + 2 - 2i] + \cdots \tag{4.5-2}$$

Having now introduced Λ we must therefore distinguish between the even and odd values of degree n, as it affects the preceding function of t^{n-2r} in (4.2-1). It can be shown that, if n is even, (3.50) is equivalent to

$$(t^2-\kappa^2)(t^2-1)\frac{d^2u_K}{dt^2}+t(2t^2-\alpha')\frac{du_K}{dt}+[p-n(n+1)t^2]u_K=0$$

where

$$\alpha'=\frac{\alpha}{h^2}=1+\kappa^2 \tag{4.6}$$

And, more relevant is the following form of (3.50)

$$(\Lambda+\kappa^2-1)\Lambda\frac{d^2u_K}{dt^2}-t(2\Lambda-2+\alpha')\frac{du_K}{dt}+[p-n(n+1)(1-\Lambda)]u_K=0 \tag{4.7}$$

Substituting (4.2-1) and (4.5) into (4.7) and equating coefficients of different powers in Λ to zero, results in the following equation in matrix form

$$\begin{pmatrix}0\\0\\\vdots\\0\\0\end{pmatrix}=\begin{pmatrix}g_0 & h_0 & & & \\ f_1 & g_1 & h_1 & & \\ & \ddots & \ddots & \ddots & \\ & & f_{r-1} & g_{r-1} & h_{r-1}\\ & & & f_r & g_r\end{pmatrix}\begin{pmatrix}b_0\\b_1\\\vdots\\b_{r-1}\\b_r\end{pmatrix}-\begin{pmatrix}b_0\\b_1\\\vdots\\b_{r-1}\\b_r\end{pmatrix}p=(\mathbf{T}_K-\mathbf{I}p)\mathbf{b} \tag{4.8}$$

where **I** denotes the identity matrix. The elements f_i,g_i,h_i in $\mathbf{T}_K$ are not the same as those given in (3.54). In this case for class *K* and even *n* we have

$$\begin{aligned}f_i&=-2(r-i+1)(2r+i-1),\\ g_i&=2r(2r+1)+4i^2(\kappa^2-2),\\ h_i&=-2(i+1)(2i+1)(\kappa^2-1)\end{aligned} \tag{4.9}$$

Hence, in order to get b_i we must solve for the r+1 eigenvalues, i.e., p_1,p_2,…,p_{r+1}, and the same number of associated eigenvectors **b** in (4.8). The components in each of the r+1 eigenvectors give the coefficients for the Lamé's functions of class *K*, even *n*. Note that the scale of the eigenvectors is not important.

The above discussion only applies to class *K* with even *n*. If *n* is odd, it can be shown that (3.50) becomes

$$\begin{aligned}&\Lambda(\Lambda+\kappa^2-1)t\frac{d^2u}{dt^2}+[2\Lambda(\Lambda+\kappa^2-1)+(\alpha'+2\Lambda-2)(\Lambda-1)]\frac{du}{dt}\\ &+t[p-\alpha'+(n+2)(n-1)(\Lambda-1)]u=0\end{aligned} \tag{4.10}$$

We need not heed *t* appearing in the above equation as it will become a common factor once we have substituted (4.5-1) into (4.10).

Thus we will have another equation in the form of (4.8) but with different f_i,g_i,h_i. The Lamé's equations of other classes will be given in Appendix A. We see that in

total there are eight such equations (two for each class) in matrix form, each of which comes with a set of coefficients f_i,g_i,h_i, for $i = 0,1,\cdots,r$. The expressions for these coefficients can be found in Dobner[38] as well as Garmier[29]. For the sake of consistency, the expressions are also provided in Appendix B. Please note that, since we use t_j rather than λ_j in the preceding functions for u_n^m in (4.2), all coefficients in our expressions differ from those provided Garmier by a common factor of h^2.

There are well established numerical schemes for solving for p and **b** in (4.8). Our experience shows that the Implicitly Shifted QR algorithm[39] suffices for our purpose.

4.1.1 Normalization of Lamé's functions based on Λ

The numerically derived coefficients of Lamé's functions are now based on t_j and Λ_j. The formulas for normalizing Lamé's functions as given in section 3.2.3 also need to be adapted. From (3.84) we see that there are four integrals to be evaluated, namely,

$$\int_0^{\sigma}\left[E_n^m(\upsilon)\right]^2 d\zeta,\ \int_0^{\sigma}\upsilon^2\left[E_n^m(\upsilon)\right]^2 d\zeta,\ \int_0^{\omega}\left[E_n^m(\mu)\right]^2 d\eta,\ \int_0^{\omega}\mu^2\left[E_n^m(\mu)\right]^2 d\eta$$

There is only need to consider two of them, i.e., those associated with either μ or υ. We shall discuss only the case for μ

$$\int_0^{\omega}\left[E_n^m(\mu)\right]^2 d\eta \quad \text{and} \quad \int_0^{\omega}\mu^2\left[E_n^m(\mu)\right]^2 d\eta$$

Expressed in t_2 and Λ_2 these two functions become

$$\begin{aligned}\int_0^{\omega}\left[E_n^m(\mu)\right]^2 d\eta &= \int_h^k \frac{\left[E_n^m(\mu)\right]^2 d\mu}{\sqrt{\mu^2-h^2}\sqrt{k^2-\mu^2}} \\ &= \int_0^{1-\left(\frac{k}{h}\right)^2} \frac{\left[E_n^m(\Lambda_2)\right]^2 d\Lambda_2}{2\sqrt{-\Lambda_2}\sqrt{1-\Lambda_2}\sqrt{h^2\Lambda_2+(k^2-h^2)}}\end{aligned} \tag{4.11-1}$$

$$\begin{aligned}&\int_0^{\omega}\mu^2\left[E_n^m(\mu)\right]^2 d\eta = \\ &\qquad \int_0^{1-\left(\frac{k}{h}\right)^2} \frac{h^2(1-\Lambda_2)\left[E_n^m(\Lambda_2)\right]^2 d\Lambda_2}{2\sqrt{-\Lambda_2}\sqrt{1-\Lambda_2}\sqrt{h^2\Lambda_2+(k^2-h^2)}}\end{aligned} \tag{4.11-2}$$

The numerators in the integrals are of the form

$$\left[E_n^m(\Lambda_2)\right]^2 = \sum_{i=0}^{n} c_i \Lambda_2^i,\ \left[\mu E_n^m(\Lambda_2)\right]^2 = \sum_{i=0}^{n+1} c_i' \Lambda_2^i \tag{4.12}$$

where c_i, c_i' are constants to be determined from the coefficients of Lamé's functions as b_i in (4.4). On the other hand, the common denominator in the integrals is

$$\begin{aligned} &\sqrt{-\Lambda_2}\sqrt{1-\Lambda_2}\sqrt{h^2\Lambda_2 + (k^2-h^2)} \\ &= \sqrt{-(k^2-h^2)\Lambda_2 + (k^2-2h^2)\Lambda_2^2 + h^2\Lambda_2^3} \\ &= \sqrt{a_1\Lambda_2 + a_2\Lambda_2^2 + a_3\Lambda_2^3} \end{aligned} \tag{4.13}$$

Following the discussion in section 3.2.3, we see that

$$\begin{aligned} &\frac{d}{d\Lambda_2}\left(\Lambda_2^l \sqrt{a_1\Lambda_2 + a_2\Lambda_2^2 + a_3\Lambda_2^3}\right) \\ &= \frac{(l+\frac{3}{2})a_3\Lambda_2^{l+2} + (l+1)a_2\Lambda_2^{l+1} + (l+\frac{1}{2})a_1\Lambda_2^l}{\sqrt{a_1\Lambda_2 + a_2\Lambda_2^2 + a_3\Lambda_2^3}} \end{aligned} \tag{4.14}$$

For some non-negative integer of l, we have

$$\left[\Lambda_2^l \sqrt{a_1\Lambda_2 + a_2\Lambda_2^2 + a_3\Lambda_2^3}\right]_0^{1-\left(\frac{k}{h}\right)^2} = 0 \tag{4.15}$$

Eq. (4.14) suggests a recursive relation analogous to (3.88). If we denote

$$I(\Lambda_2^l) = \int_0^{1-\left(\frac{k}{h}\right)^2} \frac{\Lambda_2^l d\Lambda_2}{2\sqrt{a_1\Lambda_2 + a_2\Lambda_2^2 + a_3\Lambda_2^3}} \tag{4.16}$$

Then $I(\Lambda_2^{l+2})$ can be expressed recursively by $I(\Lambda_2^{l+1})$ and $I(\Lambda_2^l)$, and this relation is valid for descending values of l through l=0, when $I(\Lambda_2^2)$ is expressed by $I(\Lambda_2)$ and $I(\Lambda_2^0)$. Eventually we should get

$$\int_0^{\omega}\left[E_n^m(\mu)\right]^2 d\eta = A \cdot I(\Lambda_2) + B \cdot I(\Lambda_2^0), \tag{4.17-1}$$

$$\int_0^{\omega}\left[\mu E_n^l(\mu)\right]^2 d\eta = A' \cdot I(\Lambda_2) + B' \cdot I(\Lambda_2^0) \tag{4.17-2}$$

It can be shown that such a relation also holds for υ. The normalization factor is

$$\gamma_n^m = \frac{(AB' - A'B)}{h^2}\frac{\pi}{2} \tag{4.18}$$

We see that the coefficients of Lamé's functions as well as the normalization factors are essentially related to the focal lengths h,k. Once we have fixed the reference

ellipsoid of ρ_0 together with the focal lengths, the coefficients are specified once and for all.

4.1.2 Computing Lamé's functions of the second kind

The computation of Lamé's functions of the second kind involves evaluating a certain integral in (3.122)

$$I(\rho) = \int_{\rho}^{+\infty} \frac{dt}{\left[E(t)\right]^2 \sqrt{t^2 - h^2}\sqrt{t^2 - k^2}}$$

It would be desirable to transform this function in such a way that the integration limits are both finite. One way is to do so via (3.126) as

$$I(\rho) = \int_{0}^{1/\rho} \frac{ds}{\left[E(s)\right]^2 \sqrt{1 - s^2h^2}\sqrt{1 - s^2k^2}} \tag{4.19}$$

Since now $E(\rho)$ is expressed as a function of s, i.e., with coefficients other than those in the Lamé's functions. For example, suppose $E(\rho)$ is of class K,

$$\begin{aligned} E(s) = E(\rho) &= a_0\rho^n + a_1\rho^{n-2} + \cdots = \rho^n\left(a_0 + \frac{a_1}{\rho^2} + \cdots\right) \\ &= \frac{1}{s^n}\left(a_0 + a_1 s^2 + \cdots\right) = \frac{1}{s^n}\tilde{E}(s) \end{aligned} \tag{4.20}$$

Therefore (3.122) can be rewritten as follows

$$I(\rho) = \int_{0}^{1/\rho} \frac{s^{2n}ds}{\left[\tilde{E}(s)\right]^2 \sqrt{1 - s^2h^2}\sqrt{1 - s^2k^2}} \tag{4.21}$$

It can be easily verified that (4.21) also holds for other classes as well. Eq. (4.21) can be integrated numerically as a quardrature problem.

Hence we see that Lamé's functions of the second kind are now of the form

$$F(\rho) = (2n+1)I(\rho)E(\rho) \tag{4.22}$$

4.2 Numerical modeling of the gravitational field via ellipsoidal harmonics

We wish to represent the gravitational potential by the EHS given by (3.118)

$$V_{\text{EHS}} = \sum_{n=0}^{\infty}\sum_{m=1}^{2n+1} c_{nm}\frac{F_n^m(\rho)}{F_n^m(\rho_0)}E_n^m(\mu)E_n^m(\upsilon)$$

In section 4.1, we have reviewed a more practical formulation for computing the

Lamé's functions, and shall decompose $F_n^m(\rho)E_n^m(\mu)E_n^m(\upsilon)$ into the following form

$$F_n^m(\rho)E_n^m(\mu)E_n^m(\upsilon) = I_n^m(\rho)E_n^m(\rho)E_n^m(\mu)E_n^m(\upsilon) \tag{4.23}$$

Note that in (4.23) the common factor $2n+1$ was dropped. The matter of computing E_n^m really comes down to computing $u(\Lambda_j)$ as in (4.3) and (4.4). Therefore we could express (4.23) further as

$$E_n^m(\rho)E_n^m(\mu)E_n^m(\upsilon) = \Phi_n^m(t_1,t_2,t_3)u_n^m(\Lambda_1)u_n^m(\Lambda_2)u_n^m(\Lambda_3) \tag{4.24}$$

The form of $\Phi_n^m(t_1,t_2,t_3)$ according to the evenness of degree n and class, is given in the Table 4.1.

Table 4.1 Expressions for the preceding function Φ_n^m for different n and m

Φ_n^m	n even	n odd
class K	1	$t_1t_2t_3 = x/h\cdot\kappa$
class L	$t_1t_2t_3\sqrt{t_1^2-1}\sqrt{t_2^2-1}\sqrt{1-t_3^2}$ $= xy/h^2\cdot\kappa\sqrt{\kappa^2-1}$	$\sqrt{t_1^2-1}\sqrt{t_2^2-1}\sqrt{1-t_3^2}$ $= y/h\cdot\sqrt{\kappa^2-1}$
class M	$t_1t_2t_3\sqrt{t_1^2-\kappa^2}\sqrt{\kappa^2-t_2^2}\sqrt{\kappa^2-t_3^2}$ $= xz/h^2\cdot\kappa^2\sqrt{\kappa^2-1}$	$\sqrt{t_1^2-\kappa^2}\sqrt{\kappa^2-t_2^2}\sqrt{\kappa^2-t_3^2}$ $= z/h\cdot\kappa\sqrt{\kappa^2-1}$
class N	$\sqrt{t_1^2-1}\sqrt{t_2^2-1}\sqrt{1-t_3^2}\cdot$ $\sqrt{t_1^2-\kappa^2}\sqrt{\kappa^2-t_2^2}\sqrt{\kappa^2-t_3^2}$ $= yz/h^2\cdot\kappa(\kappa^2-1)$	$t_1t_2t_3\sqrt{t_1^2-1}\sqrt{t_2^2-1}\sqrt{1-t_3^2}\cdot$ $\sqrt{t_1^2-\kappa^2}\sqrt{\kappa^2-t_2^2}\sqrt{\kappa^2-t_3^2}$ $= xyz/h^3\cdot\kappa^2(\kappa^2-1)$

Note that the expressions based on t_i in Table 4.1 all have sign ambiguities which result from the squares in the expressions of (3.9). However, we could always resort to the rectangular coordinates to remove such ambiguities. We shall simplify the expression of (4.23) as (for a given degree n, class and m)

$$F_n^m(\rho)E_n^m(\mu)E_n^m(\upsilon) = \Phi_n^m(x,y,z)I_n^m(\lambda_1)u_n^m(\Lambda_1)u_n^m(\Lambda_2)u_n^m(\Lambda_3)$$
$$= Y_n^m(x,y,z,\lambda_1,\lambda_2,\lambda_3) \tag{4.25}$$

This is the practical expression for the EHS.

4.2.1 Gravitational acceleration via ellipsoidal harmonics

Eq. (4.25) is a form favorable for numerically expressing the gravitational potential. Taking the gradient of (4.25) with respect to the rectangular coordinates *x*,*y*,*z* results in the gravitational acceleration. We first need to differentiate (4.25) with respect to the three ellipsoidal coordinates, and then project the resulting derivatives to the *x*,*y*,*z* directions (with the exception of elements in Φ_n^m that are based on *x*,*y*,*z*). As we shall show hereafter, computing the gravitational acceleration (and gradient) via the EHS is far more cumbersome than via the SHS.

In order to simplify our notations in this section, we drop *n*,*m* and replace variables ρ,μ,υ with subscripts '(*j*)' for the functions to indicate their exclusive dependence on λ_j (or equivalently Λ_j). Taking the gradient of (4.25) in the rectangular coordinates we obtain the following expression

$$\nabla Y = Y\left(\frac{1}{\Phi}\nabla\Phi + \frac{1}{I_{(1)}}\nabla I_{(1)} + \sum_{j=1}^{3}\frac{1}{u_{(j)}}\nabla u_{(j)}\right) \tag{4.26}$$

The expression for $\nabla\Phi$ can be easily obtained based on Table 4.1. For $\nabla I_{(1)}$ we shall have

$$\nabla I_{(1)} = \frac{dI_{(1)}}{d\lambda_1}\begin{pmatrix}\dfrac{\partial\lambda_1}{\partial x}\\ \dfrac{\partial\lambda_1}{\partial y}\\ \dfrac{\partial\lambda_1}{\partial z}\end{pmatrix} = \frac{dI_{(1)}}{d\lambda_1}\nabla\lambda_1 \tag{4.27}$$

From (3.122) we find that

$$\frac{dI_{(1)}}{d\lambda_1} = -\frac{1}{\left[E(\lambda_1)\right]^2\sqrt{\lambda_1^2-h^2}\sqrt{\lambda_1^2-k^2}} \tag{4.28}$$

We will discuss the expression of $\nabla\lambda_j$ later (given in (4.35) if one prefers). On the other hand, for $\nabla u_{(j)}$ we have

$$\nabla u_{(j)} = \frac{du_{(j)}}{d\lambda_j}\nabla\lambda_j \tag{4.29}$$

And it can be easily found that $\frac{du_{(j)}}{d\lambda_j}$ is given by

$$\frac{du_{(j)}}{d\lambda_j} = \frac{du_{(j)}}{d\Lambda_j}\frac{d\Lambda_j}{d\lambda_j} \tag{4.30}$$

with

$$\frac{du_{(j)}}{d\Lambda_j} = b_1 + 2b_2\Lambda_j \cdots + rb_r\Lambda_j^{r-1} \tag{4.31}$$

$$\frac{d\Lambda_j}{d\lambda_j} = -\frac{2\lambda_j}{h^2} \tag{4.32}$$

To express the acceleration, we find expressions for $\nabla\lambda_j$ in the following form

$$\nabla\boldsymbol{\lambda} = \nabla(\lambda_1\ \lambda_2\ \lambda_3) = \begin{pmatrix} \frac{\partial\lambda_1}{\partial x} & \frac{\partial\lambda_2}{\partial x} & \frac{\partial\lambda_3}{\partial x} \\ \frac{\partial\lambda_1}{\partial y} & \frac{\partial\lambda_2}{\partial y} & \frac{\partial\lambda_3}{\partial y} \\ \frac{\partial\lambda_1}{\partial z} & \frac{\partial\lambda_2}{\partial z} & \frac{\partial\lambda_3}{\partial z} \end{pmatrix} = \begin{pmatrix} d_1^1 & d_1^2 & d_1^3 \\ d_2^1 & d_2^2 & d_2^3 \\ d_3^1 & d_3^2 & d_3^3 \end{pmatrix} \tag{4.33}$$

Note that d_i^j means taking the derivative of λ_j with respect to the *i*th rectangular coordinate with *i*=1,2,3 indicating *x*,*y*,*z*, respectively.

However, though (3.9) gives the expressions of *x*,*y*,*z* as functions of λ_j, the reverse expressions could be formidably complicated. A practical yet seemingly mechanical method is to pursue

$$\nabla\boldsymbol{\lambda} = \begin{pmatrix} \frac{\partial x}{\partial\lambda_1} & \frac{\partial y}{\partial\lambda_1} & \frac{\partial z}{\partial\lambda_1} \\ \frac{\partial x}{\partial\lambda_2} & \frac{\partial y}{\partial\lambda_2} & \frac{\partial z}{\partial\lambda_2} \\ \frac{\partial x}{\partial\lambda_3} & \frac{\partial y}{\partial\lambda_3} & \frac{\partial z}{\partial\lambda_3} \end{pmatrix}^{-1} \tag{4.34}$$

After some derivations, one would eventually get

$$\nabla\boldsymbol{\lambda} = \begin{pmatrix} \dfrac{x(\lambda_1^2-k^2)(\lambda_1^2-h^2)}{\lambda_1(\lambda_1^2-\lambda_2^2)(\lambda_1^2-\lambda_3^2)} & \dfrac{x(k^2-\lambda_2^2)(\lambda_2^2-h^2)}{\lambda_2(\lambda_1^2-\lambda_2^2)(\lambda_2^2-\lambda_3^2)} & \dfrac{x(k^2-\lambda_3^2)(h^2-\lambda_3^2)}{\lambda_3(\lambda_1^2-\lambda_3^2)(\lambda_2^2-\lambda_3^2)} \\ \dfrac{y\lambda_1(\lambda_1^2-k^2)}{(\lambda_1^2-\lambda_2^2)(\lambda_1^2-\lambda_3^2)} & \dfrac{y\lambda_2(k^2-\lambda_2^2)}{(\lambda_1^2-\lambda_2^2)(\lambda_2^2-\lambda_3^2)} & \dfrac{-y\lambda_3(k^2-\lambda_3^2)}{(\lambda_1^2-\lambda_3^2)(\lambda_2^2-\lambda_3^2)} \\ \dfrac{z\lambda_1(\lambda_1^2-h^2)}{(\lambda_1^2-\lambda_2^2)(\lambda_1^2-\lambda_3^2)} & \dfrac{-z\lambda_2(\lambda_2^2-h^2)}{(\lambda_1^2-\lambda_2^2)(\lambda_2^2-\lambda_3^2)} & \dfrac{-z\lambda_3(h^2-\lambda_3^2)}{(\lambda_1^2-\lambda_3^2)(\lambda_2^2-\lambda_3^2)} \end{pmatrix} \tag{4.35}$$

Note that the element of d_1^3 comes with a singularity at $\lambda_3 = 0$. To address this issue, we rewrite d_1^3 as follows,

$$d_1^3 = sign(x)\frac{\lambda_1\lambda_2}{hk}\frac{(k^2-\lambda_3^2)(h^2-\lambda_3^2)}{(\lambda_1^2-\lambda_3^2)(\lambda_2^2-\lambda_3^2)} \tag{4.36}$$

And it follows that when $\lambda_3 = 0$, $d_1^3 = \dfrac{kh}{\lambda_1\lambda_2}$.

At this point, (4.26) can be evaluated without further trouble. The acceleration is given by, retrieving the notations for *n*,*m*

$$\mathbf{a}_{\text{EHS}} = \sum_{n}^{\infty}\sum_{m=1}^{2n+1} c_{nm}\frac{Y_n^m}{F_n^m(\rho_0)}\mathbf{Z}_n^m \tag{4.37}$$

and

$$\begin{aligned} \mathbf{Z}_n^m &= \frac{1}{Y_n^m}\nabla Y_n^m \\ &= \frac{1}{\Phi_n^m}\nabla\Phi_n^m + \frac{1}{I_n^m(\rho)}\nabla I_n^m(\rho) + \sum_{j=1}^{3}\frac{1}{u_n^m(\lambda_j)}\nabla u_n^m(\lambda_j) \end{aligned} \tag{4.38}$$

4.2.2 Gravitational gradient via ellipsoidal harmonics

The gravitational gradient is obtained by taking the gradient of (4.26), consider the case for given *n* and *m*,

$$\begin{aligned} \nabla\left(Y_n^m\mathbf{Z}_n^m\right) &= \mathbf{Z}_n^m\left(\nabla Y_n^m\right)^T + Y_n^m\nabla\mathbf{Z}_n^m \\ &= Y_n^m\mathbf{Z}_n^m(\mathbf{Z}_n^m)^T + Y_n^m\nabla\mathbf{Z}_n^m \end{aligned} \tag{4.39}$$

So the problem boils down to calculating $\nabla\mathbf{Z}_n^m$ which is a 3×3 symmetric matrix. The expression for $\mathbf{Z}_n^m$ is given in (4.38). Again we drop the *n*,*m* in the notations and use subscript '(*j*)' to denote the function being dependent solely on λ_j,

$$\nabla \mathbf{Z}_n^m = \frac{1}{\Phi}\left(-\frac{1}{\Phi}\nabla\Phi(\nabla\Phi)^T + \nabla(\nabla\Phi)\right) + \frac{1}{I_{(1)}}\left(-\frac{1}{I_{(1)}}\nabla I_{(1)}(\nabla I_{(1)})^T + \nabla(\nabla I_{(1)})\right) + \sum_{j=1}^{3}\frac{1}{u_{(j)}}\left(-\frac{1}{u_{(j)}}\nabla u_{(j)}(\nabla u_{(j)})^T + \nabla(\nabla u_{(j)})\right) \tag{4.40}$$

$\nabla I_{(1)}$ and $\nabla u_{(j)}$ are given by (4.27) and (4.29). Now we turn to how to evaluate the expressions $\nabla(\nabla\Phi)$, $\nabla(\nabla I_{(1)})$ and $\nabla(\nabla u_{(j)})$ in (4.40).

The elements in $\nabla(\nabla\Phi)$ are easily derived based on Table 4.1 and are omitted in our discussion. For $\nabla(\nabla I_{(1)})$, referring to (4.27),

$$\nabla(\nabla I_{(1)}) = \nabla(\nabla\lambda_1)\frac{dI_{(1)}}{d\lambda_1} + \nabla\lambda_1(\nabla\lambda_1)^T\frac{d^2 I_{(1)}}{d\lambda_1^{\,2}} \tag{4.41}$$

And the expression for $\frac{d^2 I_{(1)}}{d\lambda_1^{\,2}}$ can be directly derived from (4.28) as follows

$$\frac{d^2 I_{(1)}}{d\lambda_1^2} = -\frac{dI_{(1)}}{d\lambda_1}\left(\frac{2}{E_{(1)}}\frac{dE_{(1)}}{d\lambda_1} + \frac{\lambda_1}{\lambda_1^2 - h^2} + \frac{\lambda_1}{\lambda_1^2 - k^2}\right) \tag{4.42}$$

Let us remind ourselves that $E_{(1)}$ in (4.42) should not be taken for $u_{(1)}$, as $E_{(1)}$ also has a preceding factor that varies from one class to another, e.g., $\sqrt{\lambda_1^2 - h^2}$ for class L, $\sqrt{\lambda_1^2 - k^2}$ for M, and etc. When taking the derivative of $E_{(1)}$ this preceding factor must be taken into account. Similarly, (4.29) suggests that

$$\nabla(\nabla u_{(j)}) = \nabla(\nabla\lambda_j)\frac{du_{(j)}}{d\lambda_j} + \nabla\lambda_j(\nabla\lambda_j)^T\frac{d^2 u_{(j)}}{d\lambda_j^{\,2}} \tag{4.43}$$

$\frac{d^2 u_{(j)}}{d\lambda_j^{\,2}}$ can be calculated as

$$\begin{aligned}\frac{d^2 u_{(j)}}{d\lambda_j^{\,2}} &= \frac{d}{d\lambda_j}\left(\frac{du_{(j)}}{d\Lambda_j}\frac{d\Lambda_j}{d\lambda_j}\right)\\ &= \frac{d^2 u_{(j)}}{d\Lambda_j^{\,2}}\left(\frac{d\Lambda_j}{d\lambda_j}\right)^2 + \frac{du_{(j)}}{d\Lambda_j}\frac{d^2\Lambda_j}{d\lambda_j^{\,2}}\end{aligned} \tag{4.44}$$

where

$$\frac{d^2u_{(j)}}{d\Lambda_j^{\,2}} = 2b_2 + 3\cdot 2b_3\Lambda_j + \cdots r(r-1)b_r\Lambda_j^{r-2},\ \frac{d^2\Lambda_j}{d\lambda_j^{\,2}} = -\frac{2}{h^2} \tag{4.45}$$

So far all the expressions in (4.41) and (4.43) except $\nabla(\nabla\lambda_j)$ are known. On the other hand, $\nabla(\nabla\lambda_j)$ can be expressed as

$$\nabla(\nabla\lambda_j) = \begin{pmatrix} d_{11}^j & d_{12}^j & d_{13}^j \\ d_{21}^j & d_{22}^j & d_{23}^j \\ d_{31}^j & d_{32}^j & d_{33}^j \end{pmatrix} \tag{4.46-1}$$

with $d_{i,k}^j$ denoting the derivative of d_i^j with respect to the *k*th rectangular coordinate, i.e.,

$$\begin{aligned} d_{i,k}^j &= \sum_{l=1}^{3} \tilde{d}_{i,l}^j d_k^l, \\ \tilde{d}_{i,l}^j &= \frac{\partial(d_i^j)}{\partial\lambda_l} \end{aligned} \tag{4.46-2}$$

where d_i^j are given in (4.35). We note that there are three such matrices as in (4.46) that correspond to different λ_j. Last but not least, the total 27 expressions for $\tilde{d}_{i,l}^j$ can be directly derived from (4.35). However, as is the case for computing the acceleration, we again have to be concerned with singularities for $\lambda_3 = 0, h$ and $\lambda_2 = h, k$. For example, for several $d_{i,k}^j$ we need to remove λ_3 appearing in the denominator of $\tilde{d}_{i,l}^j d_k^l$. This issue will be discussed in Appendix C.

4.2.3 Two numerical issues encountered with the computation of ellipsoidal harmonics

The numerical scheme reviewed above come with several issues, of which two will be discussed as they have been encountered in our simulations. For a more comprehensive discussion on the numerical uncertainties of the EHS and the causes, readers are encouraged to refer to Garmier et al.[29]

Removing singularities in a certain integral

The factor $\sqrt{|\lambda_j^2 - h^2|}\sqrt{|\lambda_j^2 - k^2|}$ appears quite commonly in the denominator in

several integrals, causing singularities. For example, when evaluating the field coefficients c_{nm} in (3.115), we have to deal with the integral of the form

$$\int_h^k \int_0^h \frac{f(\mu,\upsilon)d\mu d\upsilon}{\sqrt{\mu^2-h^2}\sqrt{k^2-\mu^2}\sqrt{h^2-\upsilon^2}\sqrt{k^2-\upsilon^2}} \tag{4.47}$$

Since $0 \le \upsilon \le h$ and $h \le \mu \le k$, $\sqrt{\mu^2-h^2}$, $\sqrt{k^2-\mu^2}$ and $\sqrt{h^2-\upsilon^2}$ are all associated with singularities. One solution to this issue is to introduce different integration variables.

For the singularity associated with $\sqrt{h^2-\upsilon^2}$, we let

$$\upsilon = h\sin\theta,\ 0 \le \theta \le \frac{\pi}{2} \tag{4.48}$$

so that

$$\sqrt{h^2-\upsilon^2} = h\cos\theta,\ d\upsilon = h\cos\theta d\theta = \sqrt{h^2-\upsilon^2}d\theta \tag{4.49}$$

Therefore $\sqrt{h^2-\upsilon^2}$ cancels out in the integral.

For the singularities associated with $\sqrt{\mu^2-h^2}$ and $\sqrt{k^2-\mu^2}$, we first introduce

$$\mu = \sqrt{t^2+h^2},\ 0 \le t \le \sqrt{k^2-h^2} \tag{4.50}$$

Then

$$d\mu = \frac{t}{\mu}dt = \frac{\sqrt{\mu^2-h^2}}{\mu}dt \tag{4.51}$$

Therefore $\sqrt{\mu^2-h^2}$ is removed from the denominator. Finally we see that

$$\sqrt{k^2-\mu^2} = \sqrt{(k^2-h^2)-t^2}$$

And we let

$$t = \sqrt{k^2-h^2}\sin\vartheta,\ 0 \le \vartheta \le \frac{\pi}{2} \tag{4.52}$$

then

$$dt = \sqrt{k^2-h^2}\cos\vartheta d\vartheta = \sqrt{k^2-\mu^2}d\vartheta \tag{4.53}$$

Therefore we see that the last singularity of $\sqrt{k^2-\mu^2}$ in the integral is also cancelled out.

For $\rho \in [k,\infty]$ we rarely need to cope with the issue of singularity. Because, for

example, ρ will not be equal to k outside the reference ellipsoid of ρ_0.

Numerical singularities with normalization of Lamé's functions

Another numerical issue has been encountered when normalizing the Lamé's functions using (4.17) and (4.18). Sometimes 'Not-a-Number' result was produced in the coefficients of Lamé's functions, which was obviously caused by division by zero γ_n^p for some degrees and classes.

For example, when normalizing the Lamé's functions for the reference ellipsoid with axes of 20.5 km, 10.4 km and 7.5 km, γ_n^p turned out to be zero numerically for class L, M and N of degree 20. Let us first take a look at how these functions behave. Figure 4.1 clearly shows that the unnormalized functions seem far different from those in Figure 3.3. For example, the variation near the origin is ominously greater by order of 10^{14} than that towards $\lambda = \pm k$ where roots are tightly spaced in a narrow span of $0.05k \approx k - h$. Also, the difference of 10^{14} touches the precipice of 15 digit precision (which we used). Therefore we infer that the problem is with (4.18), i.e., $AB' - BA'$, and that this results from the subtraction of two great and close numbers leading to the loss of the significant digits.

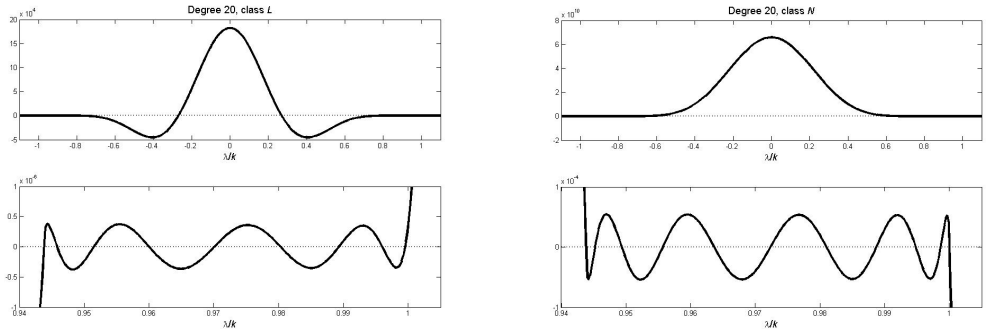

Figure 4.1 Behavior of one of the Lamé's functions for degree 20 class L (left) and N (right), in range from $-k$ to k (top) and from $0.94k$ to k (bottom).

A possible remedy is to use more significant digits since the computation and normalization of Lamé's functions are carried out only once. However, after an unsuccessful attempt to adopt this recipe with outdated versions of Fortran compilers, we retained the 15 digit precision, but resorted to an expedient approach. Namely, there is nothing that forbids us attempting to integrate (3.76) numerically to get γ_n^p

such as

$$\int_0^{\omega}\int_0^{\sigma}(\mu^2-\upsilon^2)\left[E_n^p(\mu)E_n^p(\upsilon)\right]^2 d\eta d\zeta = \tilde{\gamma}_n^p$$

Here we include the symbol '~' to explicitly indicate that such γ_n^p is numerically integrated. Even though it calls for more elaborate effort to rigorously validate this idea, our experience in simulations suggests that it at least alleviates the abrupt cancelling of trailing digits, since now the integration is performed incrementally over the reference ellipsoid.

On a further note regarding Figure 4.1, it is suggested that roots staying too close to one another may also be a stumbling block of applying the EHS beyond degree 15. Being unable to delve into this issue at this point, we found, based on our simulations afterwards that, the roots are numerically distinguishable up to degree 20 as far as the behavior of Lamé's functions is concerned. So even though the 15 digit precision may not accommodate the aforementioned large variation of some Lamé's functions which obviously could mar the result for that particular degree, we believe that such related errors are far from catastrophic.

In this chapter, we reviewed a favorable numerical scheme for applying the EHS to model the gravitational field of the attracting body. The first task is to compute the Lamé's functions not only distinguishing different classes but also according to the evenness of degree *n*. Based on the Lamé's functions computed this way, it is more desirable to represent the EHS modeled potential in the form of (3.118). The expressions for the gravitational acceleration and gradient need to be refurbished accordingly. In the next chapter we will apply the afore-discussed formulation of the EHS to model the gravitational field of the attracting body, and compare its performance with that of the SHS.

Chapter 5: Comparison of Spherical and Ellipsoidal Harmonics: Simulation Results on Modeling the Gravitational Field of Phobos and 433 Eros

In this chapter, we shall apply the SHS and EHS to model the gravitational field of two non-spherical attracting bodies, namely, the Martian moon Phobos and asteroid 433 Eros. As one of the two moons of Mars, Phobos is weakly gravitating and irregular-shaped, e.g., its apparent polar and equatorial flattening, many distinguished impact craters, and etc., all indicate distinct non-sphericity of the body. As of yet, the gravitational field of Phobos remains largely unknown due to the limitation of the quality as well as availability of observations. For example, while the mass and the mean density of Phobos has been determined to a certain accuracy (with a relative error on the order of 1%)[40], other characteristic parameters such as J_2, C_{22}, etc. are still elusive. Eros is the second largest known near-Earth asteroid (NEA)[9]. Partly owing to its close encounters with the Earth, Eros is one of the few small bodies that have been explored in detail. In particular, the spacecraft NEAR Shoemaker orbiting Eros in the year 2000 has enabled a successful attempt of recovering its gravity field[30,41]. As far as the shape is concerned, Eros is not only highly non-spherical but also more irregular than Phobos (Figure 5.1), thus regarded as a more typical example of irregular bodies in this work.

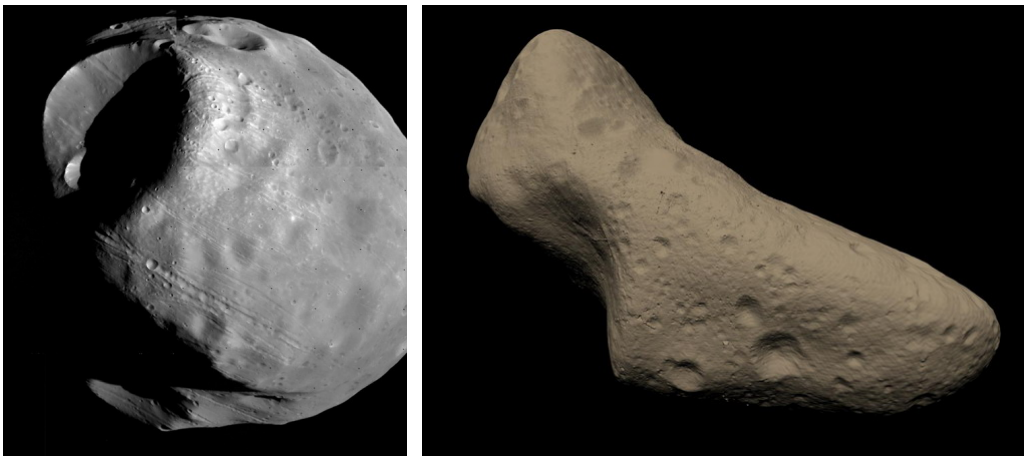

Figure 5.1 Phobos (left, credit: Bell, E. V., Viking project, JPL, NASA) and
433 Eros (right, credit: NEAR Project, NLR, JHUAPL, Goddard SVS, NASA)

5.1 Truth gravitational field via polyhedron method

The performance of either EHS or SHS will be assessed based on the discrepancies between their modeled gravitational field and the truth field. The truth field will be computed by the polyhedron method (PM)[42], which shall be briefly introduced in this part.

The PM essentially builds on the Gauss' divergence theorem. We use the rectangular coordinate system in which *X,Y,Z* are the coordinates for a differential volume *dV* of the attracting body, and *x,y,z* that for the field point P. The vector from P to *dV* is

$$\mathbf{r} = \begin{pmatrix} r_X & r_Y & r_Z \end{pmatrix}^T = \begin{pmatrix} X-x & Y-y & Z-z \end{pmatrix}^T \tag{5.1}$$

Using $\hat{\mathbf{r}}$ to denote the unit vector and r the magnitude of $\mathbf{r}$, it can be easily shown that

$$\nabla \cdot \hat{\mathbf{r}} = \frac{\partial}{\partial X}\left(\frac{r_X}{r}\right) + \frac{\partial}{\partial Y}\left(\frac{r_Y}{r}\right) + \frac{\partial}{\partial Z}\left(\frac{r_Z}{r}\right) = \frac{2}{r} \tag{5.2}$$

It follows that if the body has constant density, its gravitational potential can be calculated as follows

$$V = \iiint_v \frac{G\rho dv}{r} = \frac{G\rho}{2}\iint_S \nabla \cdot \hat{\mathbf{r}} dS = \frac{G\rho}{2}\iint_S \hat{\mathbf{n}} \cdot \hat{\mathbf{r}} dS \tag{5.3}$$

ρ is the density of the body (hopefully in this chapter distinguishable from the ellipsoid coordinate), and $\hat{\mathbf{n}}$ the unit out-pointing normal vector to the surface of *V*,

see Figure 5.2.

So (5.3) basically transforms the volume integral into surface integral over the body. The PM then seeks to approximate the attracting body as a polyhedron of a finite number of flat faces, in which case the integral in (5.3) can be arranged as

$$\iint_S \hat{\mathbf{n}} \cdot \hat{\mathbf{r}} dS = \sum_{i=1}^{N} \iint_{S_i} \hat{\mathbf{n}} \cdot \hat{\mathbf{r}} dS = \sum_{i=1}^{N} \hat{\mathbf{n}}_i \cdot \mathbf{r}_i \iint_{S_i} \frac{dS}{r} \tag{5.4}$$

where now the integer $1 \le i \le N$ refers to the *i*th face of the approximating polyhedron. We note that the dot product $\hat{\mathbf{n}}_i \cdot \mathbf{r}_i$ can be taken outside the integral as a constant because any $\mathbf{r}_i$ (from P to anywhere on the *i*th face) has the same projected length on $\hat{\mathbf{n}}_i$. On the other hand, the integral $\iint_{S_i} dS/r$ can be conveniently evaluated adopting the Green's theorem. In particular, when the face is a polygon, it can be shown that,

$$\iint_{S_i} \frac{dS}{r} = \sum_{j=1}^{M} \hat{\mathbf{n}}_{i,j} \cdot \mathbf{r}_{i,j} \int_{L_{i,j}} \frac{dL}{r} - \hat{\mathbf{n}}_i \cdot \mathbf{r}_i \omega_i \tag{5.5}$$

with subscripts of integer $1 \le j \le M$ denoting the *j*th edge associated with the *i*th face (polygon). And $\hat{\mathbf{n}}_{i,j}$ denotes the unit out-pointing normal vector to the *j*th edge and orthogonal to $\hat{\mathbf{n}}_i$, $\mathbf{r}_{i,j}$ is the vector from P to anywhere along the *j*th edge. ω_i is expressed as

$$\omega_i = \iint_{S_i} \frac{\hat{\mathbf{n}}_i \cdot \mathbf{r}_i}{r^3} dS \tag{5.6}$$

Usually one does not use (5.6) directly for computations, as ω_i can be interpreted as the signed area of the polygon projected onto the unit sphere centered at the field point or the solid angle (Figure 5.3 on the right). It is more straightforward to calculate ω_i based on this geometric meaning. The practical expressions, however, will not be discussed here.

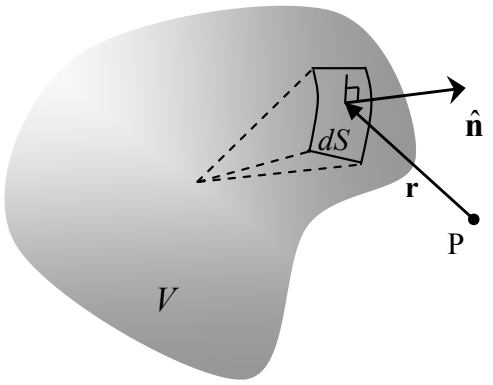

Figure 5.2 A differential surface *dS* in relation to the field point P

Even better, the curve integral in (5.5) now over a straight line can be expressed by an intrinsic function as

$$\int_L \frac{dL}{r} = \ln \frac{a+b+e}{a+b-e} \tag{5.7}$$

The scalar quantities *a*,*b*,*e* are illustrated in Figure 5.3 on the left.

So it is now understood that the gravitational potential of a polyhedron having constant density can be calculated exactly as follows

$$V = \frac{G\rho}{2} \sum_{i=1}^{N} \hat{\mathbf{n}}_i \cdot \mathbf{r}_i \left(\sum_{j=1}^{M} \hat{\mathbf{n}}_{i,j} \cdot \mathbf{r}_{i,j} \int_{L_{i,j}} \frac{dL}{r} - \hat{\mathbf{n}}_i \cdot \mathbf{r}_i \omega_i \right) \tag{5.8}$$

It is worth pointing out that, (5.2) is subject to singularities if the field point is on or inside the body, i.e., *r* may be zero. Therefore it is considered that (5.8) only strictly holds outside the attracting body[42]. Acceleration as well as gradient can also be conveniently expressed by the PM but the related discussions will be omitted here. Quite obviously, there is nothing that stands in the way of applying PM to varying density bodies, in which case one could decompose the body into different polyhedra and sum up the their respective resulting field.

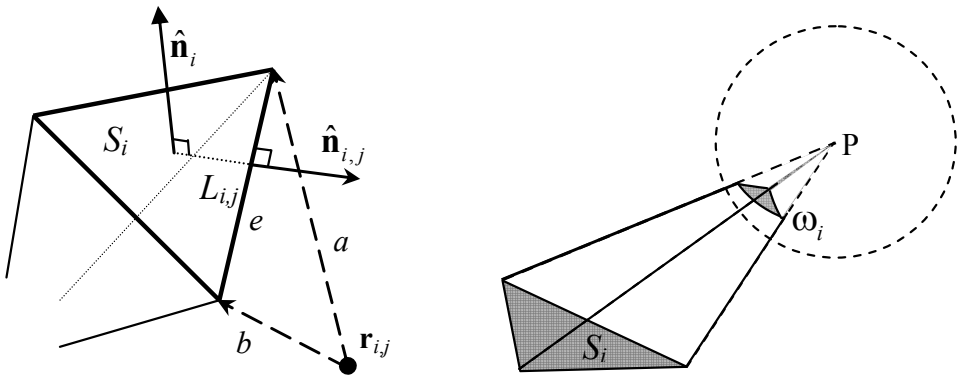

Figure 5.3 A field point in relation to a polygon on the body surface and its edges (left), and geometric meaning of ω_i (right)

Several practical expressions for PM can be greatly simplified if the body is approximated as a polyhedron consisting of triangular faces. In that case the entire body is broken up into a number of tetrahedra with the origin of the shape model as a common vertex. To find such polyhedron approximation of the body, one may find the Delaunay Triangulation (DT) useful.

We now almost come to the heart of the matter in this text. We shall approximate the shape of Phobos and Eros as two respective polyhedra. Since our goal is to assess the performance of the EHS and SHS for irregular-shaped bodies, with no loss of generality we adopt the constant density and apply the PM to simulate the truth field for both bodies. We are interested in the modeling errors, i.e., the deviations of results given by the EHS and the SHS from the truth.

5.2 Modeling the gravitational field of Phobos

A recent spherical harmonic shape model up to degree and order 17 is given by Willner[43], suggesting that the best-fitting ellipsoid of Phobos has three axes of 13.0 km, 11.4 km and 9.1 km, respectively. The gridded shape model for Phobos was obtained by discretizing the spherical harmonic model such as

$$r(\varphi,\lambda)=\sum_{n=0}^{N}\sum_{m=0}^{n}P_n^m(\sin\varphi)\left(A_{nm}\cos m\lambda+B_{nm}\sin m\lambda\right)$$

where r is the radii of the body as a function of latitude φ and longitude λ. A_{nm}, B_{nm} are the coefficients for the spherical harmonic model, and N=17 is the maximum

degree. The shape model with a grid interval of 5° in both latitude and longitude is shown in Figure 5.4 on the left. The polyhedron model, based on the shape model with a grid interval of 10°, is illustrated on the right. 1.876 g/cm^3 is used for the density of Phobos[40].

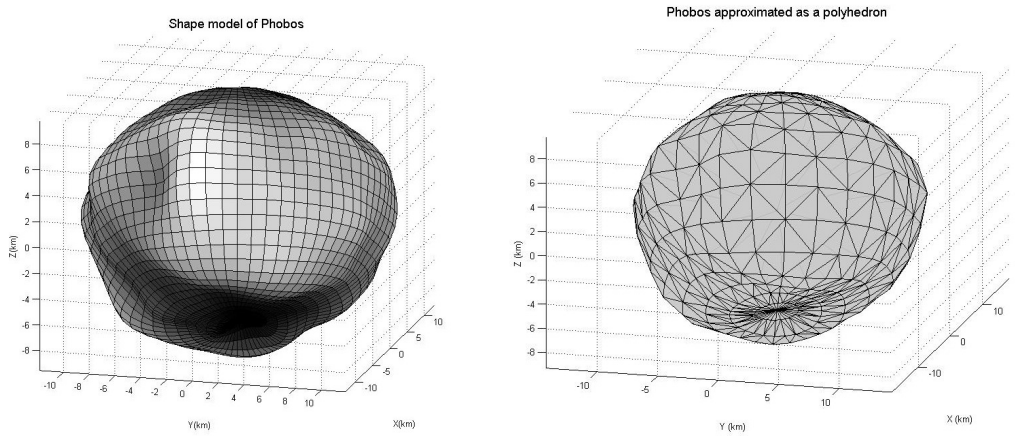

Figure 5.4 Shape model of Phobos (left), and Phobos approximated by a polyhedron (right)

5.2.1 Gravitational field via spherical harmonics on reference sphere

In this part we shall first look at how the SHS can be used to represent the gravitational field of Phobos. The reference sphere we choose is centered at the origin of the shape model and has a radius of 14 km, ensuring that the polyhedron has no vertex on or outside the reference sphere. We need to point out that this reference sphere is by no means intended to be the best choice, e.g., not the smallest sphere to the body.

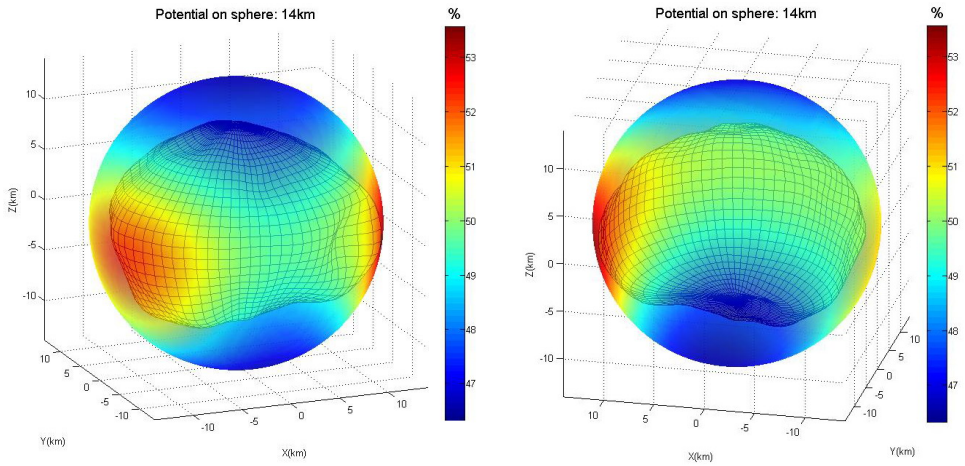

Figure 5.5 Gravitational potential on reference sphere with different views

Gravitational potentials

Using the PM, we obtained the gravitational potential on the reference sphere of 14 km as shown in Figure 5.5. The shape model is also plotted in order to better illustrate the correlation of the topography and the gravitational potential. As we have assumed that Phobos has constant density, the most powerful relation is that, the closer the body surface is to the reference sphere, the greater the potential is. The PM derived potential on the reference sphere is then used in (2.24) (for V) to calculate the field coefficients C_{nm}, S_{nm} up to degree and order 20. Specifically, V is obtained at a 100×200 grid in latitude and longitude. The resolution of the grid for V is obviously higher than that can be accounted for by the SHS up to degree 20. However, it is intended to reduce the integration error when applying (2.24), so as to prevent it from affecting the modeling error. The field coefficients for the SHS are then used in (2.22) for "backtracking" the potential of Phobos.

It would be natural to first look at the evaluated potential on the reference sphere, and see how it differs from that evaluated by the PM from which we derived the coefficients. We first look at the case of using the SHS up to degree 10 for modeling. The relative errors of the SHS in percentage are shown in Figure 5.6 as function of latitude and longitude.

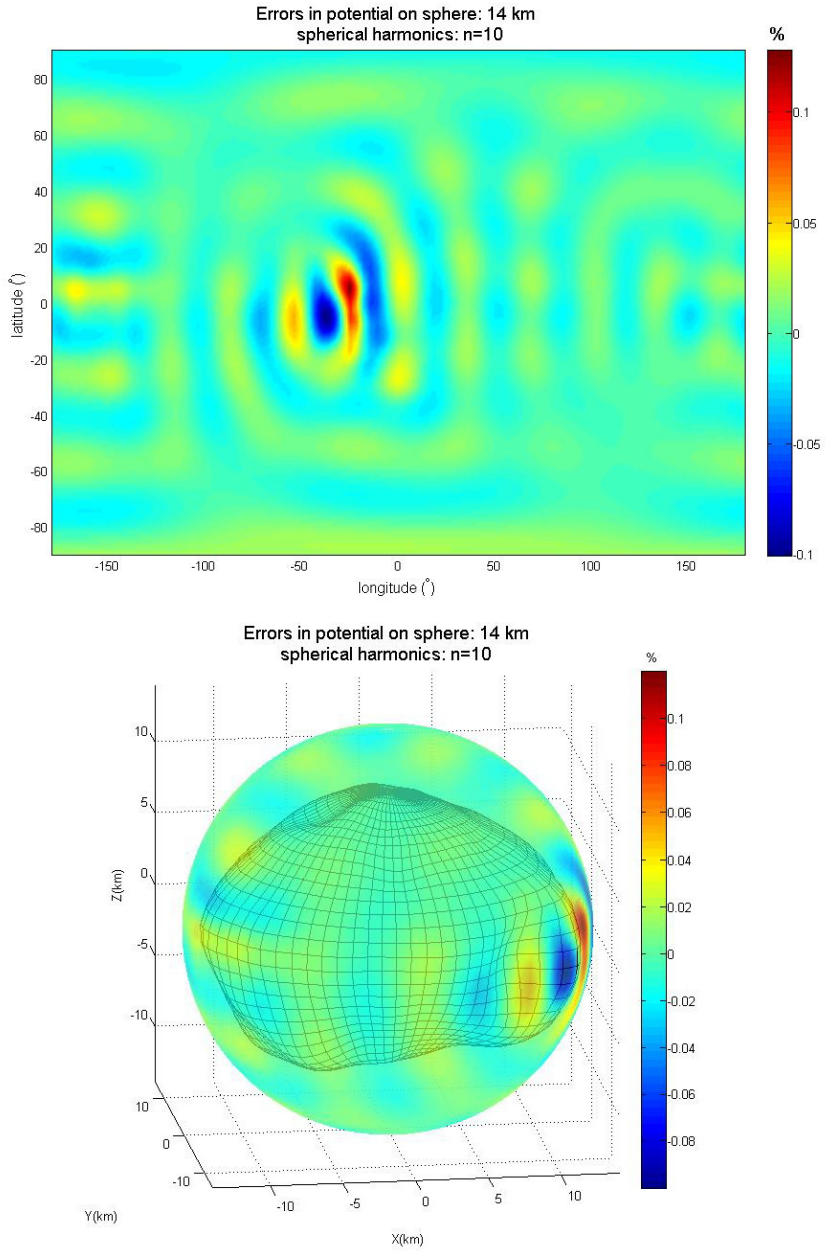

Figure 5.6 Errors in potential via spherical harmonics up to degree 10 (top); errors represented on the reference sphere (bottom)

First of all, we observe that the errors on average are on the order of 0.01%, with distinct corrugated pattern or ringing effect that is expected to have resulted from the truncation of the SHS at degree 10. E.g., the dominant contribution seems to correspond to n=11 or greater. On the other hand, the errors are altogether evenly distributed, i.e., fluctuating around zero. One area near (-40°,0°), as (longitude,latitude), shows most pronounced ringing effect with the errors reaching

the maximum of over 0.1%. To understand the reason of this observation, it is useful to look at Figure 5.6 at the bottom. Clearly, this area is where the reference sphere is the closest to the body of Phobos. In addition, we notice that a major crater of Phobos named Stickney is also located in the vicinity, adding to the high variability of the local gravitational field.

Next we increase n up to 20. The overall errors (Figure 5.7) decrease to 0.001%. While the corrugated pattern is still present, now the dominant frequencies correspond to those values of n greater than 20 that have not been accounted for. At the same time, we notice that again the SHS seems to be faltering near Stickney, as is the case for n=10.

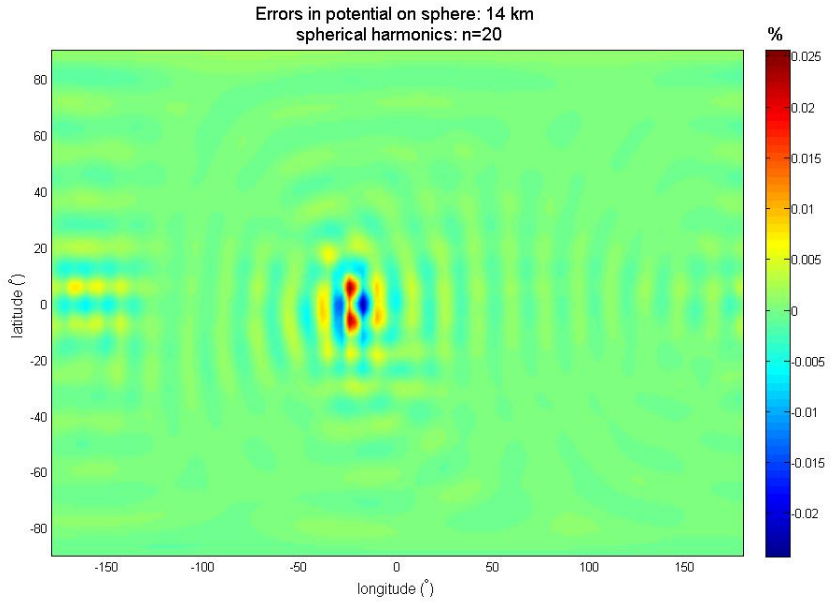

Figure 5.7 Errors in potential via spherical harmonics up to degree 20

Gravitational acceleration

For the gravitational acceleration, we shall look at the magnitude of errors in acceleration instead of each component. Figure 5.8 shows the distribution of the degree-10 SHS errors in latitude and longitude. Just as the case for the potential, errors in acceleration appear notably greater near (-40°,0°) where the topographic surface gets closer to the reference sphere. The most marked area is around Stickney.

Again the larger variations should be due to that the body is closer to the reference surface so that the topography more significantly affects variation of the gravitational field. The gridded pattern of errors in acceleration exhibits higher-frequency behavior than that in potential. This should be attributed to the fact that the acceleration is related to the differentiation of the potential, thus the higher-frequency errors are amplified. On average, the errors in the modeled acceleration reach the level of 0.1%, one order of magnitude greater than in the potential. On the other hand, using the SHS up to degree 20 sees errors decrease by one order of magnitude, though the peak errors have not been substantially abated (Figure 5.9).

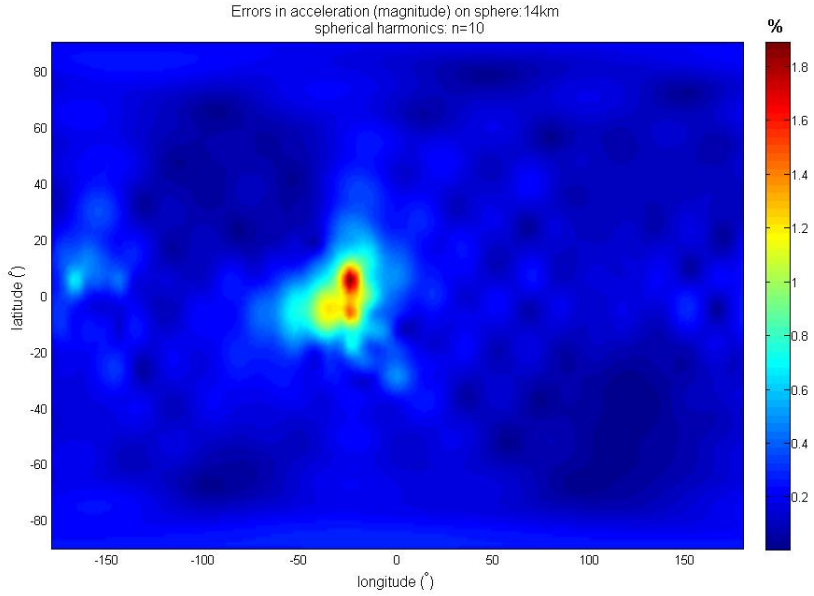

Figure 5.8 Errors in acceleration (magnitude) via spherical harmonics up to degree 10

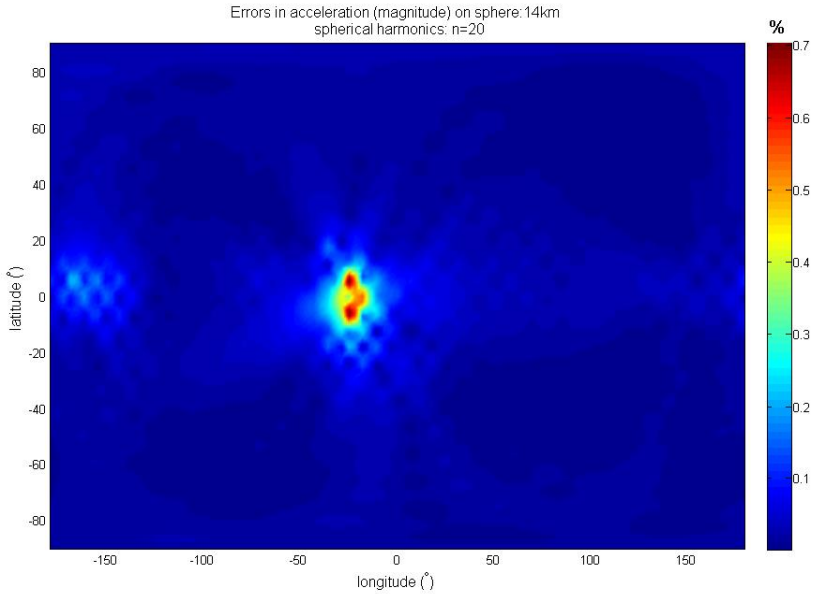

Figure 5.9 Errors in acceleration (magnitude) via spherical harmonics up to degree 20

5.2.2 Gravitational field via ellipsoidal harmonics on reference ellipsoid

Now we turn to the ellipsoidal harmonics. First, we chose the reference ellipsoid that has three axes of 14.5 km, 12.5 km and 10.5 km, respectively. The ellipsoid is centered at the origin of the shape model. We stress again that the choice of reference surface is not unique; the only rule to follow is that it must contain the entire body thus the total mass. Nevertheless it is always desirable to have the reference surface fit the body snugly to reduce the space between the reference surface and the body where the EHS (or SHS) might suffer errors due to divergence.

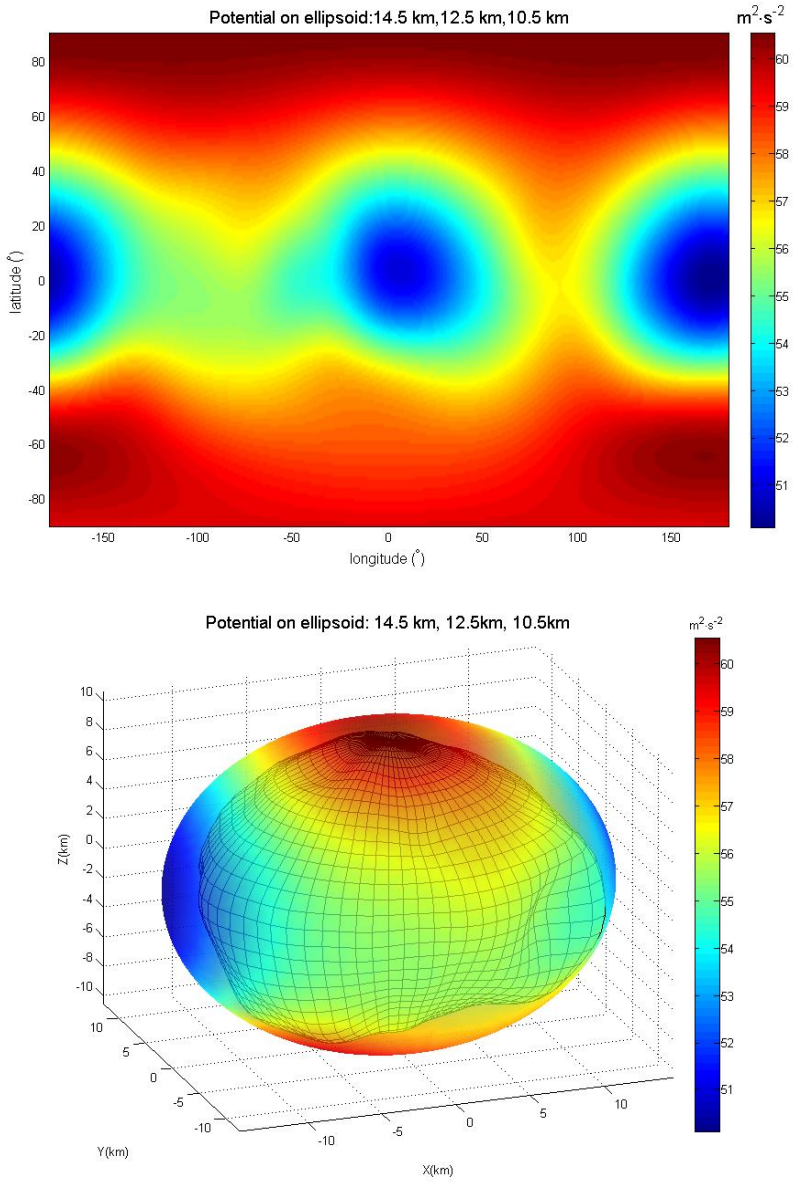

Figure 5.10 Gravitational potential on reference ellipsoid; potential represented on the reference ellipsoid (bottom)

Gravitational potential

The PM evaluated gravitational potential on the reference ellipsoid is shown in Figure 5.10. First of all, it is interesting to note the difference between Figure 5.5 and 5.10, in the former of which the potential is given on the reference sphere. Evidently, the ellipsoid being tri-axial in this case is a more arbitrary surface and thus is more apt to be a good-fitting surface to the shape of Phobos, even more so for the more irregular bodies. Since the ellipsoid overall would somewhat hug the topography

more closely, quite interestingly, the two formerly higher potential areas located along the equator where topography is outstretched to reach the reference sphere, now have become subsided on the reference ellipsoid. Obviously because along the semi-major axis the distance on the ellipsoid from the body's center of mass[1] (CoM) is the greatest. In this case, distance overwhelms the variation of topography in shaping the gravitational field.

The PM derived potential is used in (3.117) (for V) for evaluating the field coefficients c_{nm} for the EHS up to degree 20. For comparison, V is given on a 50×50 grid in υ and μ, respectively, which corresponds to 100×200 grid in latitude and longitude. The field coefficients are then substituted in (3.118) for gravitational field modeling.

We assess the errors of the EHS in the same way by comparing the EHS modeled potential with the true values. For the EHS up to degree 10, the errors in potential are plotted in Figure 5.11. Errors appear uniform in the sense that the variations over the entire ellipsoid are comparable. The peak errors now are present both near Stickney and another area around (180°,-50°). Referring to Figure 5.10, we could certainly tell that this area is very close to the reference ellipsoid. Therefore we infer that the larger errors in these areas are to be accounted for by the more pronounced topographic variations.

On the other hand, the errors are generally on the order of 0.01% with the exception of the two peak areas. We argue that it is not really reasonable to compare the EHS errors with that of the SHS, because the potentials are different on different surfaces, as is suggested by the comparison of Figure 5.5 and 5.10. Errors in potential for the EHS up to degree 20 are plotted in Figure 5.12 for comparison. The errors are reduced to the level of 0.001%; the improvement seems comparable to that for the SHS.

[1] The CoM of the polyhedron model for Phobos is offset from the origin by 106.5 m.

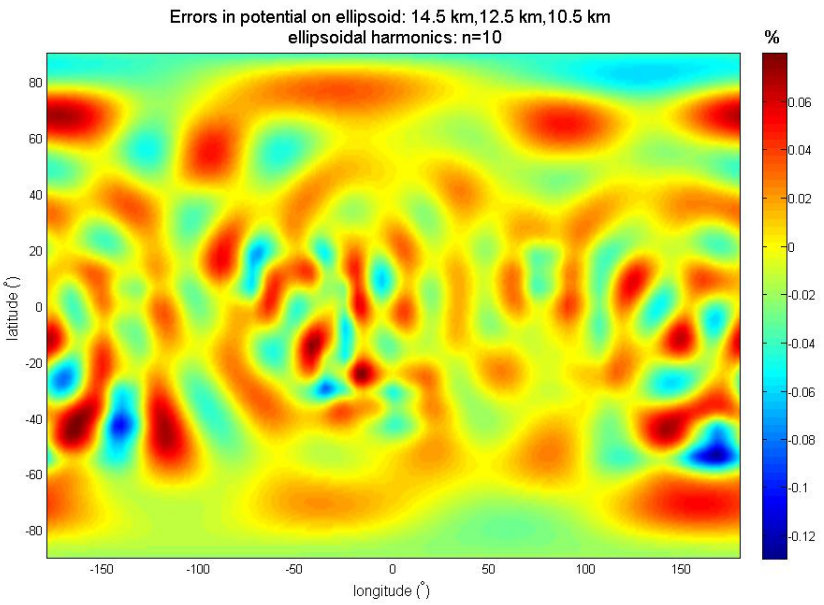

Figure 5.11 Errors in the EHS modeled potential up to degree 10

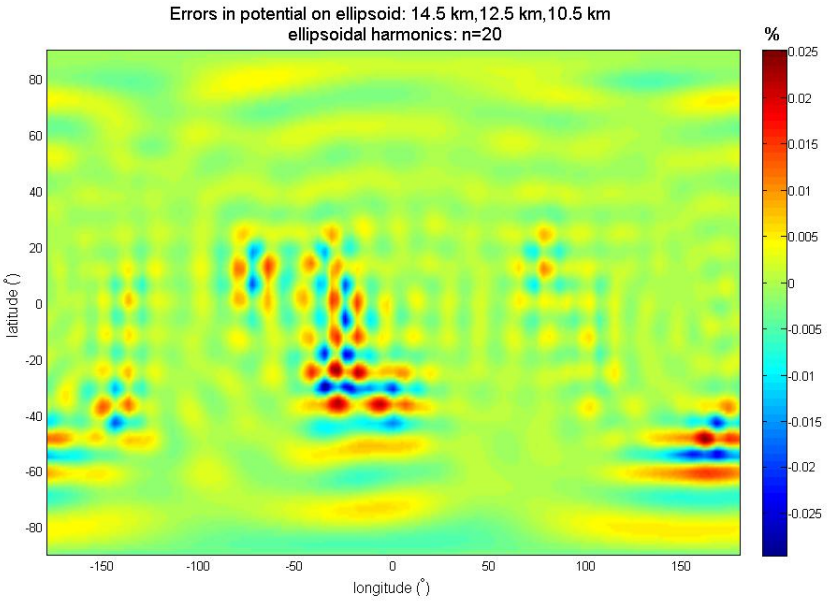

Figure 5.12 Errors in the EHS modeled potential up to degree 20

Gravitational acceleration

The relative errors of modeling the gravitational acceleration via the EHS up to degree 10 are in general on the order of 0.1%, but with peak errors in the same areas as the case of the potential (Figure 5.13). Increasing the maximum degree up to 20 causes an overall decrease of errors, as well as more even error distribution except the peak areas (Figure 5.14). The gridded pattern of errors, with higher-frequency variations than that for the potential, is also well observed with the errors in the SHS modeled acceleration, due to the ringing effect and the fact that the acceleration is related to the differentiation of the potential.

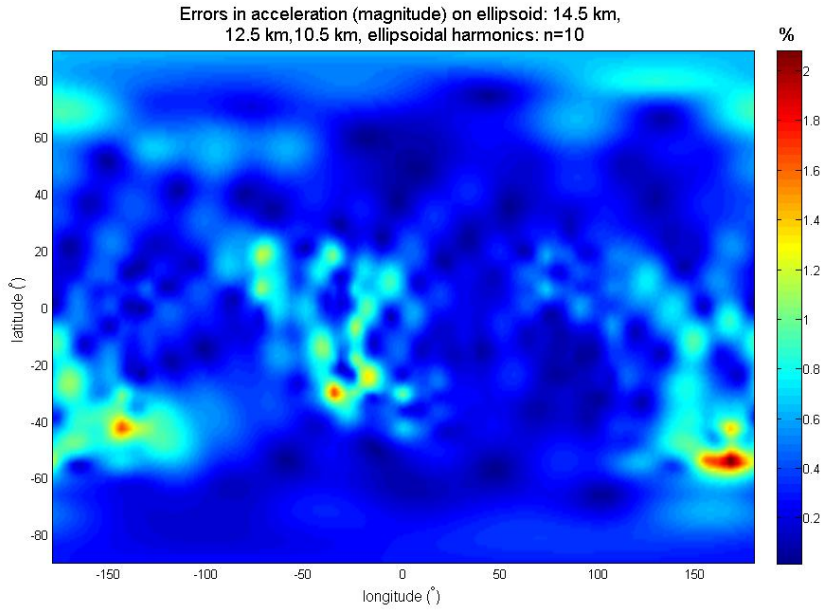

Figure 5.13 Errors (magnitude) in the EHS modeled acceleration up to degree 10

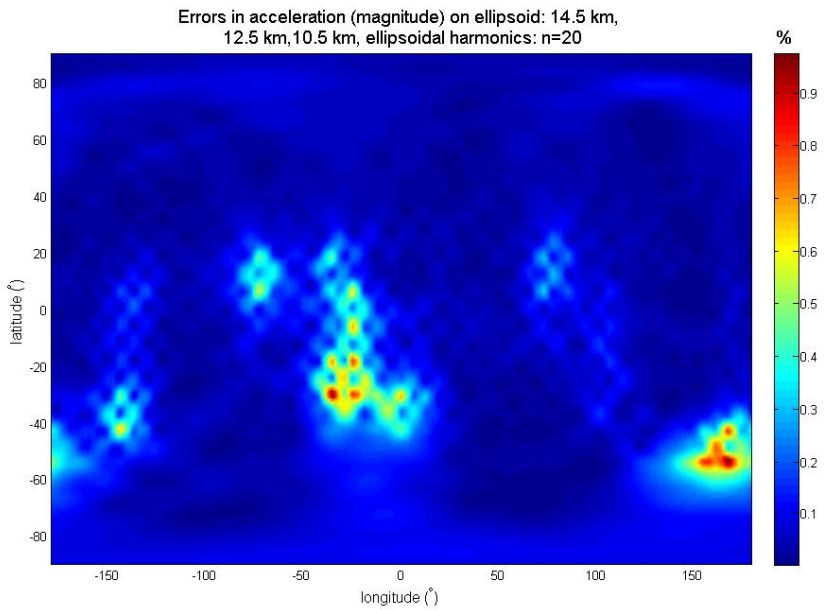

Figure 5.14 Errors (magnitude) in the EHS modeled acceleration up to degree 20

5.2.3 Comparison of spherical and ellipsoidal harmonics on arbitrary surfaces

So far we have merely looked at the performance of SHS and EHS on their respective reference surfaces. It would be difficult to compare more comprehensively the performance of the two algorithms. In this section, we shall use the SHS and EHS to model the gravitational field on more arbitrary but common surfaces that are favorable for comparison. Specifically, there are three cases to be considered: 1) EHS on the reference sphere; 2) SHS on the reference ellipsoid; 3) EHS and SHS on the topographic surface. The reference sphere has radius of 14 km, and the ellipsoid has three axes of 14.5 km, 12.5 km and 10.5 km. Therefore neither is contained entirely in the other (Figure 5.15). This is desired since it allows us to investigate both algorithms outside their respective regions of uniform convergence for case 1) and 2). On the other hand, the topographic surface is inside both reference surfaces, thus inside the divergence regions for both. We shall be able to observe how tolerant or error-prone the SHS and EHS are.

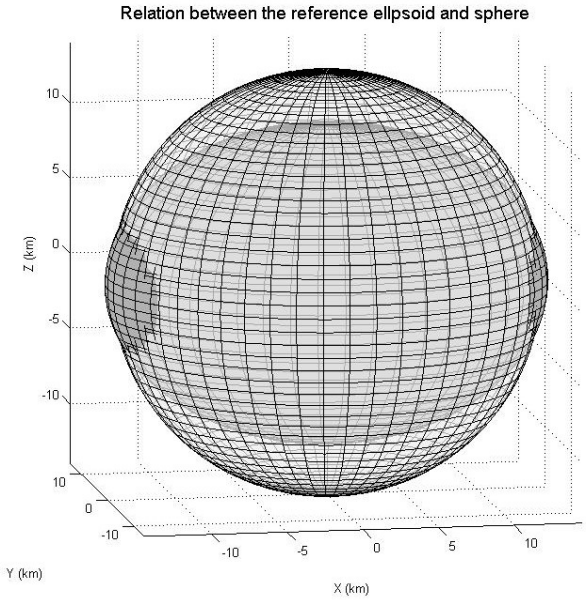

Figure 5.15 The geometric relation between the reference ellipsoid and sphere

Gravitational field via ellipsoidal harmonics on reference sphere

The radius of the reference sphere is 14 km, greater than the two semi-minor axes of 10.5 km and 12.5 km for the ellipsoid, but the sphere is inside the ellipsoid at the two ends of the semi-major axis of 14.5 km. Figure 5.16 shows the relative errors of EHS up to degree 10 in the potential. It is quite obvious that the EHS is less suited to modeling the potential near the semi-major axis, i.e., near (0°,0°) and (180°,0°). The errors in percentage reach the maximum of 0.1%, which, if not notably smaller, are at least comparable to the errors of the SHS as shown in Figure 5.6. However, Figure 5.17 shows the case for degree up to 20, where we observe that the errors are significantly reduced overall, and the peak errors decrease from 0.08% to 0.02%. This improvement suggests that the EHS remains quite reliable on the reference sphere, and, reassuringly, inside its divergence region.

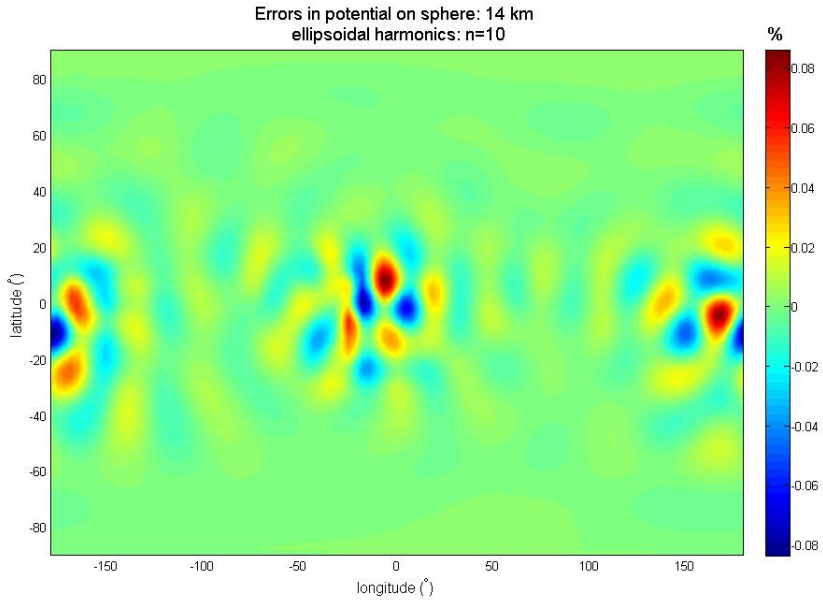

Figure 5.16 Errors in the EHS modeled potential up to degree 10 on reference sphere

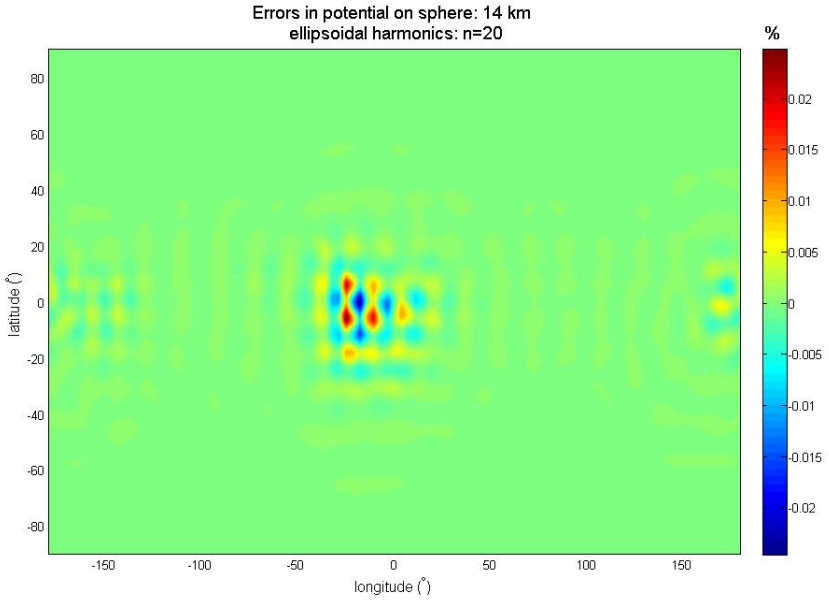

Figure 5.17 Errors in the EHS modeled potential up to degree 20 on reference sphere

Gravitational field via spherical harmonics on reference ellipsoid

Since the reference ellipsoid is for the most part inside the reference sphere, intuitively, this will put the SHS to the test, as it will be applied outside its convergence region. The errors in the SHS modeled potential are plotted in Figure

5.18 and 5.19, for up to degree 10 and 20, respectively. In both cases, the pattern of errors is markedly different from that previously observed. Now the errors show clear dependence on latitude, increasing from 0.01% in the lower latitudes (<50°) to 0.1% near the poles. This pattern is hardly unexpected, since the departure of the sphere from the ellipsoid is the greatest at the poles. On the other hand, around the equator along the semi-major axis the ellipsoid overlies the sphere, and the SHS performs normally. Along the semi-minor axis of the equator, though the ellipsoid falls underneath the sphere, the SHS does not seem to experience significant divergence in this case.

We also note that increasing the maximum degree does not yield any improvement in performance for the SHS over higher latitudes. On the contrary, the peak errors have indeed grown a bit rather than diminished. This further verifies that errors at the higher latitudes are due to divergence of the algorithm when the factor R/r is greater than unity. In this case, with $\left(\frac{R}{r}\right)^n$ being an intensifying rather than an attenuating factor, the higher the degree, the more liable is the SHS to diverge.

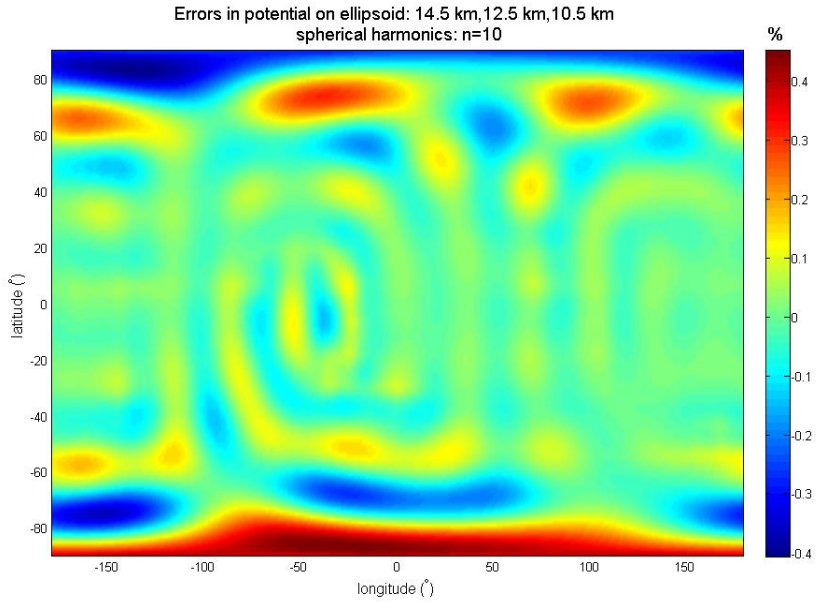

Figure 5.18 Errors in the SHS modeled potential up to degree 10 on reference ellipsoid

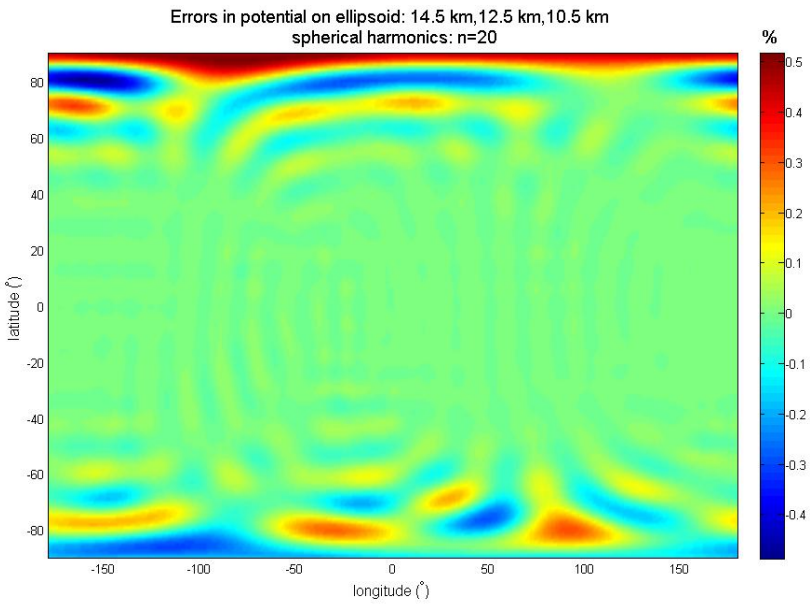

Figure 5.19 Errors in the SHS modeled potential up to degree 20 on reference ellipsoid

While the EHS is just as consistent on the reference sphere as on the reference ellipsoid, the SHS is clearly less reliable on the reference ellipsoid, particularly in higher latitudes where the ellipsoid resides in the divergence area. We have discussed and understood that such errors due to divergence cannot be lessened by increasing the degree of expansion. As a matter of fact, increasing the degree may be aggravating the divergence as the attenuation factor up to higher power, if greater than one, amplifies errors more severely.

Spherical and ellipsoidal harmonics on the surface of Phobos

A cross check was carried out above on the consistency of the EHS and SHS on a mutual surface, i.e., EHS on the reference sphere and SHS on the ellipsoid. It is of interest to know the accuracy of the modeled gravitational field near the surface of the body. For instance, calculating the landing trajectory of a spacecraft on an asteroid, analyzing the movement of surface materials of the body[44], and so forth, would all benefit from this kind of practice.

The entire body is enclosed by both reference surfaces. Both algorithms will be tested in their respective divergence regions. Again the PM is used to generate the

truth field near the surface of Phobos. In our simulation, we chose the evaluation points to be 0.1 meters above the polydedral surface, so as to guarantee they are all unequivocally outside the polyhedron. Figure 5.20 shows the relative errors in the EHS and the SHS modeled potentials, respectively, up to degree 10. The peak errors of the EHS are around 1%, and located at two known regions at the equator where the surface is the closest to the reference sphere. Let us refer to Figure 5.16 for comparison, on the reference sphere near the same locations the errors in the EHS modeled potential are at the level of 0.1%. As the body surface lies further below the reference sphere, we regard the 1% errors in this case as a sign of divergence for the EHS on the body surface. In other areas, errors are well bounded, overall on the order of 0.01%. A notable exception is the expansive area near the South Pole as shown in Figure 5.20 at the top, where errors are above 0.1%. This should be accounted for by the fact that around the South Pole the topography is distinctly caved in, thus altogether more distant from the reference ellipsoid.

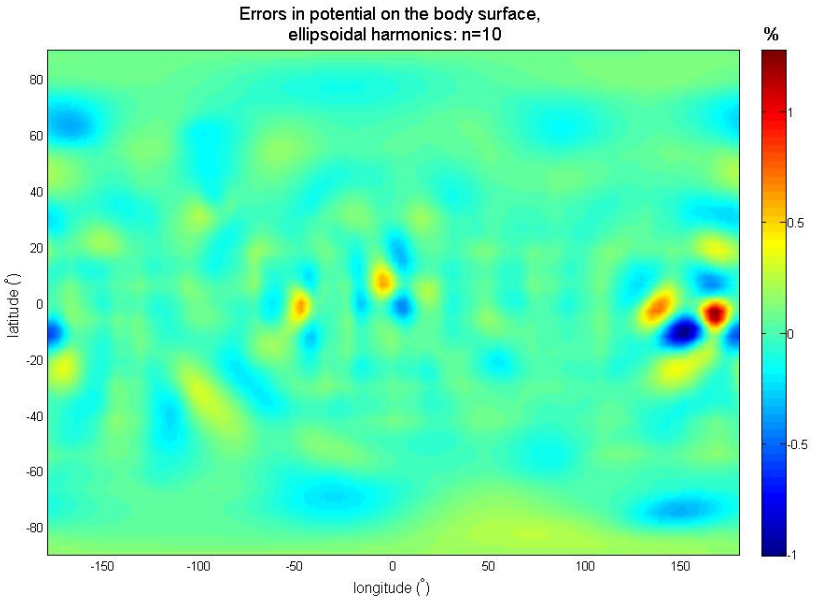

Continued

Figure 5.20 Comparison of errors in the EHS (top) and SHS (bottom) modeled potentials up to degree 10 on the body surface

Figure 5.20 continued

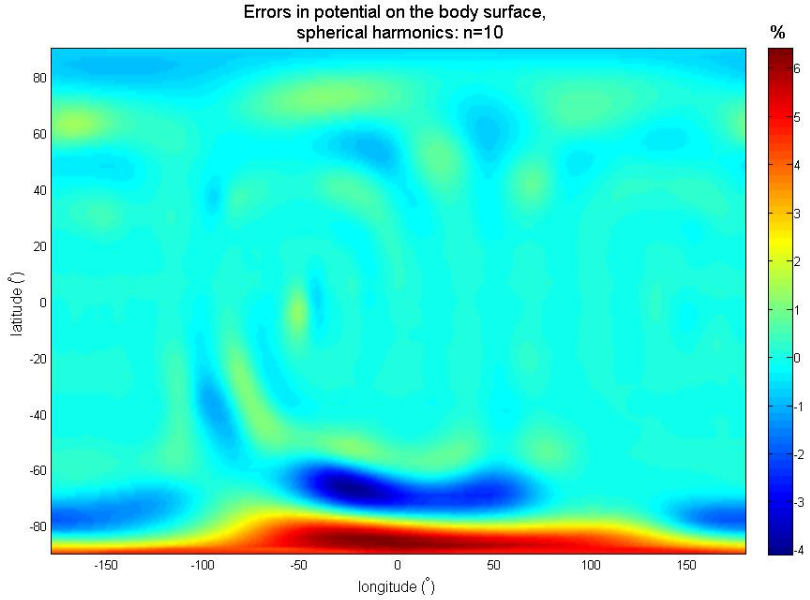

On the other hand, also near the South Pole, the SHS is hard put to tracing the field variations due to divergence with errors reaching over 1%. It is not unreasonable to infer that the topographic subsidence at the South Pole also intensifies the errors, as they do not appear as significant near the North Pole. Other than the higher latitudes, the SHS is more or less consistent with the usual, mildly undulating error pattern that we have already seen.

A more straightforward comparison of EHS and SHS errors is given in Figure 5.21, in which the errors ranging from -1% to 1% are emphasized. The figure on the right clearly shows that the SHS is an inaccurate model near the poles. Whether SHS should be used in these areas would probably depend on the error budget of the application.

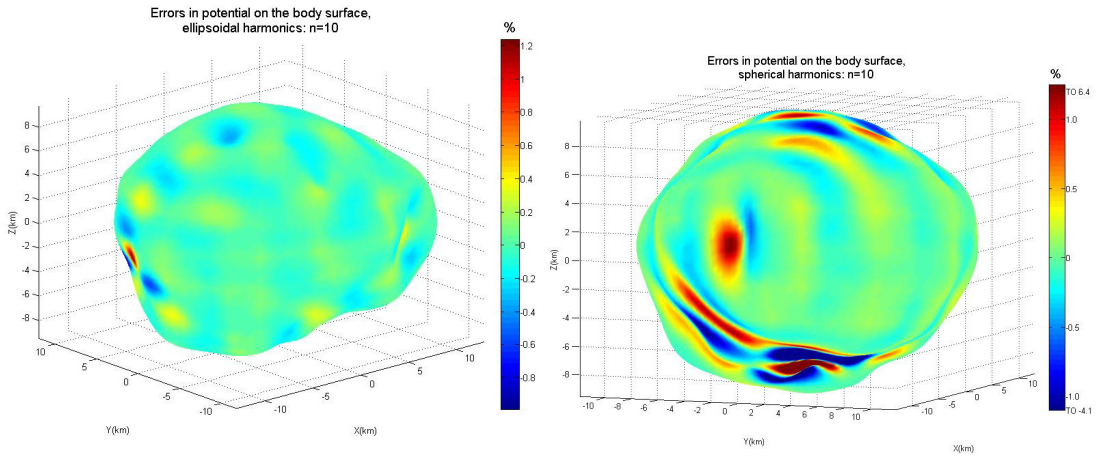

Figure 5.21 Same comparison as in Figure 5.20, with errors represented on the body surface

The errors in acceleration of the two algorithms up to degree 10 are shown in Figure 5.22. For the EHS, again the errors are one order of magnitude greater than that in the potential. The peak errors of over 20% appear at one of the most severe locations of divergence. Other scattered error-prone spots include one near the South Pole centered at (150°,-80°), and another near Stickney. If we refer back to Figure 5.20, these locations can also be discerned in the error map for the potential, though less distinguishable. For the SHS (Figure 5.22 at the bottom), the errors now exceed 100% around the South Pole and overwhelm those in other areas, where the errors could be on the order of 10% at worst. Based on this, we conclude that it would be inappropriate to use the SHS to model the field near the surface, at least not for evaluating the gravitational acceleration.

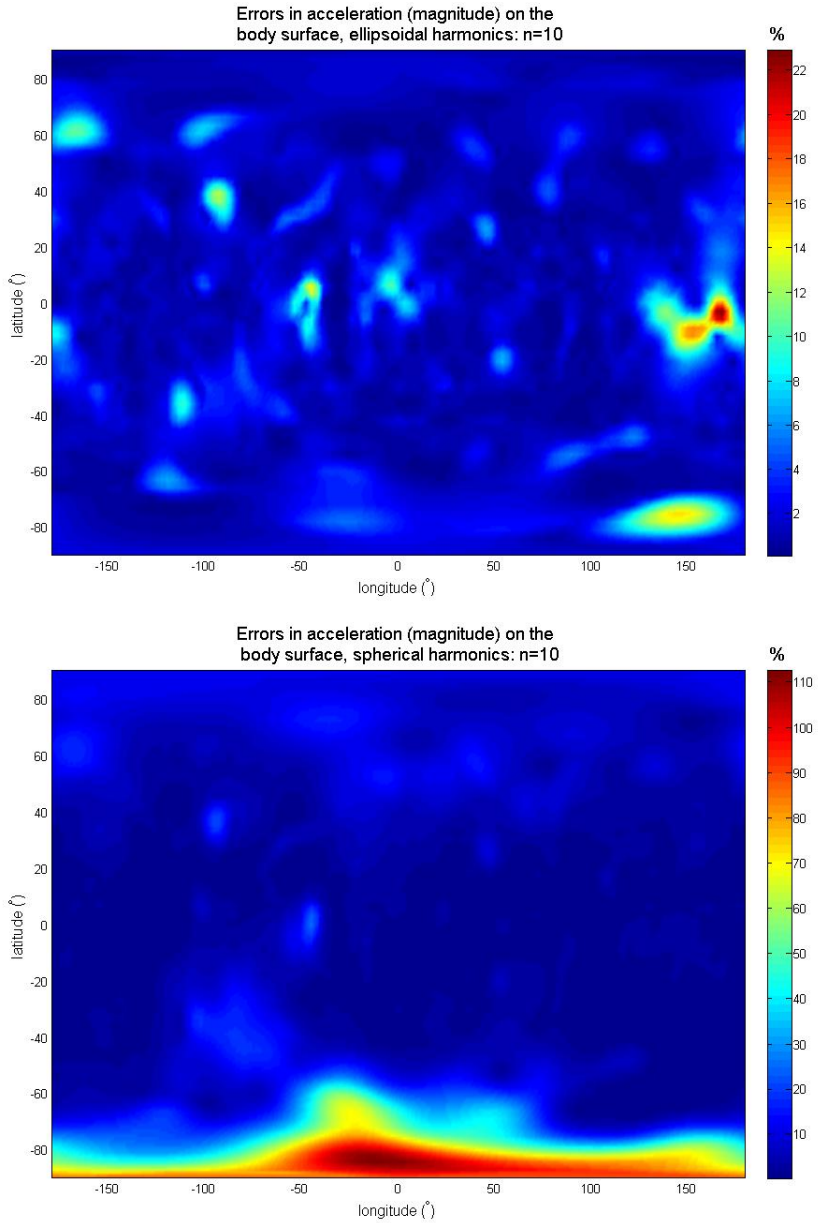

Figure 5.22 Comparison of errors (magnitude) in the EHS (top) and SHS (bottom) modeled accelerations up to degree 10, on the surface of Phobos

5.3 Modeling the gravitational field of 433 Eros

We investigated the EHS and SHS modeled gravitational field for Phobos, whose figure cannot be closely fitted by a sphere. However, Phobos is hardly as irregular as numerous asteroids, comets, and so on, in our solar system. Eros is, as far as the contents in this text are concerned, a more representative case for the non-spherical bodies. We use the spherical harmonic shape model for Eros given by Zuber[45], and

the gridded shape model of Eros with a resolution of 2° in both latitude and longitude is shown in Figure 5.23 on the left. To obtain the polyhedral approximation of Eros, we discretize the spherical harmonic model using grid interval of 10° in both latitude and longitude; the triangulation of the resulting vertices yields a 900-facet polyhedron model as shown in Figure 5.23 on the right. The density for Eros[41] is taken to be 2.67 g/cm^3.

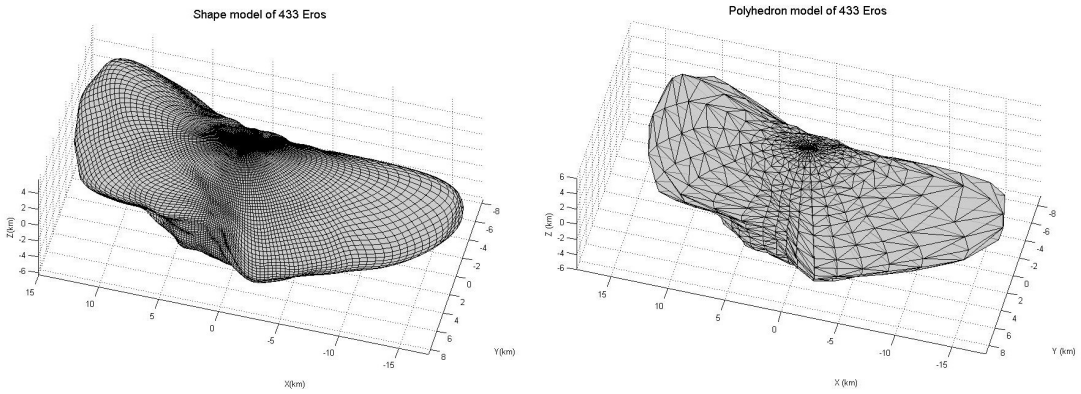

Figure 5.23 Shape and polyhedron (right) models of 433 Eros

5.3.1 Gravitational field via ellipsoidal harmonics on reference ellipsoid

The reference ellipsoid for Eros is centered at the origin of the shape model, and has three axes of 22.7 km, 10.4 km and 7.5 km, respectively. Other ellipsoids could be used so long as they contain the entire figure. The true potential of Eros on the reference ellipsoid is shown in Figure 5.24. The potential appears dominantly affected by the distance from the CoM of the body[1]: the greater the distance, the smaller the potential. Around the poles the potential is the greatest, whereas at the two ends of the semi-major axis it is the smallest.

[1] The CoM of the polyhedron model for Eros is offset from the origin by roughly 140 m.

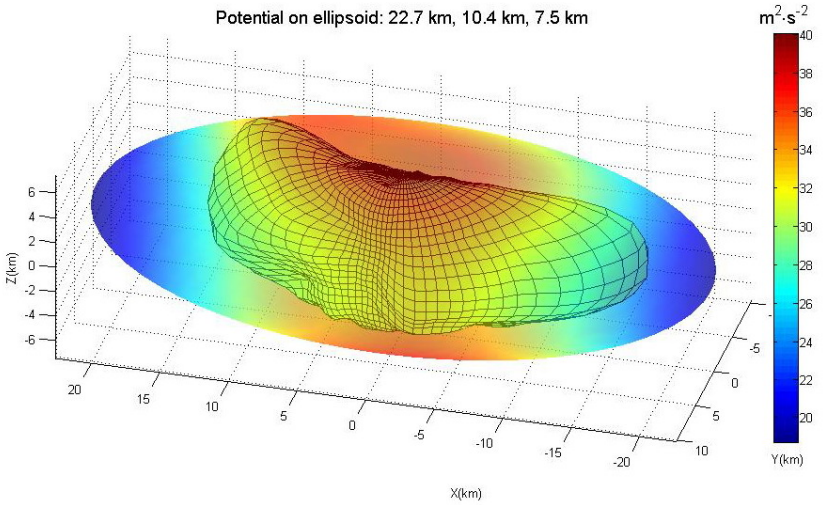

Figure 5.24 The PM derived true potential of Eros on the reference ellipsoid

The resolution of the PM derived potential on the reference ellipsoid for evaluating the field coefficients for Eros is the same as for Phobos. The errors in the degree-10 EHS modeled potential and acceleration on the ellipsoid are depicted in Figure 5.25. For a very rough comparison, we note that the errors in potential in general are greater than for the similar case of Phobos (Figure 5.11), where errors did not exceed 0.1%, compared to over 1% for Eros. Also, errors in Figure 5.25 exhibit variations over large areas on the order of 0.1%, with the maximum occurring along the semi-major axis. The area between -50° and 15° in longitude experiences more uncertainties. We believe that it is due to the outthrust topography towards the ellipsoid, a phenomenon also observed for Phobos. The peak errors in acceleration appear in the same regions reaching above 25% of the total magnitude. While in other areas they are generally at the 1% level. For comparison the error map for EHS up to degree 20 is shown in Figure 5.26.

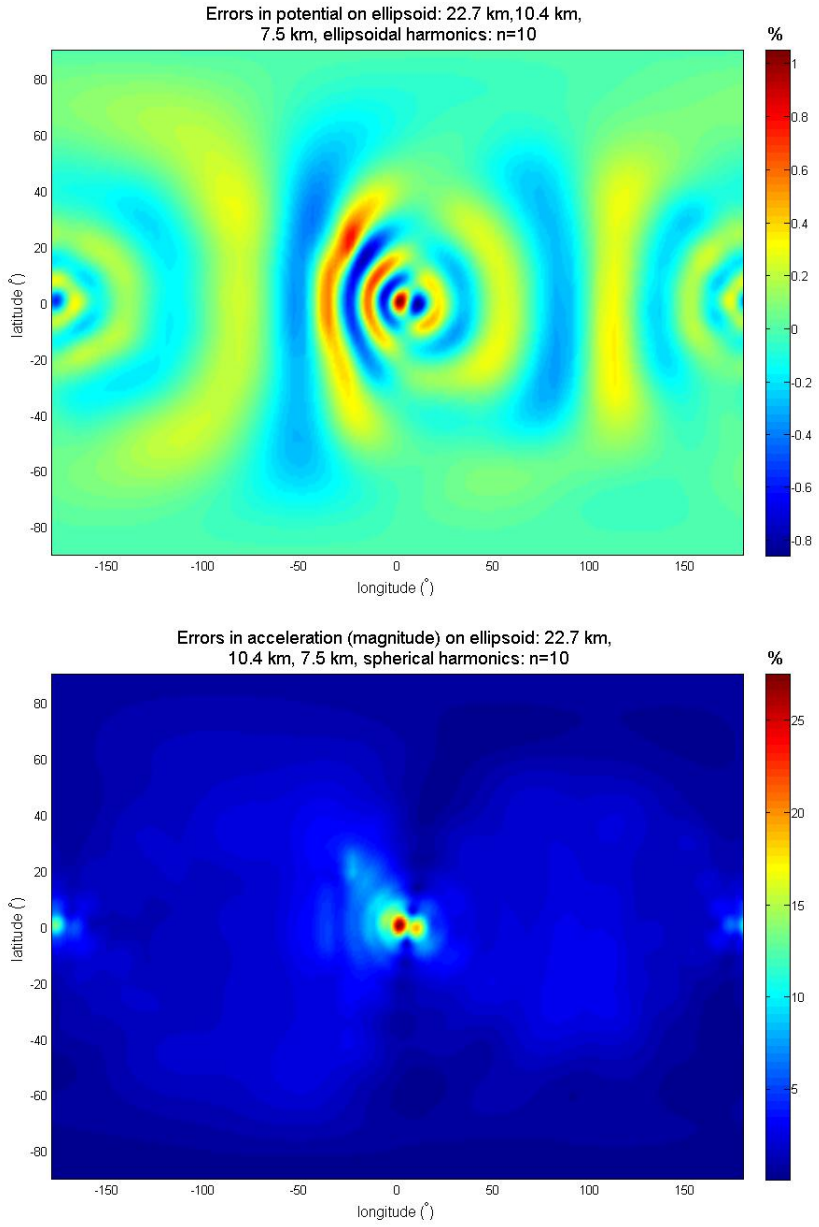

Figure 5.25 Errors in the EHS modeled potential (top) and acceleration (bottom) up to degree 10 on the reference ellipsoid

We find that increasing the maximum degree to 20 has reduced errors in both potential and acceleration by one order of magnitude, e.g., from 0.1% to 0.01% in potential. The pattern of peak errors in this case is well correlated and visible as a strip slanting northwesterly from the origin where errors are roughly 0.1%. The maximum error is no longer at the origin but offset in the same direction. We speculate that the same explanation provided for the locations of such errors based

on the case of degree 10 should apply to this case as well.

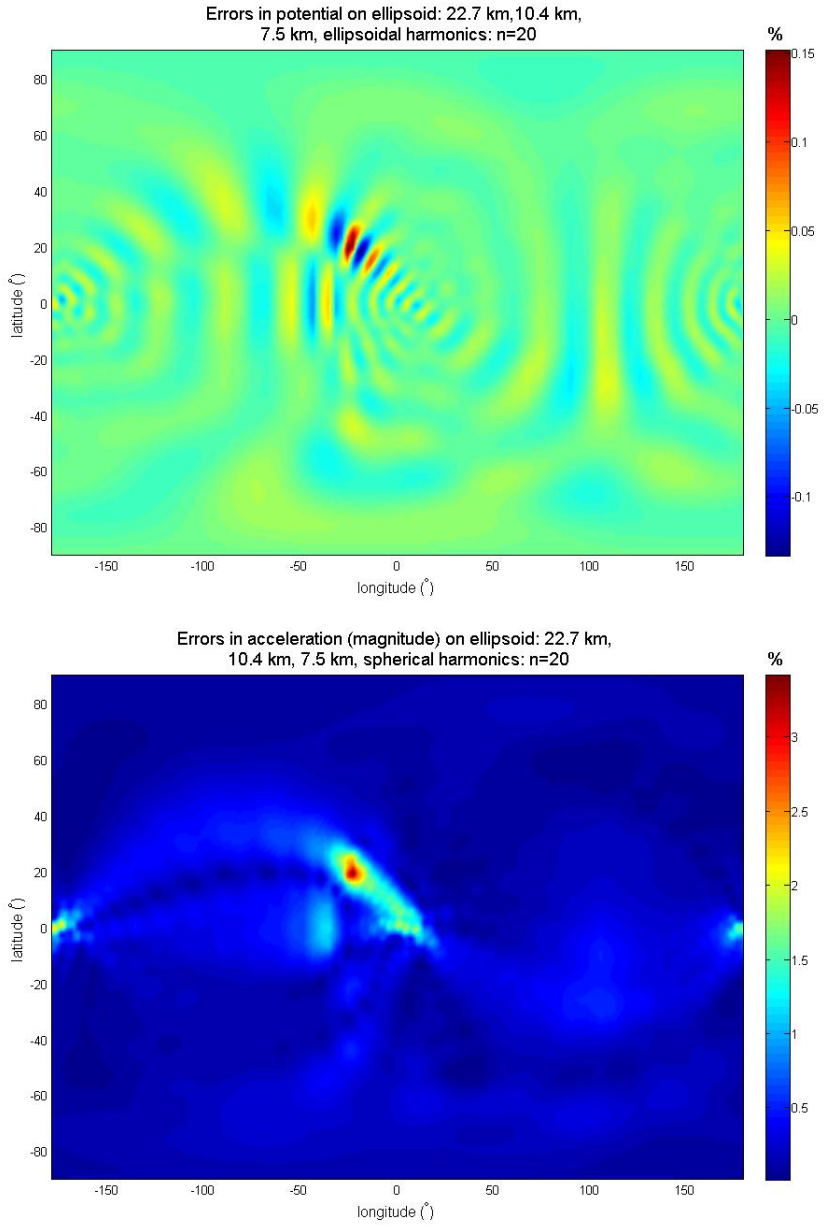

Figure 5.26 Errors in the EHS modeled potential (top) and acceleration (bottom) up to degree 20 on the reference ellipsoid

With no intention to investigate the extent to which the choice of degree affects the EHS performance, we can at least infer that using harmonic degrees up to 20 is advantageous for Eros to reduce the otherwise substantial errors in a degree-10 expansion.

The reason why overall EHS suffers larger modeling errors for Eros than for Phobos can be quite complicated. Essentially it should be attributed to Eros being much more irregular in shape than Phobos. The implication is two-fold; firstly, the highly irregular shape of Eros generates highly variable gravitational field which is undoubtedly more difficult to represent by simple mathematical models. Secondly, Eros requires a much more elongated reference ellipsoid. For example, the two focal lengths h=20.183 km and k=21.385 km are rather close to one another. By definition the second ellipsoidal coordinate must satisfy $h \le \mu \le k$. Moreover, this will cause the roots of Lamé's equations to be unevenly spaced and have very large variations (e.g., as in Figure 4.1). Clearly this has not caused significant numerical problems, as the pattern of errors is reasonable and accountable, indicating that the results do not suffer great errors. However, we certainly cannot rule out the possibility that it may have affected the modeling errors. At any rate we did not pursue this problem any further but decided to let the case present itself to be judged by readers.

5.3.2 Gravitational field via spherical harmonics on reference sphere

Let us now attend to the errors in the SHS on its reference sphere of radius 17.5 km. The true potential on the sphere is given in Figure 5.27. The error maps of the degree-10 SHS modeled potential and acceleration are given in Figure 5.28. On average, errors in potential vary on the order of 0.1%, and peak values appear at (180°,0°) where topography is the closest to the sphere (Figure 5.27). Compared to the EHS on the ellipsoid, the SHS is not challenged near (0°,0°), because here the topography remains distant from the sphere. As usual, the errors in the modeled acceleration (Figure 5.28 at the bottom) are greater than that in the potential by one order of magnitude. Near the area of peak errors in the potential, the acceleration errors reach nearly 10%.

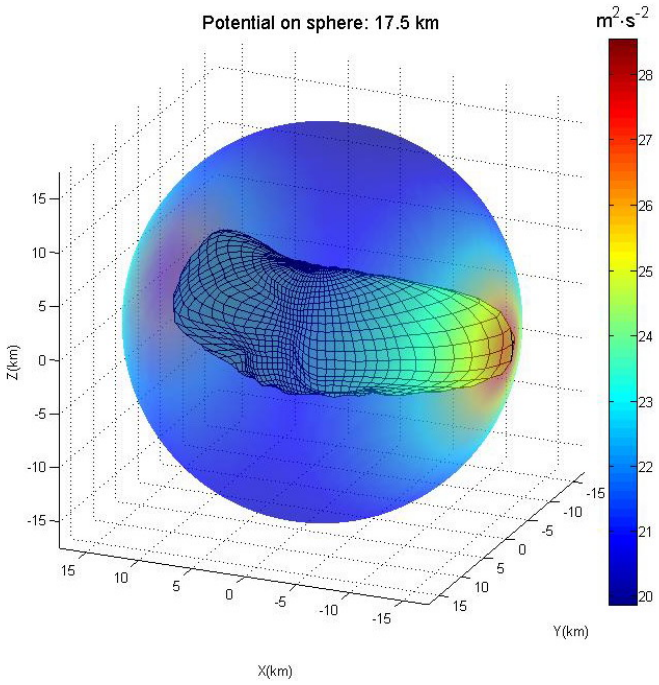

Figure 5.27 The PM derived true potential of Eros on the reference sphere

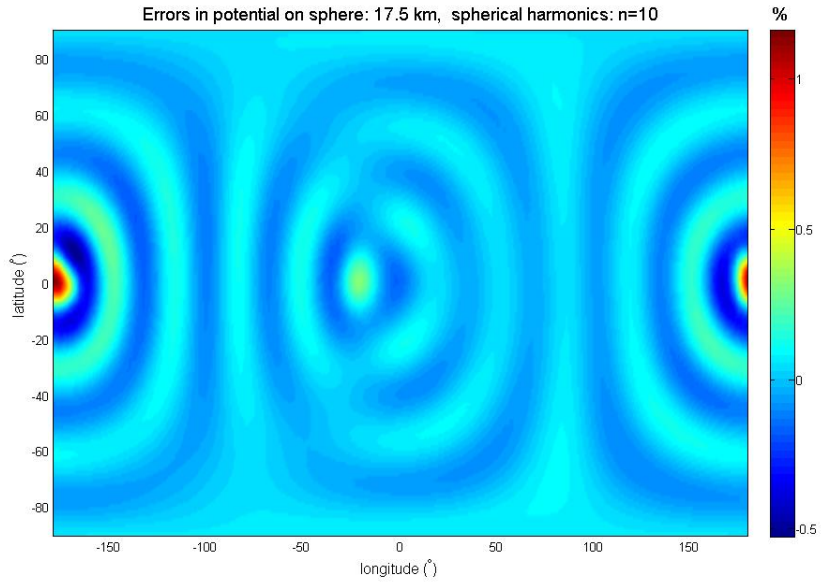

Continued

Figure 5.28 Errors in the SHS modeled potential (top) and acceleration (bottom) up to degree 10 on the reference sphere

Figure 5.28 continued

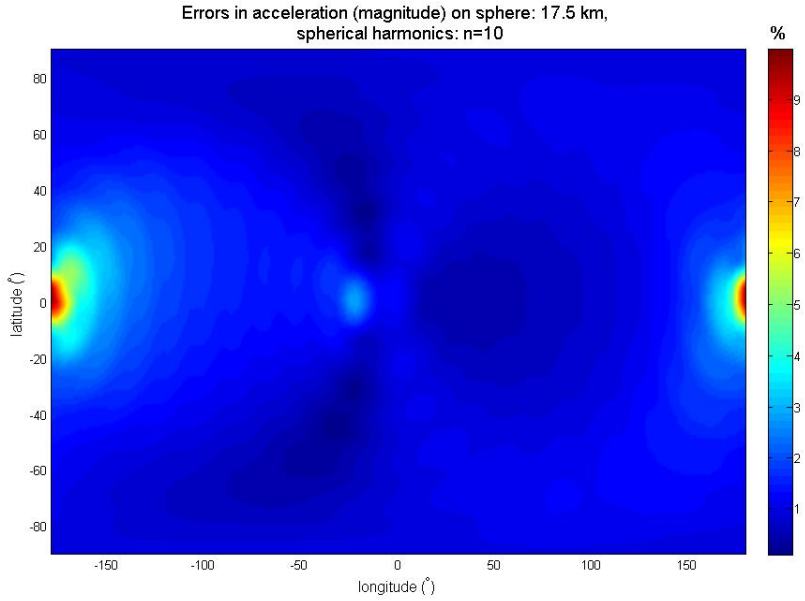

In the usual manner, when increasing the maximum degree from 10 to 20 we observe a reduction of overall errors, e.g., from 0.1% level to 0.01% in potential. Similarly, the peak errors decrease from 1% to 0.1%, again indicating the deficiency of the degree-10 SHS model as well as the validity of higher-degree expansions.

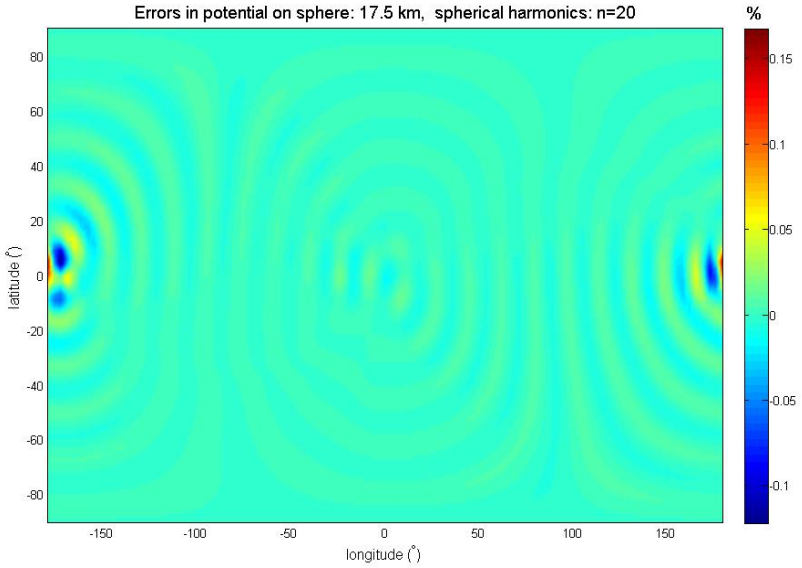

Continued

Figure 5.29 Errors in the SHS modeled potential (top) and acceleration (bottom) up to degree 20 on the reference sphere

Figure 5.29 continued

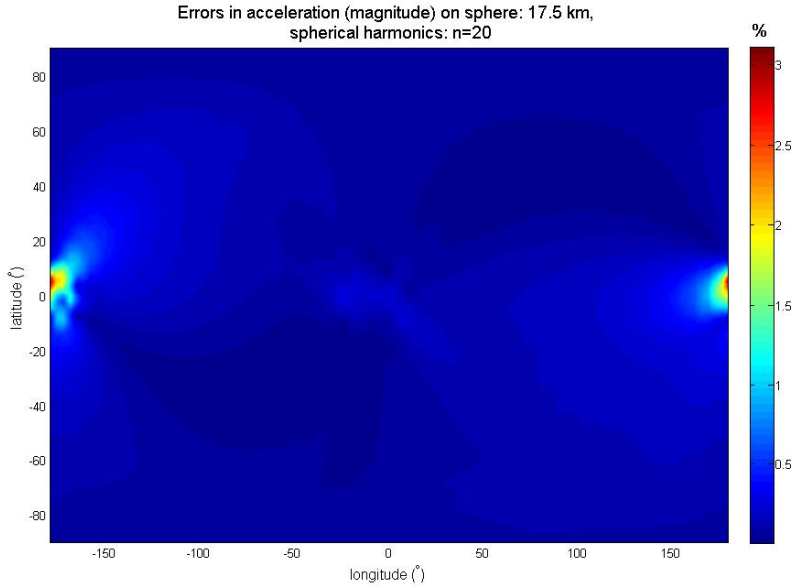

5.3.3 Comparison of spherical and ellipsoidal harmonics on arbitrary surfaces

Same as for Phobos, we shall examine the modeling errors of using the EHS and SHS for Eros on an arbitrary surface based on the following cases: 1) applying EHS on the reference sphere; 2) applying SHS on the reference ellipsoid; 3) applying EHS on the topographic surface of Eros. For case 3) we will pass over using the SHS on Eros' surface for a reason that shall become evident later. The geometric relation of the two reference surfaces can be illustrated in Figure 5.30.

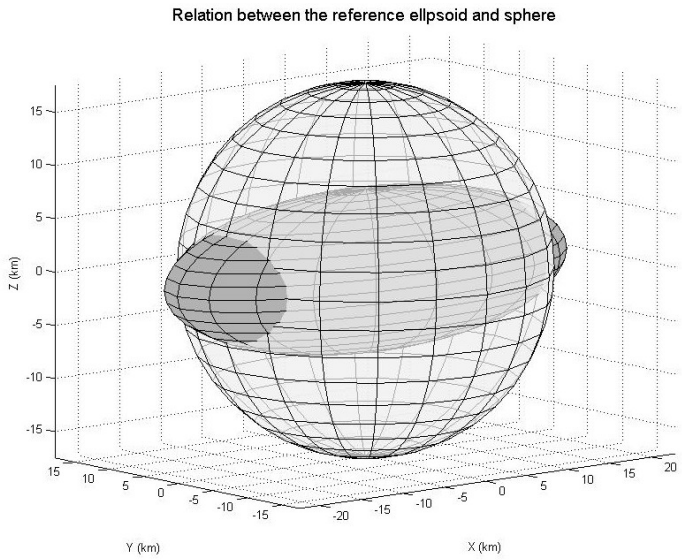

Figure 5.30 The geometric relation between the reference ellipsoid and sphere

Ellipsoidal harmonics on the reference sphere

We first look at the modeling errors of the EHS up to degree 10 in potential on the sphere (Figure 5.31). As expected, the largest errors of over 30% occur around (0°,0°) and (180°,0°) where the sphere falls the lowest beneath the ellipsoid. Such errors completely overwhelm the rest. When we zoom in over the error range from -0.5% to 0.5% we find that greater errors indeed correspond to the heart of the divergence areas for the EHS. While the convergence of EHS is doubtful in these two regions, in all other areas the errors typically fluctuate on the order of 0.01%.

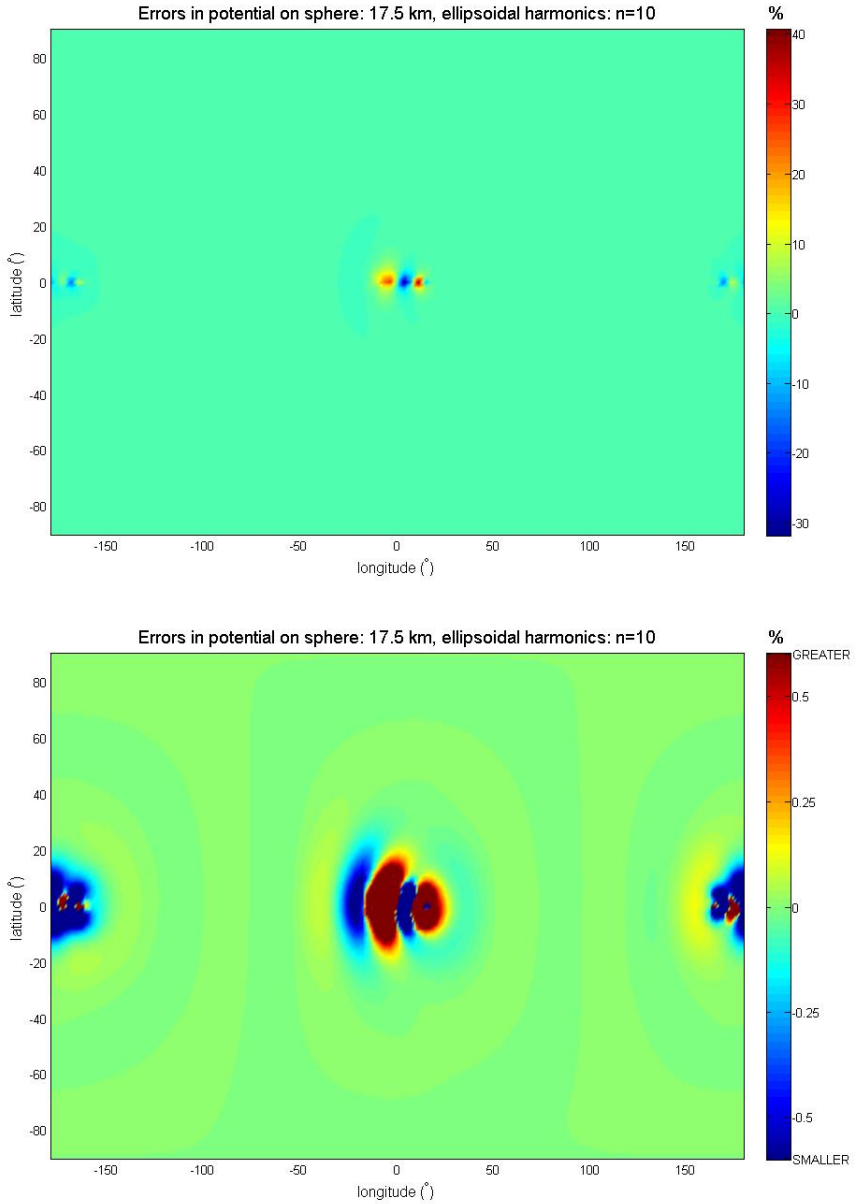

Figure 5.31 Errors in the EHS modeled potential up to degree 10 on reference sphere; errors ranging from -0.5% to 0.5% are emphasized at the bottom

Since the EHS modeled potential barely converges at the two critical locations near the equator, the modeled acceleration is not any better. Indeed the divergence is much more severe in acceleration, which can be seen in Figure 5.32. The peak errors at the center of the two locations have gone up to 1000%, suggesting that the EHS has failed altogether at these two locations. However, in all other areas EHS remains reliable. Note that in Figure 5.32, we accentuate only the error range from 0% to

10% which covers most of the errors. The errors typically vary at the level of 0.1%, which is one order of magnitude greater than the usual potential errors, a familiar condition so far and a sign that the model is stable.

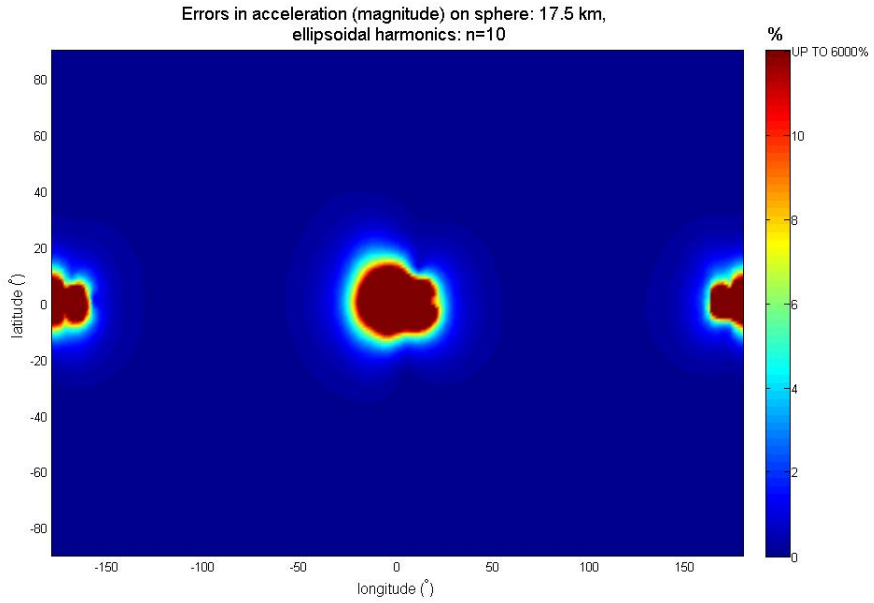

Figure 5.32 Errors in the EHS modeled acceleration up to degree 10 on the reference sphere; errors below 10% are emphasized

Finally, let us look at the EHS modeling errors for maximum degree 20. Judging from the previous cases, we do not expect that increasing the maximum degree will alleviate the divergence problem. On the contrary, the divergence will likely intensify with the higher-degree EHS. Nevertheless, in areas outside the divergence region, we expect the EHS to improve in accuracy since the algorithm is reliable. Our reasoning is clearly confirmed by Figure 5.33. The peak errors in potential increase from 40% to 1400% at the two divergence regions. Elsewhere errors overall decrease from 0.01% for degree 10 to 0.001% for degree 20, as is suggested by the fluctuating pattern.

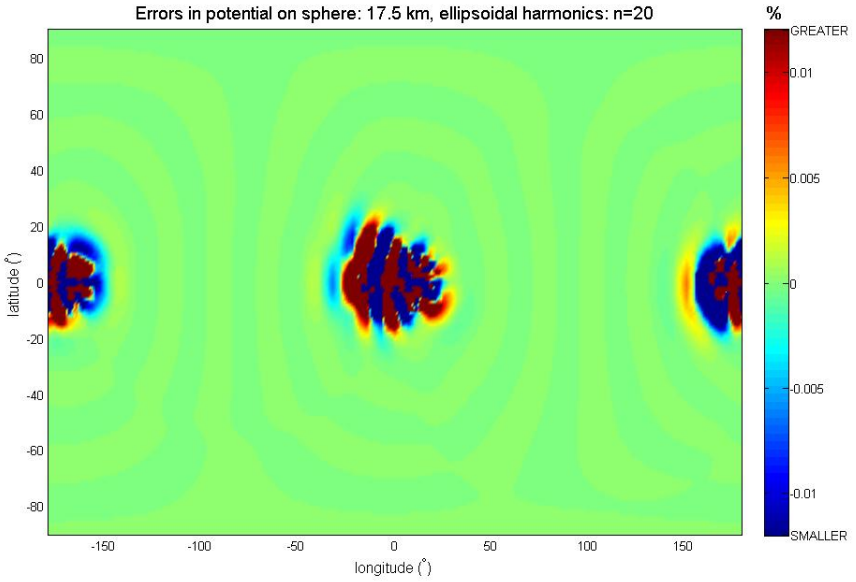

Figure 5.33 Errors in the EHS modeled potential up to degree 20 on the reference sphere; errors ranging from -0.01% to 0.01% are emphasized.

Spherical harmonics on the reference ellipsoid

When the SHS up to degree 10 is applied on the reference ellipsoid, significant errors of 800% in potential are present near the poles (Figure 5.34). Moreover, the error pattern looks almost symmetric hence we may infer that the character of errors is purely divergent (not showing any field potential variations). Figure 5.35 on the left shows the errors on the ellipsoid, with the range between -10% and 10% emphasized. It is clear that the use of SHS is overall problematic on the reference ellipsoid: only in the two restricted areas along the semi-major axis are the errors in the selected range. Figure 5.34 does not reveal the extent of divergence well enough, as the regions along the semi-minor axis in the lower latitudes also have substantial errors. This issue is not urgent for Phobos because of its moderate equatorial flattening. But the best-fitting ellipsoid of Eros has two like semi-minor axes of 5.77 km and 5.33 km with a much longer semi-major axis of 20.9 km, which proved an unmanageable case for the SHS.

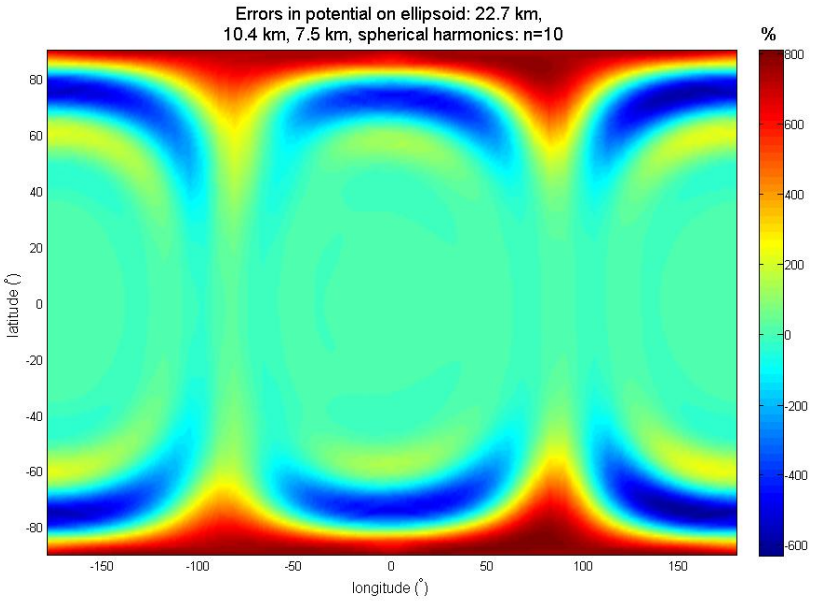

Figure 5.34 Errors in the SHS modeled potential up to degree 10 on reference ellipsoid

On the other hand, applying the EHS (up to degree 10) on the reference surface seems much less problematic. On the sphere, only in two regions of approximately 30°×30° do errors go beyond 1% in potential, as illustrated by Figure 5.35 on the right.

As should have been well anticipated at this point, the increase in maximum degree from 10 to 20 greatly exacerbates the divergence of the SHS and thus shall not be elaborated here.

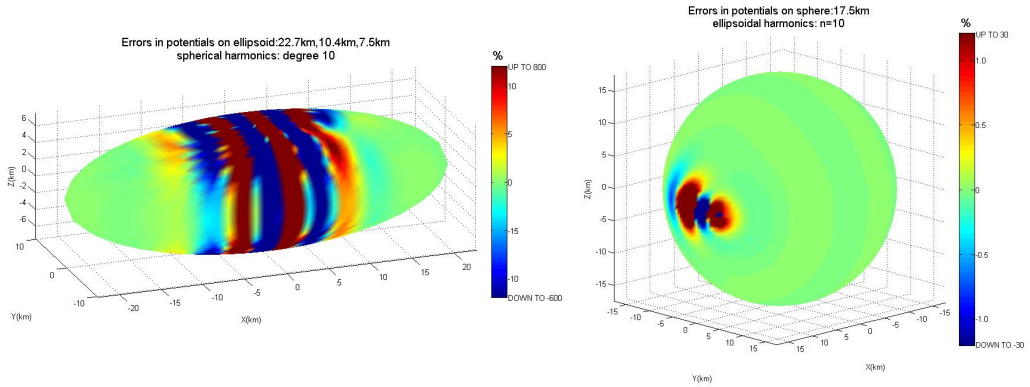

Figure 5.35 Comparison of errors in the SHS modeled potential on reference ellipsoid (left) and EHS modeled potential on sphere (right), expansions up to degree 10

Based on the above discussions, we see that the SHS is basically not suited for modeling highly irregular bodies such as Eros, especially far into the divergence region. The inferior performance of SHS on the reference ellipsoid eliminates the need of further testing it near the surface of the body.

Modeling errors of ellipsoidal harmonics near the surface of Eros

The surface points are again chosen to be slightly elevated from the topography model in order to ensure that PM strictly holds. The EHS diverged for the most part along the equator, especially those areas that are subsided far below the reference ellipsoid (Figure 5.36). The greatest errors are 60% in the potential. On the other hand, the two areas on the equator more outstretched to the ellipsoid are relieved of large errors. For the geometry of the shape model and the reference ellipsoid please refer back to Figure 5.24.

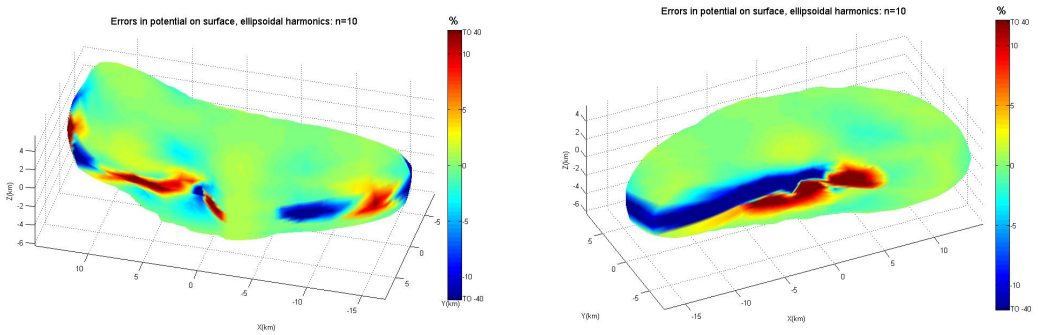

Figure 5.36 Errors in the EHS modeled potential up to degree 10 near the body surface; errors in the range from -10% to 10% are emphasized.

The errors in acceleration are akin to that in potential. Where the evaluated potential diverges the acceleration diverges, too. Subsequently, the EHS is only reliable at two areas around the equator and in higher latitudes. Figure 5.37 emphasizes the errors below 50% level in the acceleration, while the maximum errors reach 360%.

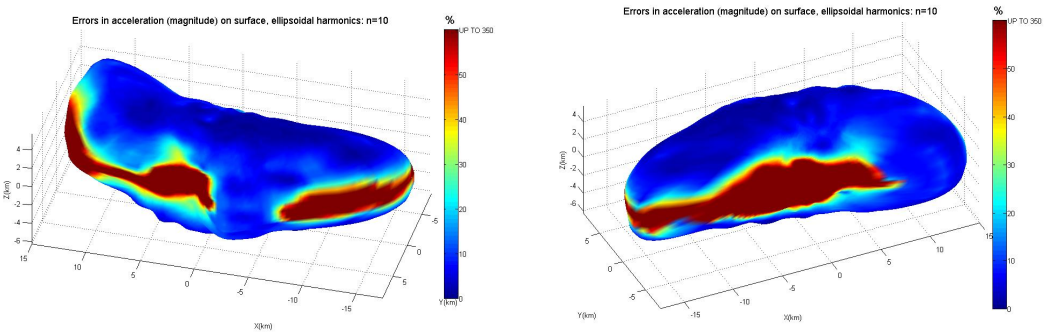

Figure 5.37 Errors (magnitude) in the EHS modeled acceleration up to degree 10 near the body surface; errors below 50% are emphasized.

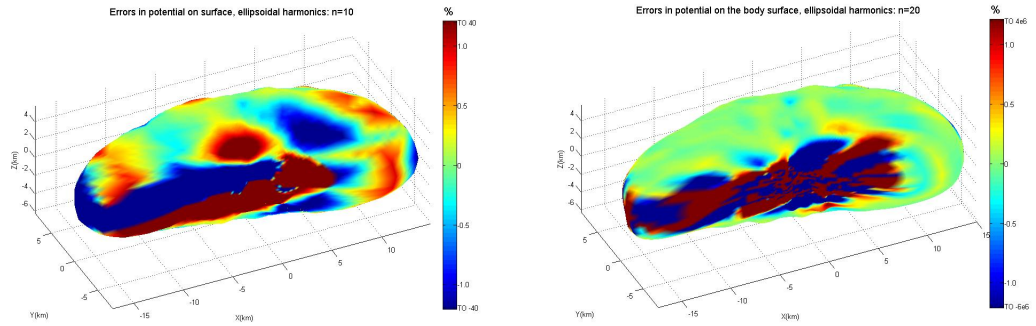

Figure 5.38 Comparison of errors in the EHS modeled potential up to degrees 10 (left) and 20 (right) near the body surface; errors ranging from -1.0% to 1.0% are emphasized

Last but not least, let us compare the errors of degree-10 and degree-20 models on the surface. We shall confine our attention to the range between -1% and 1%, as it is well known to us that increasing the maximum degree will not mitigate the divergence. Instead we shall pay attention to the parts unaffected by divergence. Note that these areas are likewise below the reference ellipsoid. We are interested in whether the expansion up to degree 20 will enhance or degrade the performance of the EHS in these areas. From Figure 5.38, we can clearly tell that for the case of Eros, increasing the maximum degree of the EHS causes errors in potential in higher latitudes to decrease significantly (though at the expense of magnifying the divergence near the equator). The results indicate that the EHS is convergent in higher latitudes, as the errors would have increased rather than decreased if the model was divergent. Note that the same scale was used for both graphs.

Chapter 6: Conclusions

Aiming at irregular-shaped attracting bodies, we compared two methods, the spherical and ellipsoidal harmonics, for gravitational field modeling. We are interested in the harmonic models mainly because they are more apt to be used for recovering the gravitational field from geodetic data. As series solutions, both methods have their respective regions of uniform convergence, which poses constraints on their application. Generally speaking, the SHS is uniformly convergent outside the enclosing reference sphere of the attracting body, while for the EHS, the uniform convergence holds outside the enclosing reference ellipsoid. When the shape of the attracting body is highly non-spherical and may not fit into any sphere closely, leaving a large volume of divergence region, the application of the SHS can be problematic. In this case, the EHS seems to be a promising alternative, because the ellipsoid, being more arbitrary-shaped than a sphere, is more likely to fit the body, thus has smaller volume of divergence than for the SHS. This is of particular importance if the field point lies close to the body.

We reviewed Hobson's discussions of the EHS theories in Chapter 3. The correspondence between the EHS and the SHS was analyzed. In particular, it was shown that the uniform convergence of the EHS is essentially governed by a factor $(\rho_0 / \rho)^{n+1}$ (for the exterior potential problem), thus analogous to the convergence problem of the SHS. The application of the EHS for gravitational field modeling was discussed in Chapter 4, following the procedures given by Garmier. It was found that a major downside of gravitational field modeling via the EHS was the numerical complexity and difficulty. To name a few reasons: there is no available recurrence relation for generating the Lamé's functions; the lack of one-to-one transformation between the ellipsoidal and rectangular coordinates adds to the computational labor of applying the EHS. In addition, the normalization of the EHS for various degrees, e.g., those above degree ten, can be problematic. The Lamé's functions for such

degrees may have zeros that are unevenly spaced, and show larger variations than can be handled by the 15-digit precision. The modeling accuracy for these degrees may be dubious, although our experience suggested that this issue at least did not pose any severe problems, e.g., introducing out-of-scale errors in the model.

In Chapter 5, the performance of the EHS was compared to that of the SHS based on the gravitational field modeling of two non-spherical bodies: Martian moon Phobos and a NEA 433 Eros. Specifically, we analyzed the modeling errors, i.e., the discrepancies between the PM derived gravitational potential and acceleration, and that modeled by the EHS or SHS.

Phobos is considered as a moderate case of the irregular-shaped body. We found that the EHS and SHS were consistent models on their respective reference surfaces. For example, the errors in potential were overall on the order of 0.01% for both expansions up to degree 10, while using the degree-20 expansions saw a decrease in errors to the level of 0.001%. On the other hand, the errors in acceleration were generally one order of magnitude greater than that in potential, not an uncommon observation since the acceleration is related to the differentiated potential, causing especially the short-wavelength errors to intensify. Next the EHS and SHS were tested on the mutual reference surfaces. On the reference sphere, the EHS was still a reliable model. Outside its convergence region, i.e., inside the reference ellipsoid, the EHS incurred greater errors in potential, they were nevertheless still on the order of 0.01%. This is because the ellipsoid does not fall far below the sphere. On the other hand, the SHS became uncertain near the poles on the reference ellipsoid, i.e., outside its convergence region. Here the errors in potential increased to 0.1%. We also observed that increasing the maximum degree of the SHS did not reduce such errors, suggesting that the errors were due to divergence of the model. To further explore this issue, we compared the EHS and SHS on the body surface, in which case both expansions were applied outside their respective convergence regions. Again the SHS model introduced large errors over 5% in potential near the poles, especially the South Pole since here the topography is distinctly caved in. The peak errors in acceleration exceeded 100% at this location. The EHS also showed mild

signs of divergence at several locations where the topography is deep below the reference ellipsoid. For example, the peak errors in potential were around 1% while that in acceleration were over 20% for the degree-10 EHS model. Obviously, the smaller modeling errors of the EHS can be attributed to the fact that the reference ellipsoid more closely fits the body thus reducing the divergence region over the body surface. Another implication is that, the distance of a field point (if outside the convergence regions for both EHS and SHS) from the reference ellipsoid is likely shorter than that from the reference sphere. Judging from such comparisons, we conclude that the EHS is a more reliable method than the SHS for field modeling in close proximity to Phobos.

The asteroid Eros is more irregularly shaped than Phobos. The figure of Eros requires a much elongated fitting ellipsoid, yet still with significant departures. The sphere yields a rather poor fit to the figure. On their respective reference surfaces, the degree-10 EHS and SHS introduced errors on the order of 0.1% in potential, whereas increasing the maximum degree to 20 reduced errors to 0.01%. The same as for Phobos, the errors in acceleration were greater than that in potential: on average 1% for degree-10 expansions, compared to 0.1% for the degree-20. The modeling errors of both expansions were larger for Eros than for Phobos. We regard this issue to be associated with the high variability of Ero's gravitational field due to the shape irregularity, rather than an artifact or lapse of the software. This is because the results given by the EHS and SHS were in agreement. Furthermore, the observed pattern of errors is accountable and similar to that for Phobos. The irregularity of Eros also causes the two reference surfaces to be markedly different. The reference ellipsoid is for the most part far inside the reference sphere. However, the two ends of its semi-major axis are outside the reference sphere by nearly 5 km. Subsequently, the EHS, when applied on the reference sphere, diverged at (below) these two locations with the largest errors in potential over 40%. The divergence of the modeled acceleration was even more severe at these locations, e.g., the peak errors were over 5000%. On the other hand, the SHS model was altogether divergent on the reference ellipsoid, with the exception of the two areas along the semi-major axis which are inside the convergence region of the SHS. The results suggest that the SHS is not

suitable for field modeling on the ellipsoid, let alone down on the body surface. Due to this reason, only the EHS was investigated on the surface of Eros. In this case, along the equator the EHS model was more vulnerable to divergence, obviously because there the topography is most varied and at many places falls far inside the reference ellipsoid. Specifically, using the degree-10 EHS, the errors in potential due to divergence were less than 50%. Away from the equator, the divergence was much less noticeable or absent. For example, we observed a decrease of errors in higher latitudes using the EHS up to degree 20, which would not be possible if the EHS was severely divergent. Whether EHS is useful for field modeling on the surface of Eros is likely a subjective matter.

Based on the above discussions, we may conclude that the EHS is a better method than the SHS for modeling the gravitational field close to the non-spherical bodies. The accuracy of the EHS, if not always significantly superior, is at least comparable to that of the SHS. More importantly, the EHS is obviously a more consistent and convergent model. In other words, it has smaller divergence region and, even if applied in its divergence region, suffers smaller errors than the SHS. Based on the comparison between Phobos and Eros, we may also infer that, the more irregular the attracting body is, the more advantageous it is to apply the EHS. However, we need to stress that such conclusions only apply to the low-degree expansions, i.e., not higher than degree 20.

Being but a rough review on the EHS in comparison with the SHS, there are numerous issues that were not addressed in this thesis. For example, one of the main concerns of applying the EHS is the numerical accuracy of the Lamé's functions. Based on our observation, we consider that the degradation of the EHS model due to the inaccuracy of the Lamé's functions is benign. However, what part did the errors of the Lamé's functions play in the modeling errors and, what would be the optimal maximum degree of the EHS with regard to such errors? Another practical question is that, while the reference ellipsoid for the EHS should fit the attracting body as closely as possible, how will the shape of this ellipsoid, i.e., ρ_0, h, k, affect the numerical accuracy of the Lamé's functions and the EHS model? The answer to

some of these questions would be interesting to explore and instrumental in practice in the future.

References

1. History of lunar missions at http://nssdc.gsfc.nasa.gov/planetary/lunar/

2. Mars Exploration Program: Historical Log at http://mars.jpl.nasa.gov/programmissions/missions/log/

3. Smith B., Soderblom L., et al. The Jupiter system through the eyes of Voyager 1, Science, vol.204, pp.951-972, Jun. 1979

4. Comprehensive list of planetary exploration missions at http://science.nasa.gov/planetary-science/missions/

5. Zuber M., Smith D., et al. The shape and internal structure of the Moon from the Clementine mission, Science, vol. 266, pp. 1839-1843, Dec. 1994

6. Zuber M., Solomon S., et al. Internal structure and early thermal evolution of Mars from Mars Global Surveyor topography and gravity, Science, vol.287, pp.1788-1793, Mar. 2000

7. Missions to asteroids at http://nssdc.gsfc.nasa.gov/planetary/planets/asteroidpage.html

8. IAU 2006 Resolution A5, Definition of a Planet at http://www.iau.org/public_press/news/detail/iau0603/

9. Bottke W. Jr., Cellino A., et al., Asteroids III, University of Arizona Press, 2002

10. Chapman C., The hazard of near-Earth asteroid impacts on Earth, Earth and Planetary Science Letters, vol.222, pp.1-15, 2004

11. Rosborough G., Tapley B., Radial, transverse and normal satellite position perturbations due to the geopotential, Celestial Mechanics, vol.40, pp.409-421, 1987

12. Smith D., Zuber M., et al., The lunar orbital laser altimeter investigation on the Lunar Reconnaissance Orbiter mission, Space Science Reviews, vol.150, pp.209-241, 2010

13. Balmino G., Gravitational potential harmonics from the shape of an homogeneous body, Celestial Mechanics and Dynamical Astronomy, vol.60, pp.331-364, 1994

14. Werner R., The gravitational potential of a homogeneous polyhedron or don't cut

corners, Celestial Mechanics and Dynamical Astronomy, vol.59, pp.253-278, 1994

15. Shi X., Willner K., et al., Working models for the gravitational field of Phobos, Science China: Physics, Mechanics and Astronomy, vol.55, pp.358-364, 2012

16. Torge W., Gravimetry, Walter de Gruyter, Berlin and New York, 1989

17. Jekeli C., Inertial Navigation Systems with Geodetic Applications, Walter de Gruyter, Berlin, 2000

18. Lerch F., Klosko S., et al., A refined gravity model from LAGEOS (GEM-L2), Geophysical Research Letters, vol.9, no.11, pp.1263-1266, Nov. 1982

19. Nerem R., Chao B., et al., Temporal variations of the Earth's gravitational field from satellite laser ranging to LAGEOS, Geophysical Research Letters, vol.20, no.7, pp.595-598, Apr. 1993

20. Jekeli C., The determination of gravitational potential differences from satellite-to-satellite tracking, Celestial Mechanics and Dynamical Astronomy, vol.75, pp.85-101, 1999

21. Tapley B., Bettadpur S., et al., GRACE measurements of mass variability in the Earth system, Science, vol.305, pp.503-505, 2004

22. Reigber C., Balmino G., et al., A high-quality global gravity field model from CHAMP GPS tracking data and accelerometry (EIGEN-1S), Geophysical Research Letter, vol.29, no.14, 1692, 2002

23. Yuan D., Sjogren W., et al., Gravity field of Mars: A 75th degree and order model, Journal of Geophysical Research, vol.106, no.E10, pp.23,377-23,401, Oct. 2001

24. Lemoine F., Smith D., et al., An improved solution of the gravity field of Mars (GMM-2B) from Mars Global Surveyor, Journal of Geophysical Research, vol.106, no.E10, pp.23,359-23,376, Oct. 2001

25. Namiki N., Iwata T., et al., Farside gravity field of the Moon from four-way doppler measurements of SELENE (Kaguya), Science, vol.323, pp.900-905, 2009

26. Jekeli C., The exact transformation between ellipsoidal and spherical harmonic expansions, Manuscripta Geodaetica, vol.13, pp.106-113, 1988

27. Hobson E., The Theory of Spherical and Ellipsoidal Harmonics, 2nd reprint, Chelsea Publishing Company, New York, 1965

28. Byerly W., An Elementary Treatise on Fourier's Series and Spherical, Cylindrical and Ellipsoidal Harmonics, with Applications to Problems in Mathematical

Physics, Dover Publications, Mineola, New York, 2003

29. Garmier R., Barriot J.-P., Ellipsoidal harmonic expansions of the gravitational potential: theory and application, Celestial Mechanics and Dynamical Astronomy, vol.79, pp.235-275, 2001

30. Garmier R., Barriot J.-P., et al., Modeling of the Eros gravity field as an ellipsoidal harmonic expansion from the NEAR Doppler tracking data, Geophysical Research Letters, vol.29, no.8, 1231, 2002

31. Dechambre D., Scheeres D., Transformation of spherical harmonic coefficients to ellipsoidal harmonic coefficients, Astronomy&Astrophysics, vol.387, pp. 1114-1122, 2002

32. Chao B., Rubincam D., The gravitational field of Phobos, Geophysical Research Letters, vol.16, no.8, pp.859-862, 1989

33. Burša M., Normal gravity model of Phobos, Studia Geophysica Et Geodaetica, vol.33, no.2, pp.109-116, 1989

34. Hofmann-Wellenhof B., Moritz H., Physical Geodesy. Springer-Verlag Wien. 2005

35. Moritz H., Report No. 165: Kinematical Geodesy II, Reports of the Department of Geodetic Science, The Ohio State University, Oct. 1971

36. Kaula W., Theory of Satellite Geodesy: Applications of Satellites to Geodesy, Dover Publications, Mineola, New York, 2000

37. Irving R., Integers, Polynomials and Rings: A Course in Algebra, Springer-Verlag New York, Inc., 2004

38. Dobner H.-J., Ritter S., Verified computation of Lamé's functions with high accuracy, Computing, vol.60, pp.81-89, 1998

39. Watkins D., The QR algorithm revisited, SIAM Review, vol.50, no.1, pp.133-145, 2008

40. Andert T., Rosenblatt P., et al., Precise mass determination and the nature of Phobos, Geophysical Research Letters, vol.37, L09202, 2010

41. Miller J., Konopliv A., et al., Determination of shape, gravity, and rotational state of asteroid 433 Eros, Icarus, vol.155, pp.3-17, 2002

42. Werner R., Scheeres D., Exterior gravitation of a polyhedron derived and compared with harmonic and mascon gravitation representations of asteroid 4769 Castalia, Celestial Mechanics and Dynamical Astronomy, vol.65, pp.313-344, 1997

43. Willner K., Oberst J., et al., Phobos control point network, rotation, and shape, Earth and Planetary Science Letters, vol.294, pp.541-546, 2010

44. Thomas P., Gravity, tides, and topography on small satellites and asteroids: application to surface features of the Martian satellites, Icarus, vol.105, pp.326-344, 1993

45. Zuber M., Smith D., et al., The shape of 433 Eros from the NEAR-Shoemaker Laser Rangefinder, Science, vol.289, pp.2097-2101, 2000

Appendix A: Lamé's Equations Based on t and Λ

Please note that $\kappa = k / h, \alpha' = 1 + \kappa^2$ in the following expressions.

Class K

n even: $E_n^m(t) = u_n^m(\Lambda)$

$$(\Lambda + \kappa^2 - 1)\Lambda \frac{d^2u}{dt^2} - t(\alpha' + 2\Lambda - 2)\frac{du}{dt} + [p + n(n+1)(\Lambda - 1)]u = 0 \qquad \text{(a.1.1)}$$

n odd: $E_n^m(t) = t \cdot u_n^m(\Lambda)$

$$\begin{aligned}&\Lambda(\Lambda + \kappa^2 - 1)t\frac{d^2u}{dt^2} + [2\Lambda(\Lambda + \kappa^2 - 1) + (\alpha' + 2\Lambda - 2)(\Lambda - 1)]\frac{du}{dt} \\ &+[p - \alpha' + (n+2)(n-1)(\Lambda - 1)]tu = 0\end{aligned} \qquad \text{(a.1.2)}$$

Class L

n even: $E_n^m(t) = t\sqrt{|t^2 - 1|} \cdot u_n^m(\Lambda)$

$$\begin{aligned}&\Lambda(\Lambda + \kappa^2 - 1)t\frac{d^2u}{dt^2} + \left[2\Lambda(\Lambda + \kappa^2 - 1) + (\alpha' + 2\kappa^2 + 4\Lambda - 4)(\Lambda - 1)\right]\frac{du}{dt} + \\ &\left[p - 3\kappa^2 - \alpha' + (n+3)(n-2)(\Lambda - 1)\right]tu = 0\end{aligned} \qquad \text{(a.1.3)}$$

n odd: $E_n^m(t) = \sqrt{|t^2 - 1|} \cdot u_n^m(\Lambda)$

$$\begin{aligned}&\Lambda(\Lambda + \kappa^2 - 1)\frac{d^2u}{dt^2} - \\ &(\alpha' + 2\kappa^2 + 4\Lambda - 4)t\frac{du}{dt} + \left[p - \kappa^2 + (n-1)(n+2)(\Lambda - 1)\right]u = 0\end{aligned} \qquad \text{(a.1.4)}$$

Class M

n even: $E_n^m(t) = t\sqrt{|t^2 - \kappa^2|} \cdot u_n^m(\Lambda)$

$$\Lambda(\Lambda+\kappa^2-1)t\frac{d^2u}{dt^2}+\left[2\Lambda(\Lambda+\kappa^2-1)+(\alpha'-2+4\Lambda)(\Lambda-1)\right]\frac{du}{dt}+$$
$$\left[p-3-\alpha'+(n+3)(n-2)(\Lambda-1)\right]tu=0 \qquad \text{(a.1.5)}$$

n odd: $E_n^m(t)=\sqrt{\left|t^2-\kappa^2\right|}\cdot u_n^m(\Lambda)$

$$\Lambda(\Lambda+\kappa^2-1)\frac{d^2u}{dt^2}-$$
$$(\alpha'+2+4\Lambda-4)t\frac{du}{dt}+\left[p-1+(n-1)(n+2)(\Lambda-1)\right]u=0 \qquad \text{(a.1.6)}$$

Class *N*

n even: $E_n^m(t)=\sqrt{\left|t^2-\kappa^2\right|}\sqrt{\left|t^2-1\right|}\cdot u_n^m(\Lambda)$

$$\Lambda(\Lambda+\kappa^2-1)\frac{d^2u}{dt^2}-$$
$$3t(\alpha'+2\Lambda-2)\frac{du}{dt}+\left[p-\alpha'+(n+3)(n-2)(\Lambda-1)\right]u=0 \qquad \text{(a.1.7)}$$

n odd: $E_n^m(t)=t\sqrt{\left|t^2-1\right|}\sqrt{\left|t^2-\kappa^2\right|}\cdot u_n^m(\Lambda)$

$$\Lambda(\Lambda+\kappa^2-1)t\frac{d^2u}{dt^2}+\left[2\Lambda(\Lambda+\kappa^2-1)+3(\alpha'+2\Lambda-2)(\Lambda-1)\right]\frac{du}{dt}+$$
$$\left[p-4\alpha'+(n+4)(n-3)(\Lambda-1)\right]tu=0 \qquad \text{(a.1.8)}$$

Appendix B: Elements of the Tridiagonal Matrix T for Determining the Coefficients of Lamé's Functions

Please note that in all the expressions in this part we have $i = 0,1,\cdots,r$, where the integer r takes different values according to the degree n and class. Please also note that $\kappa = k / h$. These expressions are also given in [29] (Annex 3).

Class K

n even

$$\begin{aligned} f_i &= -2(r-i+1)(2r+2i-1) \\ g_i &= 2r(2r+1)+4i^2(\kappa^2-2) \\ h_i &= -2(i+1)(2i+1)(\kappa^2-1) \end{aligned} \qquad \text{(a.2.1)}$$

n odd

$$\begin{aligned} f_i &= -2(r-i+1)(2r+2i+1) \\ g_i &= 2(r+1)(2r+1)-4i^2+(2i+1)^2(\kappa^2-1) \\ h_i &= -2(i+1)(2i+1)(\kappa^2-1) \end{aligned} \qquad \text{(a.2.2)}$$

with $r = \left\lfloor \frac{n}{2} \right\rfloor$.

Class L

n even

$$\begin{aligned} f_i &= -2(r-i)(2r+2i+1) \\ g_i &= 2r(2r+1)-(2i+1)^2+4(i+1)^2(\kappa^2-1) \\ h_i &= -2(i+1)(2i+3)(\kappa^2-1) \end{aligned} \qquad \text{(a.2.3)}$$

n odd

$$\begin{aligned} f_i &= -2(r-i+1)(2r+2i+1) \\ g_i &= 2(r+1)(2r+1)+(2i+1)^2(\kappa^2-2) \\ h_i &= -2(i+1)(2i+3)(\kappa^2-1) \end{aligned} \qquad \text{(a.2.4)}$$

with $r = \left\lfloor \frac{n-1}{2} \right\rfloor$.

Class *M*

n even

$$\begin{aligned} f_i &= -2(r-i)(2r+2i+1) \\ g_i &= 2r(2r+1) + (2i+1)^2(\kappa^2-2) \\ h_i &= -2(i+1)(2i+1)(\kappa^2-1) \end{aligned} \qquad \text{(a.2.5)}$$

n odd

$$\begin{aligned} f_i &= -2(r-i+1)(2r+2i+1) \\ g_i &= 2(r+1)(2r+1) - (2i+1)^2 + 4i^2(\kappa^2-1) \\ h_i &= -2(i+1)(2i+1)(\kappa^2-1) \end{aligned} \qquad \text{(a.2.6)}$$

with $r = \left\lfloor \frac{n-1}{2} \right\rfloor$.

Class *N*

n even

$$\begin{aligned} f_i &= -2(r-i)(2r+2i+1) \\ g_i &= 2r(2r+1) - 4(i+1)^2 + 2(i+1)^2(\kappa^2-1) \\ h_i &= -2(i+1)(2i+3)(\kappa^2-1) \end{aligned} \qquad \text{(a.2.7)}$$

n odd

$$\begin{aligned} f_i &= -2(r-i)(2r+2i+3) \\ g_i &= 2(r+1)(2r+1) + 4(i+1)^2(\kappa^2-2) \\ h_i &= -2(i+1)(2i+3)(\kappa^2-1) \end{aligned} \qquad \text{(a.2.8)}$$

with $r = \left\lfloor \frac{n}{2} \right\rfloor - 1$.

Appendix C: Removing the Singularities for the Computation of Gravitational Gradient Matrix

In this text, $\tilde{d}_{i,l}^{j}$ in (4.46) corresponds to $\partial P_{ij}/\partial\lambda_l$ in reference [29] (Annex 1). The complete expressions for $\tilde{d}_{i,l}^{j}$ are not given here. There are four types of singularities, namely, $\lambda_2^2-h^2$, $\lambda_2^2-k^2$, $\lambda_3^2-h^2$ and λ_3 which can be zero in the denominator. We can cancel out the first three factors while computing $\tilde{d}_{i,l}^{j}d_k^l$ when evaluating $d_{i,k}^{j}$ via (4.46).

Terms associated with $\lambda_2^2-h^2$

1) For $\tilde{d}_{2,2}^{1}=d_2^1\dfrac{\lambda_2(\lambda_1^2+\lambda_2^2-2h^2)}{(\lambda_1^2-\lambda_2^2)(\lambda_2^2-h^2)}$:

$$\tilde{d}_{2,2}^{1}d_1^2=xy\frac{\lambda_1(\lambda_1^2-k^2)(k^2-\lambda_2^2)(\lambda_1^2+\lambda_2^2-2h^2)}{(\lambda_1^2-\lambda_2^2)^3(\lambda_1^2-\lambda_3^2)(\lambda_2^2-\lambda_3^2)}, \tag{a.3.1}$$

$$\tilde{d}_{2,2}^{1}d_2^2=\frac{\lambda_1\lambda_2^2(\lambda_1^2-h^2)(\lambda_1^2-k^2)(k^2-\lambda_2^2)(h^2-\lambda_3^2)(\lambda_1^2+\lambda_2^2-2h^2)}{h^2(k^2-h^2)(\lambda_1^2-\lambda_2^2)^3(\lambda_1^2-\lambda_3^2)(\lambda_2^2-\lambda_3^2)}, \tag{a.3.2}$$

$$\tilde{d}_{2,2}^{1}d_3^2=-yz\frac{\lambda_1\lambda_2^2(\lambda_1^2-k^2)(\lambda_1^2+\lambda_1^2-2h^2)}{(\lambda_1^2-\lambda_2^2)^3(\lambda_1^2-\lambda_3^2)(\lambda_2^2-\lambda_3^2)}. \tag{a.3.3}$$

2) For $\tilde{d}_{2,2}^{2}=-y\left[\dfrac{4\lambda_2^4-(3h^2+2k^2)\lambda_2^2+h^2k^2}{(\lambda_1^2-\lambda_2^2)(\lambda_2^2-\lambda_3^2)(\lambda_2^2-h^2)}-\dfrac{2\lambda_2^2(k^2-\lambda_2^2)(2\lambda_2^2-\lambda_1^2-\lambda_3^2)}{(\lambda_1^2-\lambda_2^2)^2(\lambda_2^2-\lambda_3^2)^2}\right]$:

$$\tilde{d}_{2,2}^{2}d_1^2=-xy\left[\frac{(k^2-\lambda_2^2)(4\lambda_2^4-(3h^2+2k^2)\lambda_2^2+h^2k^2)}{\lambda_2(\lambda_1^2-\lambda_2^2)^2(\lambda_2^2-\lambda_3^2)^2}-\frac{2\lambda_2(k^2-\lambda_2^2)^2(\lambda_2^2-h^2)(2\lambda_2^2-\lambda_1^2-\lambda_3^2)}{(\lambda_1^2-\lambda_2^2)^3(\lambda_2^2-\lambda_3^2)^3}\right] \tag{a.3.4}$$

$$\tilde{d}^2_{2,2}d^2_2 = -\frac{(\lambda_1^2-h^2)(h^2-\lambda_3^2)}{h^2(k^2-h^2)}\left[\frac{\lambda_2(k^2-\lambda_2^2)(4\lambda_2^4-(3h^2+2k^2)\lambda_2^2+h^2k^2)}{\lambda_2(\lambda_1^2-\lambda_2^2)^2(\lambda_2^2-\lambda_3^2)^2}-\frac{2\lambda_2^3(k^2-\lambda_2^2)^2(\lambda_2^2-h^2)(2\lambda_2^2-\lambda_1^2-\lambda_3^2)}{(\lambda_1^2-\lambda_2^2)^3(\lambda_2^2-\lambda_3^2)^3}\right] \quad \text{(a.3.5)}$$

$$\tilde{d}^2_{2,2}d^2_3 = yz\left[\frac{\lambda_2(4\lambda_2^4-(3h^2+2k^2)\lambda_2^2+h^2k^2)}{(\lambda_1^2-\lambda_2^2)^2(\lambda_2^2-\lambda_3^2)^2}-\frac{2\lambda_2^3(k^2-\lambda_2^2)^2(\lambda_2^2-h^2)(2\lambda_2^2-\lambda_1^2-\lambda_3^2)}{(\lambda_1^2-\lambda_2^2)^3(\lambda_2^2-\lambda_3^2)^3}\right] \quad \text{(a.3.6)}$$

3) For $\tilde{d}^3_{2,2} = -d^3_2\,\frac{\lambda_2(\lambda_2^2+\lambda_3^2-2h^2)}{(\lambda_2^2-\lambda_3^2)(\lambda_2^2-h^2)}$

$$\tilde{d}^3_{2,2}d^2_1 = xy\,\frac{\lambda_3(k^2-\lambda_3^2)(k^2-\lambda_2^2)(\lambda_2^2+\lambda_3^2-2h^2)}{(\lambda_1^2-\lambda_2^2)(\lambda_1^2-\lambda_3^2)(\lambda_2^2-\lambda_3^2)^3} \quad \text{(a.3.7)}$$

$$\tilde{d}^3_{2,2}d^2_2 = \frac{\lambda_3\lambda_2^2(\lambda_1^2-h^2)(k^2-\lambda_2^2)(k^2-\lambda_3^2)(h^2-\lambda_3^2)(\lambda_2^2+\lambda_3^2-2h^2)}{h^2(k^2-h^2)(\lambda_1^2-\lambda_2^2)(\lambda_1^2-\lambda_3^2)(\lambda_2^2-\lambda_3^2)^3} \quad \text{(a.3.8)}$$

$$\tilde{d}^3_{2,2}d^2_3 = -yz\,\frac{\lambda_3\lambda_2^2(k^2-\lambda_3^2)(\lambda_2^2+\lambda_3^2-2h^2)}{(\lambda_1^2-\lambda_2^2)(\lambda_1^2-\lambda_3^2)(\lambda_2^2-\lambda_3^2)^3} \quad \text{(a.3.9)}$$

Terms associated with $k^2-\lambda_2^2$

1) For $\tilde{d}^1_{3,2} = -d^1_3\,\frac{\lambda_2(\lambda_1^2+\lambda_2^2-2k^2)}{(\lambda_1^2-\lambda_2^2)(k^2-\lambda_2^2)}$

$$\tilde{d}^1_{3,2}d^2_1 = -xz\,\frac{\lambda_1(\lambda_1^2-h^2)(\lambda_2^2-h^2)(\lambda_1^2+\lambda_2^2-2k^2)}{(\lambda_1^2-\lambda_2^2)^3(\lambda_1^2-\lambda_3^2)(\lambda_2^2-\lambda_3^2)}, \quad \text{(a.3.10)}$$

$$\tilde{d}^1_{3,2}d^2_2 = -yz\,\frac{\lambda_1\lambda_2^2(\lambda_1^2-h^2)(\lambda_1^2+\lambda_2^2-2k^2)}{(\lambda_1^2-\lambda_2^2)^3(\lambda_1^2-\lambda_3^2)(\lambda_2^2-\lambda_3^2)} \quad \text{(a.3.11)}$$

$$\tilde{d}^1_{3,2}d^2_3 = \frac{\lambda_1\lambda_2^2(\lambda_1^2-h^2)(\lambda_1^2-k^2)(\lambda_2^2-h^2)(h^2-\lambda_3^2)(\lambda_1^2+\lambda_2^2-2k^2)}{k^2(k^2-h^2)(\lambda_1^2-\lambda_2^2)^3(\lambda_1^2-\lambda_3^2)(\lambda_2^2-\lambda_3^2)} \quad \text{(a.3.12)}$$

2) For $\tilde{d}^2_{3,2} = z\left[\frac{4\lambda_2^4-(2h^2+3k^2)\lambda_2^2+h^2k^2}{(\lambda_1^2-\lambda_2^2)(\lambda_2^2-\lambda_3^2)(k^2-\lambda_2^2)}-\frac{2\lambda_2^2(\lambda_2^2-h^2)(2\lambda_2^2-\lambda_1^2-\lambda_3^2)}{(\lambda_1^2-\lambda_2^2)^2(\lambda_2^2-\lambda_3^2)^2}\right]$

$$\tilde{d}^2_{3,2}d^2_1 = xz\left[\frac{(\lambda_2^2-h^2)(4\lambda_2^4-(2h^2+3k^2)\lambda_2^2+h^2k^2)}{\lambda_2(\lambda_1^2-\lambda_2^2)^2(\lambda_2^2-\lambda_3^2)^2} - \frac{2\lambda_2(k^2-\lambda_2^2)(\lambda_2^2-h^2)^2(2\lambda_2^2-\lambda_1^2-\lambda_3^2)}{(\lambda_1^2-\lambda_2^2)^3(\lambda_2^2-\lambda_3^2)^3}\right] \tag{a.3.13}$$

$$\tilde{d}^2_{3,2}d^2_2 = yz\left[\frac{\lambda_2(4\lambda_2^4-(2h^2+3k^2)\lambda_2^2+h^2k^2)}{(\lambda_1^2-\lambda_2^2)^2(\lambda_2^2-\lambda_3^2)^2} - \frac{2\lambda_2^3(\lambda_2^2-h^2)(k^2-\lambda_2^2)(2\lambda_2^2-\lambda_1^2-\lambda_3^2)}{(\lambda_1^2-\lambda_2^2)^3(\lambda_2^2-\lambda_3^2)^3}\right] \tag{a.3.14}$$

$$\tilde{d}^2_{3,2}d^2_3 = -\frac{(\lambda_1^2-k^2)(k^2-\lambda_3^2)}{k^2(k^2-h^2)}\left[\frac{\lambda_2(\lambda_2^2-h^2)(4\lambda_2^4-(2h^2+3k^2)\lambda_2^2+h^2k^2)}{(\lambda_1^2-\lambda_2^2)^2(\lambda_2^2-\lambda_3^2)^2} - \frac{2\lambda_2^3(\lambda_2^2-h^2)^2(k^2-\lambda_2^2)(2\lambda_2^2-\lambda_1^2-\lambda_3^2)}{(\lambda_1^2-\lambda_2^2)^3(\lambda_2^2-\lambda_3^2)^3}\right] \tag{a.3.15}$$

3) For $\tilde{d}^3_{3,2} = d^3_3\,\dfrac{\lambda_2(\lambda_2^2+\lambda_3^2-2k^2)}{(\lambda_2^2-\lambda_3^2)(k^2-\lambda_2^2)}$

$$\tilde{d}^3_{3,2}d^2_1 = -xz\,\frac{\lambda_3(\lambda_2^2-h^2)(h^2-\lambda_3^2)(\lambda_2^2+\lambda_3^2-2k^2)}{(\lambda_1^2-\lambda_2^2)(\lambda_1^2-\lambda_3^2)(\lambda_2^2-\lambda_3^2)^3}, \tag{a.3.16}$$

$$\tilde{d}^3_{3,2}d^2_2 = -yz\,\frac{\lambda_3\lambda_2^2(h^2-\lambda_3^2)(\lambda_2^2+\lambda_3^2-2k^2)}{(\lambda_1^2-\lambda_2^2)(\lambda_1^2-\lambda_3^2)(\lambda_2^2-\lambda_3^2)^3} \tag{a.3.17}$$

$$\tilde{d}^3_{3,2}d^2_3 = \frac{\lambda_3\lambda_2^2(\lambda_1^2-k^2)(\lambda_2^2-h^2)(h^2-\lambda_3^2)(k^2-\lambda_3^2)(\lambda_2^2+\lambda_3^2-2k^2)}{k^2(k^2-h^2)(\lambda_1^2-\lambda_2^2)(\lambda_1^2-\lambda_3^2)(\lambda_2^2-\lambda_3^2)^3} \tag{a.3.18}$$

Terms associated with $h^2-\lambda_3^2$

1) For $\tilde{d}^1_{2,3} = -d^1_2\,\dfrac{\lambda_3(\lambda_1^2+\lambda_3^2-2h^2)}{(\lambda_1^2-\lambda_3^2)(h^2-\lambda_3^2)}$

$$\tilde{d}^1_{2,3}d^3_1 = -xy\,\frac{\lambda_1(\lambda_1^2-k^2)(k^2-\lambda_3^2)(\lambda_1^2+\lambda_3^2-2h^2)}{(\lambda_1^2-\lambda_2^2)(\lambda_1^2-\lambda_3^2)^3(\lambda_2^2-\lambda_3^2)} \tag{a.3.19}$$

$$\tilde{d}^1_{2,3}d^3_2 = \frac{\lambda_1\lambda_3^2(\lambda_1^2-h^2)(\lambda_1^2-k^2)(\lambda_2^2-h^2)(k^2-\lambda_3^2)(\lambda_1^2+\lambda_3^2-2h^2)}{h^2(k^2-h^2)(\lambda_1^2-\lambda_2^2)(\lambda_1^2-\lambda_3^2)^3(\lambda_2^2-\lambda_3^2)} \tag{a.3.20}$$

$$\tilde{d}^1_{2,3}d^3_3 = yz\,\frac{\lambda_1\lambda_3^2(\lambda_1^2-k^2)(\lambda_1^2+\lambda_3^2-2h^2)}{(\lambda_1^2-\lambda_2^2)(\lambda_1^2-\lambda_3^2)^3(\lambda_2^2-\lambda_3^2)} \tag{a.3.21}$$

2) For $\tilde{d}^2_{2,3} = -d^2_2 \dfrac{\lambda_3(\lambda_2^2+\lambda_3^2-2h^2)}{(\lambda_2^2-\lambda_3^2)(h^2-\lambda_3^2)}$

$$\tilde{d}^2_{2,3}d^3_1 = -xy\frac{\lambda_2(k^2-\lambda_2^2)(k^2-\lambda_3^2)(\lambda_2^2+\lambda_3^2-2h^2)}{(\lambda_1^2-\lambda_2^2)(\lambda_1^2-\lambda_3^2)(\lambda_2^2-\lambda_3^2)^3} \tag{a.3.22}$$

$$\tilde{d}^2_{2,3}d^3_2 = \frac{\lambda_2\lambda_3^2(\lambda_1^2-h^2)(\lambda_2^2-h^2)(k^2-\lambda_2^2)(k^2-\lambda_3^2)(\lambda_2^2+\lambda_3^2-2h^2)}{h^2(k^2-h^2)(\lambda_1^2-\lambda_2^2)(\lambda_1^2-\lambda_3^2)(\lambda_2^2-\lambda_3^2)^3} \tag{a.3.23}$$

$$\tilde{d}^2_{2,3}d^3_1 = yz\frac{\lambda_2\lambda_3^2(k^2-\lambda_2^2)(\lambda_2^2+\lambda_3^2-2h^2)}{(\lambda_1^2-\lambda_2^2)(\lambda_1^2-\lambda_3^2)(\lambda_2^2-\lambda_3^2)^3} \tag{a.3.24}$$

3) For $\tilde{d}^3_{2,3} = -y\left[\dfrac{4\lambda_3^4-(3h^2+2k^2)\lambda_3^2+h^2k^2}{(\lambda_1^2-\lambda_3^2)(\lambda_2^2-\lambda_3^2)(h^2-\lambda_3^2)} - \dfrac{2\lambda_3^2(k^2-\lambda_3^2)(2\lambda_3^2-\lambda_1^2-\lambda_2^2)}{(\lambda_1^2-\lambda_3^2)^2(\lambda_2^2-\lambda_3^2)^2}\right]$

$$\begin{aligned}\tilde{d}^3_{2,3}d^3_1 = &-\mathrm{sign}(x)\cdot y\lambda_1\lambda_2\frac{(k^2-\lambda_3^2)(4\lambda_3^4-(3h^2+2k^2)\lambda_3^2+h^2k^2)}{hk(\lambda_1^2-\lambda_3^2)^2(\lambda_2^2-\lambda_3^2)^2}\\ &+xy\frac{2\lambda_3(k^2-\lambda_3^2)^2(h^2-\lambda_3^2)(2\lambda_3^2-\lambda_1^2-\lambda_2^2)}{(\lambda_1^2-\lambda_3^2)^3(\lambda_2^2-\lambda_3^2)^3}\end{aligned} \tag{a.3.25}$$

$$\begin{aligned}\tilde{d}^3_{2,3}d^3_2 = &\frac{(\lambda_1^2-h^2)(\lambda_2^2-h^2)}{h^2(k^2-h^2)}\left[\frac{\lambda_3(k^2-\lambda_3^2)(4\lambda_3^4-(3h^2+2k^2)\lambda_3^2+h^2k^2)}{(\lambda_1^2-\lambda_3^2)^2(\lambda_2^2-\lambda_3^2)^2}\right.\\ &\left.-\frac{2\lambda_3^3(k^2-\lambda_3^2)^2(h^2-\lambda_3^2)(2\lambda_3^2-\lambda_1^2-\lambda_2^2)}{(\lambda_1^2-\lambda_3^2)^3(\lambda_2^2-\lambda_3^2)^3}\right]\end{aligned} \tag{a.3.26}$$

$$\begin{aligned}\tilde{d}^3_{2,3}d^3_3 = &yz\left[\frac{\lambda_3(4\lambda_3^4-(3h^2+2k^2)\lambda_3^2+h^2k^2)}{(\lambda_1^2-\lambda_3^2)^2(\lambda_2^2-\lambda_3^2)^2}\right.\\ &\left.-\frac{2\lambda_3^3(h^2-\lambda_3^2)(k^2-\lambda_3^2)(2\lambda_3^2-\lambda_1^2-\lambda_2^2)}{(\lambda_1^2-\lambda_3^2)^3(\lambda_2^2-\lambda_3^2)^3}\right]\end{aligned} \tag{a.3.27}$$

The singularities in $\tilde{d}^1_{1,3}$ and $\tilde{d}^2_{1,3}$ associated with λ_3 can be removed directly such as

$$\begin{aligned}\tilde{d}^1_{1,3} &= d^1_1\frac{\lambda_1^2+\lambda_3^2}{\lambda_3(\lambda_1^2-\lambda_3^2)} = \frac{x(\lambda_1^2-k^2)(\lambda_1^2-h^2)}{\lambda_1(\lambda_1^2-\lambda_2^2)(\lambda_1^2-\lambda_3^2)}\frac{(\lambda_1^2+\lambda_3^2)}{\lambda_3(\lambda_1^2-\lambda_3^2)}\\ &= \mathrm{sign}(x)\cdot\frac{\lambda_2(\lambda_1^2-k^2)(\lambda_1^2-h^2)(\lambda_1^2+\lambda_3^2)}{hk(\lambda_1^2-\lambda_2^2)(\lambda_1^2-\lambda_3^2)^2}\end{aligned} \tag{a.3.28}$$

$$\tilde{d}_{1,3}^2 = d_1^2 \frac{\lambda_2^2 + \lambda_3^2}{\lambda_3(\lambda_2^2 - \lambda_3^2)} = \frac{x(k^2 - \lambda_2^2)(\lambda_2^2 - h^2)}{\lambda_2(\lambda_1^2 - \lambda_2^2)(\lambda_2^2 - \lambda_3^2)} \frac{(\lambda_2^2 + \lambda_3^2)}{\lambda_3(\lambda_2^2 - \lambda_3^2)}$$
$$= \text{sign}(x) \cdot \frac{\lambda_1(k^2 - \lambda_2^2)(\lambda_2^2 - h^2)(\lambda_2^2 + \lambda_3^2)}{hk(\lambda_1^2 - \lambda_2^2)(\lambda_2^2 - \lambda_3^2)^2} \qquad \text{(a.3.29)}$$